Designing Electrocatalysts via Atomic Layer Deposition For the Carbon Dioxide Reduction and Hydrogen Evolution Reaction

Li, M.

DOI
10.4233/uuid:d4352026-c3fb-42ad-9b08-d6144b50934d

Publication date
2025

Document Version
Final published version

Citation (APA)
Li, M. (2025). *Designing Electrocatalysts via Atomic Layer Deposition For the Carbon Dioxide Reduction and Hydrogen Evolution Reaction*. [Dissertation (TU Delft), Delft University of Technology]. https://doi.org/10.4233/uuid:d4352026-c3fb-42ad-9b08-d6144b50934d

Designing Electrocatalysts via Atomic Layer Deposition

For the Carbon Dioxide Reduction and Hydrogen Evolution Reaction

Designing Electrocatalysts via Atomic Layer Deposition

For the Carbon Dioxide Reduction and Hydrogen Evolution Reaction

Dissertation

for the purpose of obtaining the degree of doctor

at Delft University of Technology

by the authority of the Rector Magnificus, prof.dr.ir. T.H.J.J. van der Hagen,

Chair of the Board for Doctorates

to be defended publicly on

Monday 6 January 2025 at 10:00 o'clock

by

Ming LI

Master of Science in Materials Engineering,

Beihang University, China

born in Hunan, China

This dissertation has been approved by the promotors.

Composition of the doctoral committee:

Rector Magnificus	chairperson
Prof.dr.ir. J.R. van Ommen	Delft University of Technology, promotor
Dr. R. Kortlever	Delft University of Technology, promotor

Independent members:

Prof.dr. A.J. Houtepen	Delft University of Technology
Prof.dr. E.A. Pidko	Delft University of Technology
Dr. T.E. Burdyny	Delft University of Technology
Dr. A. Forner-Cuenca	Eindhoven University of Technology
Prof.dr. J. Dendooven	Ghent University, Belgium

The research described in this thesis was conducted in the Chemical Engineering Department from the Faculty of Applied Science and the Process and Energy Department from the Faculty of Mechanical Engineering of the Delft University of Technology, and co-financed by the China Scholarship Council (CSC).

Keywords: Electrochemical CO_2 reduction, Electrocatalysts, Atomic layer deposition, Catalyst protection, Water splitting

Printed by: Ridderprint | www. ridderprint.nl

Front & Back: Designed by Ming Li & Aaliyah van Ballegooijen

ISBN: 978-94-6506-836-7

To family and friends

Contents

Summary iii

Samenvatting vii

1. Introduction 1

1.1 The potential of CO_2 reduction 3

1.2 Research objectives 3

1.3 Atomic layer deposition (ALD) mechanism.. 4

1.4 The application of ALD in catalyst research 5

1.5 The application of ALD in electrocatalysts for CO_2 reduction....................... 8

1.6 Molecular layer deposition (MLD) mechanism 11

1.7 Molecular layer deposition in catalyst research 11

1.8 Research questions 13

1.9 Thesis outline.. 14

References 15

2. Nanostructuring Pt-Pd bimetallic electrocatalysts for CO_2 reduction using atmospheric pressure atomic layer deposition 19

2.1 Introduction 21

2.2 Results and Discussion... 22

2.3 Conclusion 28

2.4 Experimental Section.. 28

References 31

Supporting Information for Chapter 2 39

3. Enhancing the durability of Pt nanoparticles for water electrolysis using ultrathin SiO_2 layers... 43

3.1 Introduction 45

3.2 Experimental Section.. 46

3.3 Results and Discussion... 48

3.4 Conclusions 55
References 57
Supporting information for chapter 3 61
4. The effects of SO_2 impurities on CO_2 electroreduction on bare silver and SiO_2 coated silver in different cell geometries 69
4.1 Introduction 71
4.2 Results and discussion 73
4.3 Conclusions 84
4.4 Experimental Section 84
Reference 89
Supporting information for chapter 4 93
5. Tuning the wettability of a Ag electrocatalyst by Atomic and Molecular Layer Deposition 101
5.1 Introduction 103
5.2 Wettability 104
5.3 The interaction of wetting on different surfaces 105
5.4 Wettability measuring methods 106
5.5 Electrowetting 106
5.6 Experimental methods 107
5.7 Results and discussion 108
5.8 Conclusions 117
5.9 Further experiments and recommendations 117
References 119
6. Conclusions and Outlook 121
6.1 Conclusions 123
6.2 Outlook 125
Acknowledgements 127
Curriculum vitae 131
List of Publications 133

Summary

The severe effects of climate change, along with the rising global energy demand, have driven extensive research efforts into the development of sustainable technologies for energy generation, conversion, storage, distribution, and CO_2 removal from various industrial sectors. Electrocatalysis is expected to play a pivotal role in achieving these goals, as it can utilize intermittent renewable energy sources such as wind, geothermal, hydropower and solar energy, together with CO_2 directly captured from the air or from flue gas, and H_2O, to store energy into chemical building blocks. Meanwhile, the catalyst is indispensable in these electrochemical conversions, as it enables the reduction of the reaction energy barrier, thereby lowering the electrochemical overpotential required to initiate reactions. Moreover, it facilitates the direction of reactions along specific pathways without itself being consumed in the process, thereby enhancing reaction rates and improving the efficiency. This thesis focuses on the electrocatalysts used for CO_2 reduction and water splitting, and uses atomic layer deposition (ALD) and molecular layer deposition (MLD) to precisely control the catalyst structure and protect the catalysts from degradation and poisoning.

In electrocatalysis, the catalyst must be conductive to facilitate electron transfer among the reactants, the catalyst, and the electrode. To ensure the desired reaction proceeds efficiently, the catalyst should adsorb reactant molecules onto its surface and activate them into reaction intermediates through electron transfer between the molecule and the catalyst. The catalyst also plays a crucial role in mediating the recombination of these reactive intermediates into new products. Moreover, the product should be easily desorbed from the catalyst surface to allow for the catalysts regeneration and subsequent catalytic reaction cycles. Therefore, bimetallic catalysts are crucial for synthesizing superior catalysts, as they allow for the tuning of binding energy between the catalysts and reactants by adjusting the ratio and combination structure of the two metals. We employed ALD to synthesize Pt-Pd bimetallic electrocatalysts with precisely controlled core-shell and alloy structures aimed at reducing CO_2 to formic acid. By controlling the catalyst structures at the sub-nanometer scale, we were able to investigate the influence of these configurations on Pt-Pd bimetallic catalysts. Our results indicate that by controlling the particle size and bimetallic composition, individually changing the structure of the catalyst can have a significant impact on the selectivity. The Pt-Pd alloy catalyst has superior selectivity towards formic acid, achieving more than twice the faradaic efficiency of the core-shell structure catalyst. Furthermore, we found that core-shell bimetallic catalysts (Pd@Pt and Pt@Pd) are unstable under electroreduction conditions. During the electrochemical reduction process, these catalysts

undergo structural rearrangements to form thermodynamically more stable configurations, such as segregated clusters or alloy particles, which in turn alters their catalytic selectivity.

After recognizing the critical issue of nanostructured catalyst stability in electrochemistry, we explored methods to enhance stability using ALD. We applied an ultrathin SiO_2 layer on Pt/ carbon black (CB) electrocatalysts to prevent deactivation during water electrolysis. Our results showed that the untreated Pt/CB catalyst experienced a 34 % reduction in current density at -0.2 V vs. RHE after an accelerated durability test (ADT). In contrast, Pt/CB catalysts coated with 2 cycles of SiO_2 ALD showed only a 7% reduction, and those with 5 cycles exhibited a mere 2% decrease under the same conditions. Additionally, the Pt particle size increased by 16% after ADT without SiO_2 coating but only by 3% with 5 cycles of SiO_2 deposition. Significant Pt detachment was observed in the uncoated Pt/CB catalyst, with the Pt concentration in the electrolyte rising to 8.9 mg/L post-ADT. However, the ultrathin SiO_2 coating markedly reduced this detachment, with 5 cycles of SiO_2 ALD reducing Pt detachment/dissolution to one-fifth of the level observed with the uncoated sample. In summary, a nanoscale SiO_2 protective layer significantly minimizes Pt agglomeration and detachment during the hydrogen evolution reaction in acidic conditions, effectively preserving electrocatalytic activity with just a few ALD cycles.

Building on the discovery of SiO_2's protective effect on Pt catalysts, we explored whether it could also prevent catalyst poisoning. We investigated the performance of the Ag/CB catalyst under SO_2 impurities for CO_2 electrolysis in two electrochemical reactor systems: an H-cell reactor and a MEA reactor. The catalysts behavior differed significantly between these systems concerning SO_2 contamination. In the H-cell, the impact of SO_2 on Ag/CB catalysts was substantial, whereas in the MEA system, it was nearly negligible. This discrepancy is due to the greater solubility of SO_2 in the electrolyte compared to CO_2, leading to an accumulation effect and a much higher liquid-phase concentration of SO_2 in the H-cell. Consequently, the performance of the Ag/CB catalyst in the H-cell decreased more significantly than in the MEA system when exposed to the same concentration of SO_2 impurities. An ultrathin SiO_2 coating synthesized via ALD effectively protected the Ag/CB catalyst in the H-cell against SO_2 impurities. This is likely due to differences in SO_2 and CO_2 permeability through SiO_2 coatings, with CO_2 having much higher permeability compared to SO_2 (or SO_2-derived ions). This permeability difference significantly obstructs the interaction of SO_2 with the catalyst, potentially reducing the SO_2 concentration after the SiO_2 coatings. We have demonstrated that SiO_2 coatings synthesized by ALD are effective in mitigating the performance degradation of an Ag-based electrocatalyst caused by SO_2 impurities in the feed stream.

After these studies, we continued to investigate the effect of catalyst wettability on performance and explored altering catalyst wettability with ALD and MLD. We found that

ALD and MLD are effective for modifying electrocatalyst wettability. These techniques enable the application of ultra-thin coatings (at the sub-nanometer scale) to significantly alter the catalyst surface wettability. Specifically, MLD was used for PET deposition to increase the catalysts' hydrophobicity. A linear relationship was observed between the water contact angle (WCA) and the number of deposition cycles. The WCA of the electrocatalyst increased from 119 ± 2° to 137 ± 2° after 8 PET cycles, representing an approximate 15% increase. Conversely, SiO_2 deposition effectively tuned the electrocatalyst to be more hydrophilic. However, unlike PET deposition, the WCA did not exhibit a clear linear correlation with the number of deposition cycles. The WCA of the catalysts varied considerably between the two sets of samples, likely due to the woven structure of the carbon fiber, which prevents the formation of a complete film on the carbon paper surface. Additionally, SiO_2 deposition is less effective in improving the film integrity of the catalyst surface compared to PET deposition. This results in high fluctuations in the SiO_2 ALD modification outcomes, showing only a decreasing trend rather than a linear correlation between WCA and the number of deposition cycles.

Overall, compared to traditional wet chemistry methods, ALD and MLD have shown to be valuable techniques for electrocatalyst synthesis, offering additional advantages in catalyst design and protection strategies.

Samenvatting

De ernstige effecten van klimaatverandering, samen met de stijgende wereldwijde vraag naar energie, hebben geleid tot uitgebreide onderzoeksinspanningen naar de ontwikkeling van duurzame technologieën voor energieopwekking, -omzetting, -opslag, -distributie en CO_2-verwijdering uit verschillende industriële sectoren. Elektrokatalyse wordt verwacht een cruciale rol te spelen bij het bereiken van deze doelen, omdat het periodiek hernieuwbare energiebronnen zoals wind, geothermie, waterkracht en zonne-energie kan benutten, samen met CO_2 die direct uit de lucht of uit rookgas wordt opgevangen, en H_2O, om energie op te slaan in chemische bouwstenen. Ondertussen is de katalysator onmisbaar in deze elektrochemische omzettingen, omdat het de reactieve energiebarrière verlaagt, waardoor de elektrochemische overpotentiaal die nodig is om reacties te starten, wordt verminderd. Bovendien faciliteert het de richting van reacties langs specifieke routes zonder zelf te worden verbruikt in het proces, wat de reactiesnelheden verhoogt en de efficiëntie verbetert. Dit proefschrift richt zich op de elektrokatalysatoren die worden gebruikt voor CO_2-reductie en watersplitsing, en maakt gebruik van atoomlaagafscheiding (ALD) en moleculaire laagafscheiding (MLD) om de katalysatorstructuur nauwkeurig te controleren en de katalysatoren te beschermen tegen degradatie en vergiftiging.

In de elektrokatalyse moet de katalysator geleidend zijn om de elektronoverdracht tussen de reactanten, de katalysator en de elektrode te vergemakkelijken. Om ervoor te zorgen dat de gewenste reactie efficiënt verloopt, moet de katalysator reactantmoleculen aan het oppervlak adsorberen en deze activeren tot reactieve tussenstoffen door elektronoverdracht tussen het molecuul en de katalysator. De katalysator speelt ook een cruciale rol bij het bemiddelen van de recombinatie van deze reactieve intermediairen tot nieuwe producten. Bovendien moet het product gemakkelijk van het katalysatoroppervlak desorberen om de regeneratie van de katalysator en de daaropvolgende katalytische reactiecycli mogelijk te maken. Daarom zijn bimetale katalysatoren van groot belang voor het synthetiseren van superieure katalysatoren, omdat ze de bindingsenergie tussen de katalysator en de reactanten kunnen afstemmen door de verhouding en structuur van de twee metalen aan te passen. We hebben ALD gebruikt om Pt-Pd bimetale elektrokatalysatoren te synthetiseren met nauwkeurig gecontroleerde kern-schil- en legeringsstructuren, gericht op de reductie van CO_2 tot mierenzuur. Door de katalysatorstructuren op sub-nanometerschaal te controleren, konden we de invloed van deze configuraties op Pt-Pd bimetale katalysatoren onderzoeken. Onze resultaten geven aan dat door de deeltjesgrootte en bimetale samenstelling te controleren, het individueel veranderen van de structuur van de katalysator een aanzienlijke invloed kan hebben op de selectiviteit. De Pt-Pd legeringskatalysator heeft een superieure selectiviteit voor mierenzuur, met meer dan twee keer de faradische efficiëntie van de kern-schilstructuurkatalysator. Bovendien ontdekten we dat kern-schil bimetale katalysatoren (Pd@Pt en Pt@Pd) instabiel zijn onder elektro-reductieomstandigheden. Tijdens het elektrochemische reductieproces ondergaan deze katalysatoren structurele herschikkingen om thermodynamisch stabielere configuraties te vormen, zoals gesegregeerde clusters of legeringsdeeltjes, wat op zijn beurt hun katalytische selectiviteit verandert.

Na het herkennen van het kritieke probleem van de stabiliteit van nanogestructureerde katalysatoren in de elektrochemie, hebben we methoden onderzocht om de stabiliteit te verbeteren met behulp van ALD. We hebben een ultradunne SiO_2-laag op Pt/koolstof (carbon black, CB) elektrokatalysatoren aangebracht om deactivering tijdens water-elektrolyse te voorkomen. Onze resultaten toonden aan dat de onbehandelde Pt/CB-katalysator een vermindering van 34% in stroomdichtheid bij -0,2 V vs. RHE ondervond na een versnelde duurzaamheidstest (ADT). Daarentegen vertoonden Pt/CB-katalysatoren bedekt met 2 cycli SiO_2 ALD slechts een vermindering van 7%, en die met 5 cycli vertoonden slechts een afname van 2% onder dezelfde omstandigheden. Bovendien nam de Pt-deeltjesgrootte met 16% toe na ADT zonder SiO_2-coating, maar slechts met 3% bij 5 cycli SiO_2-afzetting. Aanzienlijke Pt-loslating werd waargenomen in de onbehandelde Pt/CB-katalysator, waarbij de Pt-concentratie in het elektrolyt steeg tot 8,9 mg/L na ADT. De ultradunne SiO_2-coating verminderde deze loslating echter aanzienlijk, waarbij 5 cycli SiO_2 ALD de Pt-loslating/ontbinding tot een vijfde van het gemeten niveau bij het onbehandelde monster verminderde. Samengevat: een nanoschaal SiO_2-beschermingslaag minimaliseert significant Pt-agglomeratie en loslating tijdens de waterstofontwikkelingsreactie in zure omstandigheden, waardoor de elektrokatalytische activiteit effectief behouden blijft met slechts enkele ALD-cycli.

Voortbouwend op de ontdekking van het beschermende effect van SiO_2 op Pt-katalysatoren, onderzochten we of het ook katalysatorvergiftiging kon voorkomen. We onderzochten de prestaties van de Ag/CB-katalysator onder SO_2-onzuiverheden voor CO_2-elektrolyse in twee elektrochemische reactorsystemen: een H-celreactor en een MEA-reactor. Het gedrag van de katalysatoren verschilde aanzienlijk tussen deze systemen wat betreft SO_2-verontreiniging. In de H-cel was de impact van SO_2 op Ag/CB-katalysatoren aanzienlijk, terwijl deze in het MEA-systeem vrijwel verwaarloosbaar was. Dit verschil is te wijten aan de grotere oplosbaarheid van SO_2 in het elektrolyt vergeleken met CO_2, wat leidt tot een accumulatie-effect en een veel hogere vloeistoffaseconcentratie van SO_2 in de H-cel. Als gevolg hiervan daalden de prestaties van de Ag/CB-katalysator in de H-cel aanzienlijk meer dan in het MEA-systeem bij blootstelling aan dezelfde concentratie SO_2-onzuiverheden. Een ultradunne SiO_2-coating, gesynthetiseerd via ALD, beschermde de Ag/CB-katalysator in de H-cel effectief tegen SO_2-onzuiverheden. Dit is waarschijnlijk te verklaren door verschillen in SO_2- en CO_2-doorlaatbaarheid door SiO_2-coatings, waarbij CO_2 een veel hogere doorlaatbaarheid heeft in vergelijking met SO_2 (of SO_2-afgeleide ionen). Dit verschil in doorlaatbaarheid belemmert aanzienlijk de interactie van SO_2 met de katalysator, wat mogelijk de SO_2-concentratie na de SiO_2-coatings vermindert. We hebben aangetoond dat SiO_2-coatings, gesynthetiseerd door ALD, effectief zijn in het verminderen van de prestatieverslechtering van een Ag-gebaseerde elektrokatalysator, veroorzaakt door SO_2-onzuiverheden in de toevoer.

Na deze studies hebben we verder onderzoek gedaan naar het effect van de bevochtigbaarheid van de katalysator op de prestaties en hebben we onderzocht hoe de bevochtigbaarheid van de katalysator kan worden veranderd met ALD en MLD. We ontdekten dat ALD en MLD effectieve technieken zijn voor het aanpassen van de bevochtigbaarheid van elektrokatalysatoren. Deze technieken maken het mogelijk om ultradunne coatings (op sub-nanometerschaal) aan te brengen om de bevochtigbaarheid van het katalysatoroppervlak aanzienlijk te veranderen. Specifiek werd MLD gebruikt voor PET-afzetting om de waterafstotendheid van de katalysator te vergroten. Er werd een lineaire relatie waargenomen tussen de watercontacthoek (WCA) en het aantal afzettingscycli. De WCA van de elektrokatalysator nam toe van 119 ± 2° tot 137 ± 2° na 8 PET-cycli, wat een toename van ongeveer 15% inhoudt. Omgekeerd maakte SiO_2-afzetting de elektrokatalysator effectief meer hydrofiel. Echter, in tegenstelling tot PET-afzetting vertoonde de WCA geen duidelijke lineaire correlatie met het aantal afzettingscycli. De WCA van de katalysatoren varieerde aanzienlijk tussen de twee sets monsters, waarschijnlijk door de geweven structuur van de koolstofvezel, die de vorming van een complete film op het koolstofpapiervlak verhindert. Bovendien is SiO_2-afzetting minder effectief in het verbeteren van de filmintegriteit van het katalysatoroppervlak vergeleken met PET-afzetting. Dit resulteert in hoge fluctuaties in de resultaten van SiO_2-ALD-modificaties, die alleen een dalende trend vertonen in plaats van een lineaire correlatie tussen WCA en het aantal afzettingscycli.

Al met al hebben ALD en MLD, vergeleken met traditionele natte chemische methoden, zich bewezen als waardevolle technieken voor de synthese van elektrokatalysatoren, met extra voordelen op het gebied van katalysatorontwerp en beschermingsstrategieën.

1

Introduction

The continuous increase of the carbon dioxide (CO_2) concentration leading to climate change has obtained global attention. Converting CO_2 into value-added chemicals or fuels is one of the potential solutions to tackle this problem [1-2]. Less carbon dioxide will be released into the atmosphere by factories, which will help reduce the greenhouse effect. The chemicals obtained from this process can continue to be used as bulk chemicals in factories, allowing the factory's carbon emissions to become circular. Electroreduction of CO_2 into valuable products has garnered significant attention as a promising approach to mitigate greenhouse gas emissions, and achieve sustainability goals. Various catalyst materials, synthesis strategies, and electrochemical reactors have been explored to enhance the efficiency, stability and selectivity of CO_2 reduction reactions and the possibility of large-scale applications. The work presented in this thesis is aimed at designing electrocatalysts via atomic layer deposition for carbon dioxide reduction and hydrogen evolution reaction.

1.1 The potential of CO_2 reduction

Up to date, the major energy source worldwide is still fossil energy such as coal, crude oil and natural gas[3]. Growing human activities have increased the usage of fossil fuels and the emission of greenhouse gas into the air, disrupting the carbon balance that has been maintained in nature for thousands of years. Since the late 19th century, the concentration of CO_2 in the air has soared from 270 ppm to over 400 ppm[4]. Under these appalling circumstances, finding useful technologies to decrease the concentration of CO_2 in the air has become an urgent challenge for governments, companies and researchers all over the world. Among a host of feasible strategies, the technology of reducing CO_2 via electrochemical reduction and turning it into fuels and bulk chemicals that are profitable to humans is very attractive. This can provide solutions to transport sectors such as aviation that are very hard to decarbonize and the chemical industry that will always require hydrocarbon feedstock to make a large range of products.

Renewable electricity such as wind energy and solar energy can be used for the electrocatalytic version of CO_2 info useful chemicals. However, the industrial feasibility of CO_2 reduction is still challenging. This is mostly because CO_2 has a strong C=O double bond with a bonding energy of 750 kJ/mol, which is much larger than the C-C bond of 336 kJ/mol, the C-O bond of 327 kJ/mol, or the C-H bond of 411 kJ/mol[5]. This leads to electrocatalytic CO_2 reduction with very limited conversion efficiency and low selectivity. To make the problem even more complicated, the CO_2 reduction may need the transfer of 2, 4, 6, 8, 12 or even more electrons in several different routes [6]. The final reduction products can include carbon monoxide (CO), methane (CH_4), methanol (CH_3OH), ethylene (C_2H_4), methanol (CH_5OH), formic acid (HCOOH), and other (oxygenated) hydrocarbons. The actual composition of the product mixture strongly depends on the experimental conditions (local pH, temperature, pressure, reactant concentration, etc. [7]) as well as on the electrocatalyst applied.

1.2 Research objectives

The composition, structure, particle size, number of active sites and morphology have a large impact on the performance of electrocatalysts. It is important to understand how these factors affect catalyst performance as this will help to design better catalysts. Unfortunately, this is difficult to achieve with traditional methods such as impregnation, colloidal synthesis, and ion exchange methods which offer limited control over the catalyst properties. Moreover, they lead to contamination and separation issues when the final product is a solid material. Therefore, novel approaches are needed to carry out enhanced catalyst research. One promising solution is to use atomic layer deposition (ALD) to fabricate the electrocatalysts. ALD is a deposition method to grow conformal films or ultrafine nanoparticles with sub-nanometer precision. The method alternately uses different gas-phase reactants to absorb and react on the surface of the support materials[8]. By controlling the number of reaction cycles, temperature, pressure and other parameters, the thickness and morphology of the coating can be tuned. Another benefit of using ALD is that it operates in the gas phase, and therefore it does not require the use of solvents or surfactants for catalysts production. It also enables faster mass transfer because reactants diffuse faster in gas than in liquid. The product contamination will also be reduced, while simultaneously avoiding the problem of separating the final solid product from the solvent[9]. Since ALD is a cyclic gas phase deposition method, it facilitates the deposition of sub-nanometer coatings in each cycle, enabling the design of products at the atomic level. This allows for precise control of the particle size, morphology, and thickness of the film which is deposited on the substrate. In combination with other advanced electrochemical analysis, the catalytic processes mechanisms could be revealed, allowing for the rational design of new electrocatalysts.

In this thesis, ALD was employed to investigate various aspects of electrocatalyst performance. To explore the catalyst activity, ALD was utilized to synthesize catalysts with core-shell/alloy structures, which allowed for the examination of reaction mechanisms. Additionally, molecular layer deposition (MLD) was utilized to create a hydrophobic layer on the catalyst surface, providing insights into the catalyst selectivity aspect. Finally, the catalyst stability was enhanced by employing ALD to apply a protective layer on the catalyst surface. By using these precise deposition techniques, it was possible to obtain valuable insights into the activity, selectivity, and stability of the synthesized catalysts.

1.3 Atomic layer deposition (ALD) mechanism

As a technology that can accurately coat thin films and particles on substrates, ALD has attracted more and more interest in a range of fields, such as energy conversion and storage, biomedicine, sensor design and catalysis. Functionalizing particles using ALD to improve their performance and introducing special properties are common requirements in these emerging applications. ALD shows self-limiting behaviour: the reactant molecules can only reactor with a limited number of surface sites. One ALD cycle is usually composed of four steps[10]. The first step is to pass the precursor to the reactor chamber and let it chemisorb on the substrate. After saturation, the purging gas is purged into the reactor to remove by-products and the unadsorbed precursor to achieve a single layer adsorption on the substrate (less than a full monolayer). Then, the co-reactant is introduced to the reactor to react with

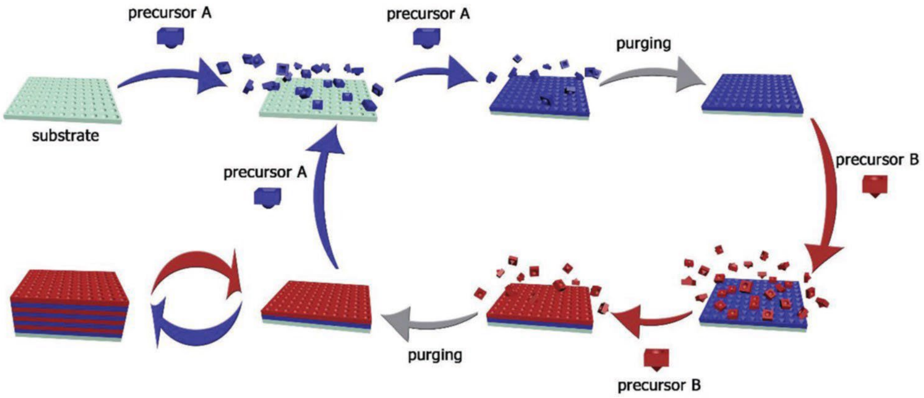

Figure 1.1. The schematic of the self-terminating surface mechanism of ALD[13]. Reprinted with permission from Wiley.

the precursor which was adsorbed on the substrate, and finally the excess co-reactants and the by-products of the reaction are washed out by the second purging step. After those four steps, an ALD cycle is completed. Figure 1.1 shows an interpretation diagram of a simple ALD process. It should be noted that the actual reaction will be more complicated and not as perfect as is described here. Different precursors have different substrate adsorption behaviors, which will lead to different growth behaviors in repeated cycles, such as substrate-enhanced growth, substrate-inhibited growth, etc. Moreover, in actual operation, the adsorption of precursors on the substrate will yield less than a monolayer[11-12].

1.4 The application of ALD in catalyst research

Since ALD can coat a uniform and conformal film on the surface of the substrate, some researchers have applied this method to protect catalysts. Kennedy et al. compared the effects of alumina and titania films on Pt/$SrTiO_3$ catalysts for the hydrogenation of acrolein [14]. Their experimental results show that the titania overlayer improves the selectivity of the catalyst while the alumina coating does not. This is related to the selective deposition on different sites of the catalyst. Alumina deposited by ALD is mainly located on the $SrTiO_3$ surface and surrounding the Pt nanoparticles. But titania deposited by ALD is present on the surface of both Pt and $SrTiO_3$. Further studies by Lu et al. found that alumina overlayers on palladium nanoparticles can effectively reduce deactivation caused by sintering and coking when the catalyst operates at high-temperature[15]. This is achieved by covering the edge and corner atoms of palladium catalysts by an ALD alumina layer.

Duan et al. prepared efficient and stable Al_2O_3/Pd/SiO_2 catalysts for the methane combustion reaction[16]. They found that the Al_2O_3 film coated on Pd particles had a strong

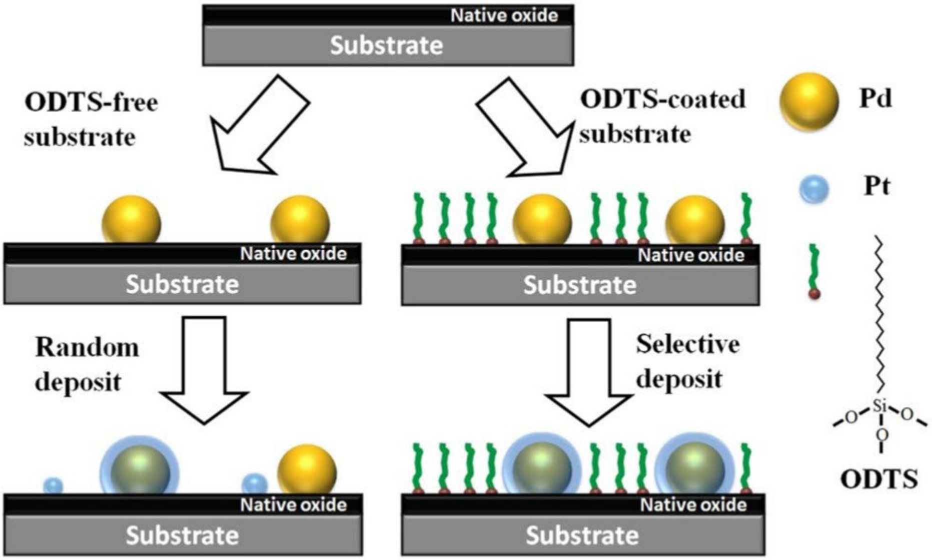

Figure 1.2. Schematic illustration of the core-shell nanoparticles prepared by AS-ALD[17]. Unrestricted reproduction permission from Springer Nature.

interaction with the PdO_x phases on the adjacent Pd surface. This is one of the main reason why the ALD protective layer works. Additionally, Cao et al. used the pinholes of a self-assembled monolayer as a template to fabricate Pd/Pt core/shell nanoparticles by ALD[17]. Figure 1.2 shows a schematic of this preparation method. This method can ensure the formation of core-shell structure without the existence of single-phase metal particles. This procedure has demonstrated a novel approach to study the structure-property relationship of bimetallic catalysts.

It is worth noting that in some cases, the protective coating layer may also completely block the particle surface, resulting in reduced catalytic activity which is undesirable. To prevent this from happening, some researchers have developed porous coating approaches that ensure exposure of the substrate surface to the solvent by providing nanopore channels. Cheng et al. developed the encapsulation of Pt in a zirconia nanocage by area-selective ALD[18]. They deposited Pt nanoparticles onto N-doped carbon nanotubes (NCNT) and then used oleylamine as an adsorbent on the surface of Pt particles as a blocking agent. After that, ZrO_2 was selectively deposited around the Pt nanoparticles to form a cage and stabilize the Pt nanoparticles. Lastly, the oleylamine was removed by heating and oxidizing at 200 °C. This method improves the stability of the Pt catalyst effectively and prevents the loss of the electrochemical surface area of the catalyst after the reaction. After 4000 cycles of cyclic voltammetry, which is an electrochemical technique that cycles the potential of working electrode while measuring the corresponding current, the ALD ZrO_2-Pt/NCNT catalysts only lost 8% of electrochemical surface area (ECSA), whereas the ALD Pt/NCNT catalysts lost 74% of ECSA. The catalyst activity towards the oxygen reduction reaction is also improved by the synergetic effects of ZrO_2 nanocage on Pt catalyst.

Another approach to enhance the stability of electrocatalysts is by increasing the stability of the catalyst support material. The catalyst support is prone to collapse or corrode during electrochemical reactions, owing to the extreme pH environment and continuous oxidation or reduction processes. To solve this problem, Marichy et al. used SnO_2 deposited on Pt/carbon fibers (CF) by ALD to increase the stability of the catalyst support and ultimately, improve the overall stability of the catalyst[19]. SnO_2 has inherently high electrochemical stability, and it has a strong interaction with Pt which can improve the activity of the catalyst through this interaction. However, the common problem with metal oxides is that their low electrical conductivity will limit electron transport. High resistivity will affect the electron transfer and reduce the reaction rate. Therefore, in order to avoid the side effect of SnO_2 metal oxides and use its attractive features, Marichy et al. used ALD to deposit a thin layer of SnO_2 on the electrospun Pt/CF electrocatalyst to enhance the stability of the catalyst which can prevent CF from corrosion during the long-term electrocatalysis process. The SnO_2 film deposited by ALD is uniformly coated on the surface of the support and the atomic-level thickness of SnO_2 also minimizes its negative effects. The authors applied an accelerated degradation protocol by performing 10000 CV cycles and monitoring the ECSA decrease to define the stability of the catalyst. Their results demonstrate that the Pt/CF electrocatalyst with SnO_2 modification is twice as stable as the pristine catalyst.

Additionally, in order to improve stability of catalysts, the selection of a more stable substrate for a given operating conditions is a viable solution. A Pt/carbon black catalyst is the conventional oxygen reduction reaction (ORR) catalyst and carbon black is the most widely used support material for many electrocatalysts due to its high conductivity, controllable production and low price. Nevertheless, carbon black is easy to corrode during long-term use, which will lead to catalyst deactivation and contamination of the product. To solve this problem, Cheng et al. used ZrC as support material instead of carbon black to synthesize Pt/ZrC catalyst by ALD[20]. Through accelerated durability tests (ADT) by potential cycling between 0.6 and 1.2 V vs RHE at a scan rate of 50 mV s^{-1} and comparing the calculated ECSA, they show that ALD- Pt/ZrC electrocatalyst was 5-fold more stable than commercial Pt/C electrocatalyst and 3-fold more stable than a conventional chemical reduction fabricated CW-Pt/ZrC electrocatalyst. Replacing carbon black with ZrC as the catalyst support material significantly improves the stability of the catalyst. ALD can form a chemical bond between the initial layer of Pt particles and the surface of ZrC during the first cycle which ensures a strong interaction between Pt and the ZrC. Their X-ray absorption near edge structures (XANES) analysis also showed that the electronic structure of Pt on ALD-Pt/ZrC has changed compared with the chemical reduction fabricated CW-Pt/ZrC catalyst, which may be the reason why the ORR catalytic activity of the catalyst is facilitated.

1.5 The application of ALD in electrocatalysts for CO_2 reduction

The preparation of electrocatalysts by ALD with a well-controlled composition and structure has received more and more attention in recent years. Figure 1.3 shows some basic strategies for the preparation of electrocatalysts by ALD[21]. Nevertheless, there are many more possibilities of using ALD in electrocatalysts research. For example: some researchers use ALD technology to add S or N adatoms into the catalyst to modulate the coordination sites and crystal structure of the catalyst, which can decrease the activation energy barrier of the reaction and improve the selectivity. Zheng et al. used SnS_x deposited by ALD to fabricate a sulfur-modulated tin (Sn(S)) catalysts[22]. They achieved a controllable sulfur-doped Sn film through ALD, followed by a reduction process to precisely control the S content. The optimal sulfur content to maximize the selectivity of the catalyst was researched, and the role of sulfur in the reaction was also well explained. Some researchers have come up with some very creative ideas to use ALD to create new catalyst structures for carbon dioxide reduction reactions. Chen et al. discovered that the Ru(II) polypyridyl carbine complex molecular catalyst can be used to electrochemically reduce CO_2 to syngas, but this molecule is very unstable and cannot be tightly fixed on the electrode surface[23-24]. To solve this problem, they used ALD to design a new catalyst structure. A layer of TiO_2, fabricated by ALD, was used to bind the molecules to the electrode and a layer of carbon nanotubes is sandwiched between them to decrease the electron transfer resistance. Another thin layer of TiO_2 is applied to the outer surface of the molecular catalyst for surface stabilization purposes[7]. Furthermore, the same research group immobilized another molecule Ru^{II} complex $[Ru(PO_3Et_2\text{-ph-tpy})(6\text{-mbpy})(NCCH_3)]^{2+}$ on the titanium dioxide electrode and used ALD to deposit a NiO layer to protect the molecule[26] and then tested the electrocatalytic performance of the catalyst.

Directly using metal electrodes such as copper, palladium and gold electrodes for carbon dioxide reduction has been extensively studied since the 20th century allowing for their reaction mechanism to be clearly explained. These fundamental studies provide a solid foundation for subsequent research. Although these pure metal electrodes are useful for mechanistic studies, they will encounter various problems in practical application. In order to solve these problems, researchers modified the electrode surface with ALD to achieve unique properties. For example, Schreier et al. deposited SnO_2 on a CuO nanowires electrode using ALD to tune the electrochemical reduction products mainly towards CO[26]. Zhang et al. applied ALD to deposit a thin layer of zinc oxide on the surface of the copper electrode to study the effect on the selectivity and overpotential of the electrode[27].

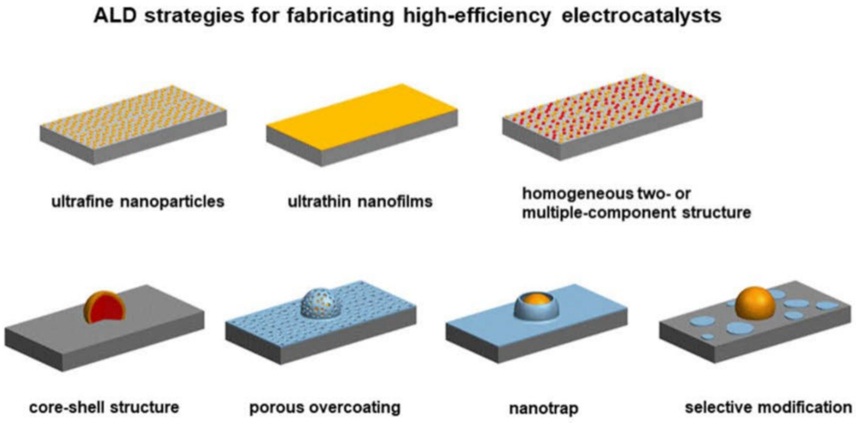

Figure 1.3. ALD strategies for fabricating high-efficiency electrocatalysts[21]. Reprinted with permission from Wiley.

In order to obtain a single-atom catalyst structure to maximize the usage of metal catalyst atoms, researchers have proposed a metal–organic framework (MOF) to fix the single atom in the center of the molecular MOF, which can effectively prevent the single atom agglomeration effect. ALD can be used to assist the MOF skeleton construction. Kornienko et al. synthesized an atomically precise thin film of a cobalt porphyrin MOF by ALD for CO_2 reduction reaction to CO[28]. The porphyrin units of this MOF materials are linked with aluminium oxide rods to construct a 3D porous structure. Their synthesis process involves depositing a metal oxide film as the metal precursor onto the electrode by ALD, and then put the ALD coated electrode and the linker in a microwave reactor with dimethylformamide (DMF) solvent to synthesize a cobalt porphyrin MOF. This new type of catalyst shows high selectivity of CO with more than 76% faradaic efficiency and remains active for 7 hours, with a turnover number (TON) of 1400. Adopting a similar approach, Yang's research group synthesized $Al_2(OH)_2TCPP\text{-}H_2$ [$TCPP\text{-}H_2$ = 4, 4', 4'', 4'''-(porphyrin-5,10,15,20-tetrayl) tetrabenzonate] MOF material and introduced gaseous diethylzinc precursors and co-reactant to the ALD reactor to coordinate on the porphyrin ring with the nitrogen atoms, which is called vapor phase infiltration[29]. Kung et al. used this method to create elastic strain in the MOF porous structure and through systematic research of the internal strain, the catalyst performance was significantly improved. This technology can be used to expand the research of MOF materials as catalysts application. Hupp et al. also applied the same idea and embedded copper nanoparticles into the zirconium MOF NU-1000[30]. Table 1.1 gives a summary of the application of ALD to make electrocatalyst for CO_2 reduction.

Table 1.1. The performance of reported ALD-based electrocatalysts for the electrochemical CO_2 reduction reaction.

Electrocatalyst	Substrate	Main reduction products	E (V vs RHE)	Faradaic efficiency(%)	Current density (mA cm^{-2})	Reference
Ru(II) polypyridyl carbene catalyst	Fluorine-doped tin oxide (FTO) electrodes	CO, H_2	−1.16	-	-	7
SnS	Au	Formate	-0.75	93%	55	22
SnO_2	CuO nanowires	CO	-0.55	81%	11.57	26
Al_2O_3	Cobalt porphyrin MOF	CO	-0.7	76%	5.9	28
ZnO	Cu nanoclusters	CH_3OH, CH_4	-	-	-	27
NiO	TiO_2 electrode	CO	-1.68	62.5%	-	25
Zn	$Al_2(OH)_2$TCPP-H_2 MOF	CO	-1.8	100%	4.5	29
Cu	NU-1000 MOF	Formate	-0.82	31%	-1.2	30

1.6 Molecular layer deposition (MLD) mechanism

Molecular Layer Deposition (MLD) is a vapor-phase deposition technique that is based on the self-limiting surface reaction in a sequential cycle[31]. It involves the sequential introduction of gas-phase organic molecules reactants that react with a substrate surface in a self-limiting manner, ensuring that only a single monolayer of molecules is deposited per cycle. The process typically consists of two main steps per cycle: exposure to a precursor and a subsequent reaction with a second precursor or reagent. Each of these steps is followed by purging with an inert gas to remove any unreacted precursor and by-products. Theoretically speaking, MLD is similar to the well-established ALD techniques, but ALD is limited to inorganic coatings, the precursors used in MLD usually are small, bifunctional organic molecules that can form an organic coating on the substrate eventually. This process allows the organic layer to grow in a process similar to polymerization, while also allowing two types of building blocks to be linked together in a controlled manner to build organic-inorganic hybrid materials. This process involves the alternating use of organic and inorganic reactants. Initially, either an inorganic or organic precursor is introduced into the reaction chamber to react with the substrate, followed by a purge step. Then, the corresponding organic or inorganic precursor is introduced to react with the previously deposited layer, and any unreacted precursors and by-products are purged. These steps are repeated in sequence to accumulate the desired number of layers, with each cycle adding one organic-inorganic bilayer.

1.7 Molecular layer deposition in catalyst research

Liang et al. obtained an ultra-thin microporous-mesoporous carbon-metal oxide film by carbonizing an aluminium alkoxide (alucone) film in an inert gas[32]. By changing the deposition cycles, the authors precisely controlled the thickness of the protective layer, and by tuning the etching conditions such as etching time and temperature, the size distribution and density of the holes in the film can also be controlled for different purposes. Gould et al. synthesized Ni/Al_2O_3 catalysts with Ni particles by the ALD method. The catalyst was coated with a heterogeneous alucone MLD layer which was subsequently calcined into a porous alumina layer covered on the surface of Ni/Al_2O_3 catalyst[33]. The calcination and reduction temperatures will greatly affect the structure of the MLD layer and the catalytic behavior of the dry reforming of methane of the catalyst. The large available surface area of the 5-MLD cycles catalyst produced the best dry reforming of methane. The porous alumina MLD layer was shown to stabilize the Ni catalyst for more than 180 h under the high-temperature extremes conditions.

Qin's research group used an MLD assisted route to prepare the Cu-ZnO catalyst. This catalyst is used to hydrogenate levulinic acid to valerolactone[34]. Zn-polyurea organic-inorganic hybrid film was coated by MLD on Cu doped multiwalled carbon nanotubes. After calcination and reduction in H_2 flow under 300 °C, Cu-ZnO interface sites (Cu^0Zn) was created. They found that the new Cu-ZnO interface sites (Cu^0Zn) can reduce the apparent activation energy and enhances the selectivity and activity of the catalyst. Some Zn is oxidized to ZnO_x because of the electron transfer between Cu and ZnO.

Further exploring the capabilities of MLD, Zhang et al. tried to deposit Pt particles on MLD-derived interlayer[35]. They used trimethylaluminum (TMA) and glycerol (GLY) as the precursors to form an alucone interlayer on nitrogen-doped carbon nanotubes. To avoid the low conductivity problem caused by this MLD layer, the authors annealed the MLD layer to form an MLD-derived carbon-based interlayer. The remained carbon after annealing in the coating can increase conductivity. After this Pt particles were deposited on the MLD-derived interlayer. They found that the MLD-derived surface has abundant pores which are useful for anchoring the Pt particles and avoiding the aggregation and detachment. X-ray absorption spectroscopy results show that Pt deposited on the MLD-derived interlayer resulted in the transfer of electrons from Pt to the substrate. They also found that the deposition of Pt particles on the MLD-derived surface shortened the Pt-Pt bond distance and thus improved the catalytic activity of the Pt particles. Their work provides a new avenue for stabilizing the catalysts through an MLD mid layer.

Further analysis developed in the same research group found that MLD can deposit a polyimide film on the surface of vertically oriented TiO_2 nanotube arrays (TNTAs). The polyimide film was carbonized and hydrogenated later and an ultrathin nitrogen-doped carbon membranes were formed conformally on the surface of TNTAs[36]. This kind of core-shell nanostructure gives a larger heterogeneous junction interface, which greatly reduces the photogenic electron-hole pairs recombination. The N-doped carbon film can be used as a catalyst for the oxygen evolution reaction (OER), where the highly reactive N-doped carbon enhances the kinetics of water splitting and results in the applied potential required to drive photo-assisted water splitting to shift cathodically by 100 mV. It can also act as a protective layer that prevents hydrogen-treated TiO_2 nanotubes from being oxidized by electrolyte or air. The authors used chronoamperometric measurements to test the performance of different samples. They found that without the carbon film, the photocurrent of TNTAs decreases rapidly after a few cycles. However, by decorating the N-doped carbon film on the surface of the catalyst, the photocurrent stays almost unchanged in the test. The N-doped carbon film can prevent the oxidation of Ti^{3+} in the TNTAs surface. In the end, N-doped carbon film-coated TNTAs showed significant improvement in photocurrent and optical stability. Under the illumination power of 100 mW cm^{-2}, TNTAs with N-doped carbon film

(~1 nm) generated a current density of 3.6 mA cm^{-2} considering 0 V vs Ag / AgCl, a 5-fold increase than the pristine TNTAs.

1.8 Research questions

ALD has emerged as an attractive technique for designing and producing catalytic materials with atomic precision and a robust way to protect the catalyst. The main research questions of this thesis are to demonstrate how this atomic precision can be used to understand the relationships between catalyst structure and properties, and how the coating thickness can influence the catalyst protection performance. We have sub-divided these main research questions into a number of sub-research questions.

1. How can fluidized bed reactor ALD be used to synthesize a metal catalyst with a precisely controlled nanostructure and homogeneous distribution?

2. How do core-shell and alloy structures of bimetallic catalysts affect the performance for CO_2 reduction and how do core-shell and alloy structure of the bimetallic catalysts changes during the electrochemical reaction?

3. How can ALD be used to protect electrocatalysts, and how do super-thin coatings created by ALD affect the activity and stability of the catalyst for water splitting?

4. What is the function of an ALD coated film in preventing catalyst poisoning in CO_2 electro-reduction?

5. How can the water contact angle of a catalyst via ALD/MLD coating be controlled to regulate the activity and selectivity of the catalyst for electrochemical CO_2 reduction?

The upcoming chapters will delve into these questions, providing insight in the rational design of electrocatalysts via ALD and exploring more possibilities of using ALD for future catalyst research.

1.9 Thesis outline

This thesis contains 6 chapters. The first chapter is the introduction of the whole PhD project, including the motivation of this research project and the main research questions that will be addressed in the upcoming chapters.

In Chapter 2, we used ALD to synthesize catalysts with core-shell/alloy structures, which allowed for the examination of reaction mechanisms. By creating materials with controlled attributes such as size, composition, and active sites, ALD enables the development of catalysts with enhanced activity and selectivity across different conditions.

In Chapter 3, we employed an ultrathin SiO_2 layers on the surface of Pt/Carbon black catalysts via ALD to prevent its deactivation during water electrolysis. The Pt agglomeration and detachment during the hydrogen evolution reaction in acidic conditions was suppressed by this ultrathin SiO_2 layers.

In Chapter 4, we investigated the impact of SO_2 impurities on CO_2 electroreduction in two electrochemical reactor systems: an H-cell reactor system and a membrane electrode assembly (MEA) system. We observed distinct behavior of the Ag on carbon black (Ag/CB) catalyst under SO_2 impurities in the H-cell compared to the MEA reactor. SO_2 exhibited a more pronounced effect on Ag/CB catalysts in the H-cell than in the MEA system. By depositing a very thin SiO_2 coating on the outermost surface of the Ag/CB catalyst using atomic layer deposition (ALD), the impact of SO_2 on the catalysts selectivity diminished.

In Chapter 5, we tuned the wettability of the Ag/CB catalyst on the carbon paper electrode and found that the hydrophobicity of the catalyst-loaded carbon paper electrode can be proportionally adjusted using PET MLD modification.

Finally, in the last chapter, we discussed the future prospects of ALD-derived catalytic materials, highlighting the challenges that lie ahead and the promising areas for gaining scientific insights and making practical impacts.

References

1. Kibria, M.G., et al., *Electrochemical CO_2 Reduction into Chemical Feedstocks: From Mechanistic Electrocatalysis Models to System Design.* Adv Mater, 2019. **31**(31): p. e1807166.

2. Spurgeon, J.M. and B. Kumar, *A comparative technoeconomic analysis of pathways for commercial electrochemical CO_2 reduction to liquid products.* Energy & Environmental Science, 2018. **11**(6): p. 1536-1551.

3. *BP Statistical Review of World Energy-2018.*

4. Zhang, L., Z.J. Zhao, and J. Gong, *Nanostructured Materials for Heterogeneous Electrocatalytic CO_2 Reduction and their Related Reaction Mechanisms.* Angew Chem Int Ed Engl, 2017. **56**(38): p. 11326-11353.

5. Wu, J., et al., *CO_2 Reduction: From the Electrochemical to Photochemical Approach.* Adv Sci (Weinh), 2017. **4**(11): p. 1700194.

6. Topuz, F. and T. Uyar, *Atomic layer deposition of palladium nanoparticles on a functional electrospun poly-cyclodextrin nanoweb as a flexible and reusable heterogeneous nanocatalyst for the reduction of nitroaromatic compounds.* Nanoscale Advances, 2019. **1**(10): p. 4082-4089.

7. Wang, Y., et al., *Single-Site, Heterogeneous Electrocatalytic Reduction of CO_2 in Water as the Solvent.* ACS Energy Letters, 2017. **2**(6): p. 1395-1399.

8. Markku Leskela, M.R., *Atomic layer deposition (ALD): from precursors to thin film structures.* Thin Solid Films, 2002. **409**(1): p. 138-146.

9. Goulas, A. and J.R. van Ommen, *Scalable Production of Nanostructured Particles using Atomic Layer Deposition.* KONA Powder and Particle Journal, 2014. **31**(0): p. 234-246.

10. George, S.M., *Atomic Layer Deposition: An Overview.* Chem. Rev., 2010. **110**: p. 111–131.

11. Lin, Y.-S., et al., *Nucleation engineering for atomic layer deposition of uniform sub-10 nm high-K dielectrics on $MoTe_2$.* Applied Surface Science, 2019. **492**: p. 239-244.

12. Liu, J., et al., *Atomic Layer Deposition-Assisted Construction of Binder-Free Ni@N-Doped Carbon Nanospheres Films as Advanced Host for Sulfur Cathode.* Nano-Micro Letters, 2019. **11**(1): 64.

13. Chen, Z., et al., *Rational Design of Novel Catalysts with Atomic Layer Deposition for the Reduction of Carbon Dioxide.* Advanced Energy Materials, 2019. **9**(37): 1900889.

14. Kennedy, R.M., et al., *Replication of SMSI via ALD: TiO_2 Overcoats Increase Pt-Catalyzed Acrolein Hydrogenation Selectivity.* Catalysis Letters, 2018. **148**(8): p. 2223-2232.

15. Junling Lu, B.F., Mayfair C. Kung, Guomin Xiao, Jeffrey W. Elam, Harold H. Kung, Peter C. Stair, *Coking- and Sintering-Resistant Palladium Catalysts Achieved Through Atomic Layer Deposition.* Science, 2012. VOL **335**: p. 1205-1208.

16. Duan, H., et al., *Pentacoordinated Al(3+) -Stabilized Active Pd Structures on $Al_2 O_3$ -Coated Palladium Catalysts for Methane Combustion.* Angew Chem Int Ed Engl, 2019. **58**(35): p. 12043-12048.

17. Cao, K., et al., *Controlled Synthesis of Pd/Pt Core Shell Nanoparticles Using Area-selective Atomic Layer Deposition.* Sci Rep, 2015. **5**: 8470.

18. Cheng, N., et al., *Extremely stable platinum nanoparticles encapsulated in a zirconia nanocage by area-selective atomic layer deposition for the oxygen reduction reaction.* Adv Mater, 2015. **27**(2): p. 277-281.

19. Marichy, C., et al., *ALD SnO_2 protective decoration enhances the durability of a Pt based electrocatalyst.* Journal of Materials Chemistry A, 2016. **4**(3): p. 969-975.

20. Cheng, N., et al., *Atomic scale enhancement of metal–support interactions between Pt and ZrC for highly stable electrocatalysts.* Energy & Environmental Science, 2015. **8**(5): p. 1450-1455.

21. Yang, H., Y. Chen, and Y. Qin, *Application of atomic layer deposition in fabricating high-efficiency electrocatalysts.* Chinese Journal of Catalysis, 2020. **41**(2): p. 227-241.

22. Zheng, X., et al., *Sulfur-Modulated Tin Sites Enable Highly Selective Electrochemical Reduction of CO_2 to Formate.* Joule, 2017. **1**(4): p. 794-805.

23. Chen, Z., et al., *Electrocatalytic reduction of CO_2 to CO by polypyridyl ruthenium complexes.* Chem Commun (Camb), 2011. **47**(47): p. 12607-12609.

24. Chen, Z., et al., *Splitting CO_2 into CO and O_2 by a single catalyst.* Proc Natl Acad Sci U S A, 2012. **109**(39): p. 15606-15611.

25. Li, T.T., et al., *Electrocatalytic CO_2 Reduction with a Ruthenium Catalyst in Solution and on Nanocrystalline TiO_2.* ChemSusChem, 2019. **12**(11): p. 2402-2408.

26. Schreier, M., et al., *Solar conversion of CO_2 to CO using Earth-abundant electrocatalysts prepared by atomic layer modification of CuO.* Nature Energy, 2017. **2**: 17087

27. Zhang, Z., et al., *Atomic layer deposition of ZnO on Cu-nanoclusters for methanol synthesis.* Journal of Vacuum Science & Technology A: Vacuum, Surfaces, and Films, 2013. **31**(1): 01A144.

28. Kornienko, N., et al., *Metal-organic frameworks for electrocatalytic reduction of carbon dioxide.* J Am Chem Soc, 2015. **137**(44): p. 14129-14135.

29. Yang, F., et al., *Tuning Internal Strain in Metal-Organic Frameworks via Vapor Phase Infiltration for CO_2 Reduction.* Angew Chem Int Ed Engl, 2020. **59**(11): p. 4572-4580.

30. Kung, C.-W., et al., *Copper Nanoparticles Installed in Metal–Organic Framework Thin Films are Electrocatalytically Competent for CO_2 Reduction.* ACS Energy Letters, 2017. **2**(10): p. 2394-2401.

31. Steven M. George, B.Y., et al., *Surface Chemistry for Molecular Layer Deposition of Organic and Hybrid Organic-Inorganic Polymers.* Accounts of chemical research, 2009. **42**(4): p. 498-508.

32. Liang, X., et al., *Ultra-thin microporous-mesoporous metal oxide films prepared by molecular layer deposition (MLD).* Chem Commun (Camb), 2009(46): p. 7140-7142.

33. Gould, T.D., et al., *Stabilizing Ni Catalysts by Molecular Layer Deposition for Harsh, Dry Reforming Conditions.* ACS Catalysis, 2014. **4**(8): p. 2714-2717.

34. Zhang, B., et al., *High Efficiency Cu-ZnO Hydrogenation Catalyst: The Tailoring of Cu-ZnO Interface Sites by Molecular Layer Deposition.* ACS Catalysis, 2015. **5**(9): p. 5567-5573.

35. Zhang, L., et al., *Rational design of porous structures via molecular layer deposition as an effective stabilizer for enhancing Pt ORR performance.* Nano Energy, 2019. **60**: p. 111-118.

36. Tong, X., et al., *Enhanced photoelectrochemical water splitting performance of TiO2 nanotube arrays coated with an ultrathin nitrogen-doped carbon film by molecular layer deposition.* Nanoscale, 2014. **6**(12): p. 6692-6700.

2

Nanostructuring Pt-Pd bimetallic electrocatalysts for CO_2 reduction using atmospheric pressure atomic layer deposition

This study demonstrates a way of synthesizing well-controlled core-shell and alloy catalysts by ALD on the surface of the powder substrate material. Pt-Pd bimetallic catalysts have been synthesized and used for the CO_2 electro-reduction reaction. The effect of nanostructuring on bimetallic catalysts' selectivity was investigated

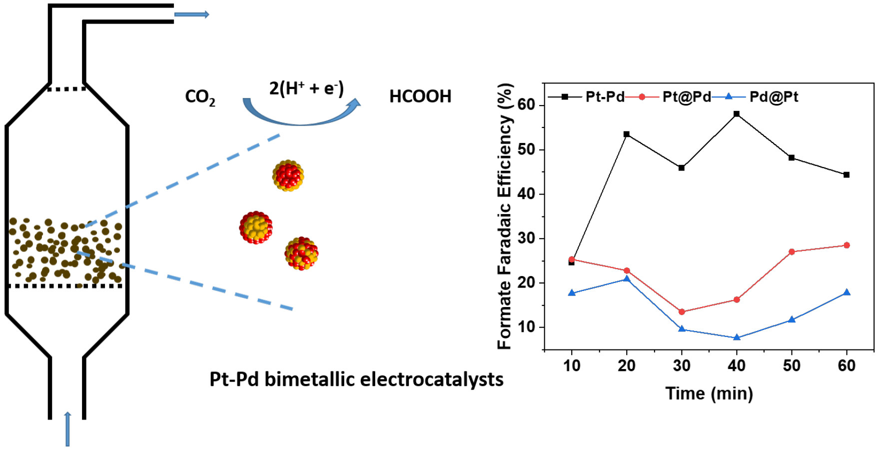

Abstract: Preparing supported nanoparticles with a well-defined structure, uniform particle size, and composition using conventional catalyst synthesis methods, such as impregnation, precipitation, and deposition-precipitation is challenging. Furthermore, these liquid phase methods require significant solvent consumption, which has sustainable issues and requires complex purification processes, usually leaving impurities on the catalyst, affecting its selectivity and activity. In this work, we employed atomic layer deposition (ALD, a vapor phase synthesis method) to synthesize electrocatalysts with well-controlled core-shell and alloy structures for CO_2 reduction to formic acid. With this approach, the structural control of the catalysts is down to the atomic scale, and the effect of core-shell and alloy structure on Pt-Pd bimetallic catalysts has been investigated. It is shown that the Pt-Pd alloy catalyst displays a 46 % faradaic efficiency toward formic acid, outperforming Pt@Pd and Pd@Pt core-shell structures that show faradaic efficiencies of 22 % and 11 %, respectively. Moreover, both core-shell bimetallic catalysts (Pd@Pt and Pt@Pd) are not stable under electroreduction conditions. These catalysts restructure to more thermodynamically stable structures, such as segregated clusters or alloy particles, during the electrochemical reduction reaction, altering the catalytic selectivity.

This chapter has been published in *ChemCatChem, 2022,14, e202200949*

2.1 Introduction

The electrochemical reduction of CO_2 provides an attractive pathway to convert waste CO_2 with water and renewable electricity into chemicals or fuels[38]. It can thereby provide a way to store intermittent electricity in the form of chemical bonds and aid in the defossilization of the chemical industry, paving the way for a carbon-neutral economy. Among the currently available catalysts and targeted products, the commercialization of electrochemically produced formic acid is profitable in comparison with other options[39]. Formic acid is a suitable energy storage medium, and the two-electron pathway for formic acid production requires much less energy input compared to the multi-electron pathways that generate more complex products[2]. However, the most commonly reported catalysts for reducing CO_2 to formic acid, such as In, Sn, Bi, and Pb, suffer from very high overpotentials of more than 1 V or stability issues[40-42]. The activity and selectivity of a catalyst strongly depend on the particle size, shape, and structural uniformity of these particles[43]. The conventional catalyst synthesis methods, such as impregnation, precipitation, deposition-precipitation and sol-gel, usually fail to control these structural properties well[44-45]. Moreover, these methods typically require significant amounts of solvent, which generally leave impurities and contaminate the catalyst, affecting its selectivity and activity. Synthesis of catalysts using vapor phase methods offers a viable solution for these issues. The possibility of large-scale production using gas phase methods also promises scalable production of microstructurally well-controlled catalysts.

Various approaches have been proposed to electrochemically reduce CO_2 to formic acid. For example, Zhao et al. reported an electrodeposited Sn electrode that gives a 91% faradaic efficiency for formic acid production at -1.4 V vs. saturated calomel electrode (SCE)[46]. A bulk In electrode can reach a faradaic efficiency of ~95% at -1.06 V vs. reversible hydrogen electrode (RHE) for the conversion of CO_2 to formic acid[47]. Metallic Pd has been shown to reduce CO_2 to formic acid with low overpotentials and high selectivity[48]. Nevertheless, it is easily poisoned by CO produced during the reaction. Chatterjee and co-workers designed nanoporous Pd alloy electrocatalysts, np-PdX (X = Ag, Cu, Ni, Co), and studied the deactivation process of the electrodes[49]. Pt-Pd bimetallic electrocatalysts have been reported as a promising candidate for this process[50]. This is based on the theory that for a two-electron transfer reaction, the catalyst should be able to catalyze both the forward and reverse reactions[51]. Pt-Pd bimetallic electrocatalysts have been proven to be reputable catalysts for formic acid electro-oxidation. Therefore, they should also be suitable catalysts for the reverse reaction, the electrochemical synthesis of formic acid[52]. Previous studies have established that electrodeposited palladium on a platinum electrode is capable of reducing CO_2 to formic acid from -0.05 V vs. RHE[52]. Furthermore, Pt-Pd bimetallic nanoparticles can reduce CO_2 to formic acid at 0 V vs. RHE and reach a faradaic efficiency of

88% at -0.4 V vs. RHE. The optimized Pd:Pt ratio for this bimetallic electrocatalyst was found to be 7:3 for CO_2 reduction purposes[50].

All of the previously mentioned studies provide a good foundation to study Pt-Pd bimetallic electrocatalysts for the electroreduction of CO_2 to formic acid. However, none of the previously mentioned studies have investigated the effect of the morphology of Pt-Pd bimetallic structures on its electrocatalytic performance. Atomic layer deposition (ALD), a vapor phase synthesis technique, provides atomic-scale precision in deposition, thereby offering a good opportunity to study the structure effect on catalysts without the influence of other factors[53]. Here, we demonstrate the ability of ALD to make bimetallic electrocatalysts with nano precision control over the morphology. We synthesize well-controlled Pt-Pd electrocatalysts on carbon black support with core-shell and alloy structures using atmospheric pressure ALD[54]. These Pt-Pd structures were subsequently tested for their electrocatalytic properties toward CO_2 reduction to formate.

2.2 Results and Discussion

2.2.1 Component and Microstructure Characterization

First, the Pt and Pd ALD growth behavior was studied in a custom-built vibrated fluidized bed reactor operated at atmospheric pressure[54]. 0.5 gram of carbon black was used as substrate in all experiments conducted. Figure S2.1a shows the saturation behavior of the

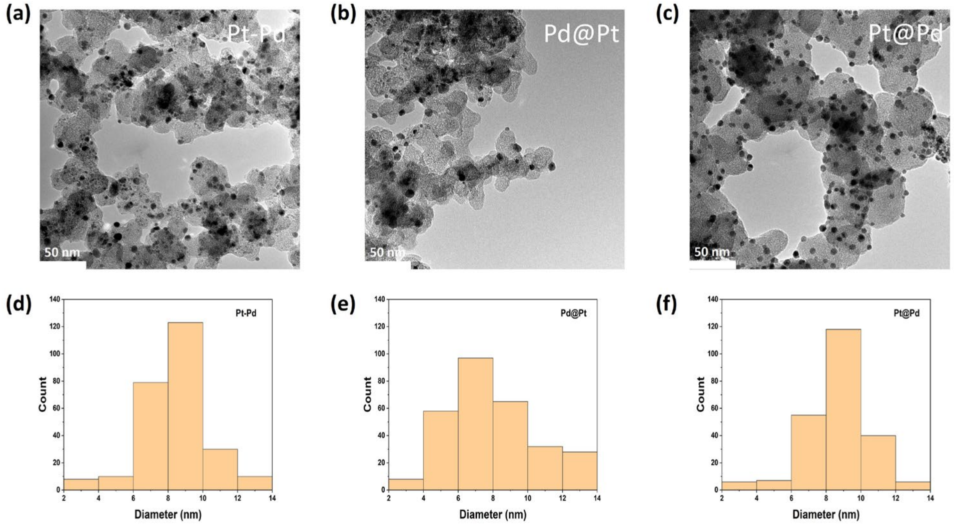

Figure 2.1. TEM images and particle size distribution of Pt-Pd alloy (a and d), Pd@Pt core-shell (b and e), and Pt@Pd core-shell (c and f) catalysts.

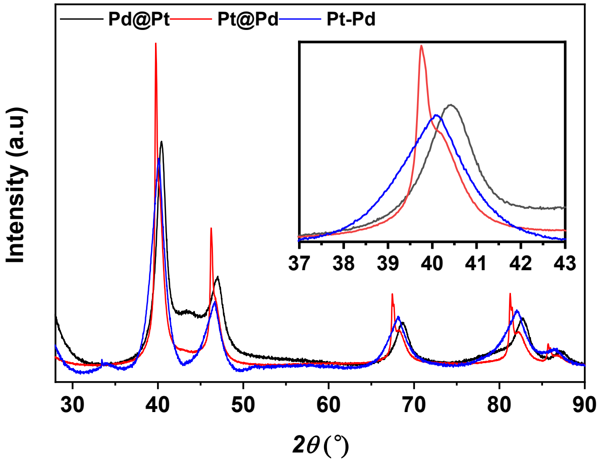

Figure 2.2. X-ray diffraction patterns of Pt@Pd core-shell, Pd@Pt core-shell, and Pt-Pd alloy catalysts. The inset shows the position of (111) diffraction peak.

trimethyl(methylcyclopentadienyl) platinum(IV) ($MeCpPtMe_3$) precursor on carbon black substrate. The Pt content in the samples increases with $MeCpPtMe_3$ dosing time and reaches a plateau after 12 minutes. This indicates that the $MeCpPtMe_3$ precursor reaches self-limiting adsorption on the surface of the substrate. When considering the growth rate of Pt ALD, we found that it reaches a substrate-enhanced growth behavior. After the first cycles of deposition, an average increase of 1.1 wt% per cycle is observed with an increase in cycle numbers (Figure S2.1b). For Pd deposition, in contrast, the gradual saturation of the formalin co-reactant can be observed in Figure S2.2a. After 3 minutes of formalin dosing, the Pd content reaches a plateau. This means that the self-limiting phenomena is observed in the formalin dosing curve. However, when it comes to the palladium(II) hexafluoroacetylacetonate ($Pd(hfac)_2$) dosing curve (Figure S2.2b), no saturation behavior is observed, not even after 30 minutes of continuous $Pd(hfac)_2$ dosing. This observation is in agreement with Liang et al.[55], who observed that the Pd particle size continues to grow when overdosing the precursor, especially for high specific surface area substrates[55]. It appears that the atomic layer deposition, in this case, has a significant chemical vapor deposition (CVD) component. The growth per cycle (GPC) of Pd deposition was found to be 0.41 wt% per cycle in this study (Figure S2.2c). Both Pt and Pd depositions showed constant GPC after the first atomic layer deposition cycle.

We synthesized three different Pt-Pd bimetallic catalysts via ALD with a well-defined structure to investigate the nanostructure effects on the electrocatalytic performance for CO_2 electroreduction: a Pt@Pd core-shell, a Pd@Pt core-shell, and a Pt-Pd alloy. As can be seen from Figure 2.1, Pt-Pd bimetallic nanoparticles of all three morphologies can be clearly seen on the surface of the carbon black substrate. They show comparable particle size distributions and an average particle size of around 8.6 nm. The metal loading and Pd:Pt ratio of these bimetallic samples were determined by inductively coupled plasma-optical emission spectrometry (ICP-OES) and can be found in Table S2.1. The overall metal loading of all these samples is around 6.7 wt%, and their Pd: Pt ratio are all roughly 65:35. This similarity in particle size and chemical composition helps to exclude the particle size and metal loading effects on the performance of the catalysts with different structure and maintains a single variable in this work. Powder X-ray diffraction (XRD) was conducted to study the crystallinity of these three Pt-Pd bimetallic catalysts. The observed diffraction peaks in Figure 2.2 can be indexed as (111), (200), (220), and (221) reflections of the fcc structure of Pt and Pd. The peak position of the (111) planes of pure Pt and Pd are located at 39.8° and 40.2°, respectively[46]. For Pt@Pd, the peak corresponding to the (111) plane is shifted to 39.8°, while for Pd@Pt it is shifted to 40.4° and for Pt-Pd alloy it is shifted to 40.1°. This peak position shift indicates lattice distortion in these samples, suggesting that the different nanostructures lead to minor variations in lattice spacing of Pt-Pd bimetallic catalysts [56]. Additionally, the defects and nano-size effects also contribute to this peak shift.

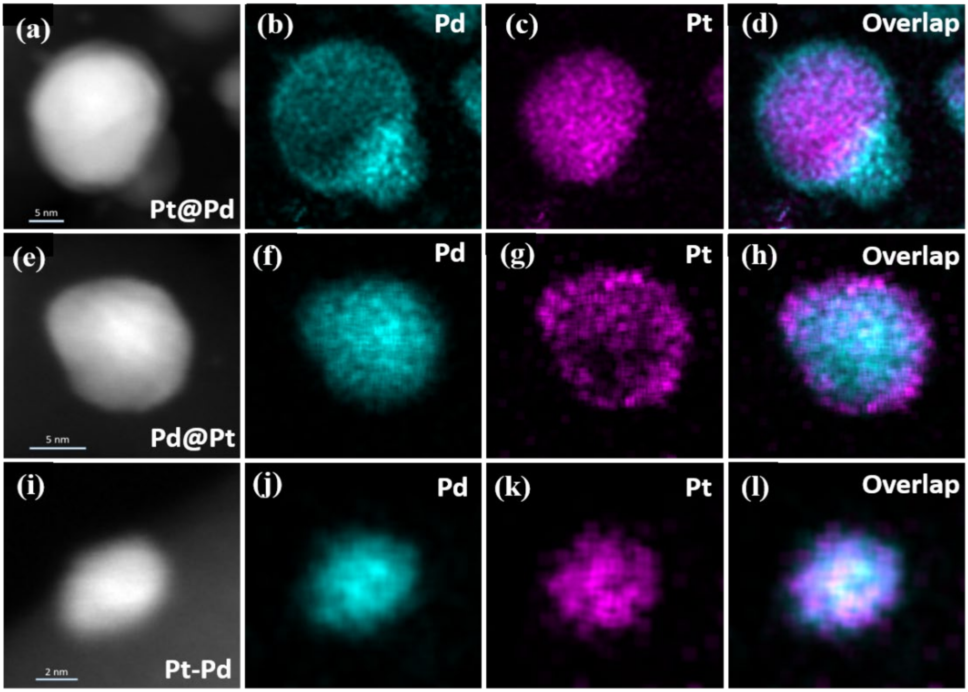

Figure 2.3. STEM-EDX elemental mappings of the Pt@Pd core-shell (a-d), Pd@Pt core-shell (e-h), and Pt-Pd alloy structure catalysts (i-l).

In Figure 2.3 and Figure S2.3, the structure of the Pt@Pd and Pd@Pt core-shell nanoparticles, and Pt-Pd alloy are investigated using scanning transmission electron microscopy energy-dispersive X-ray elemental mapping (STEM-EDX mapping) and line-scanning EDX. From Figure 2.3d, we can see that the Pt particles are encapsulated in a Pd shell, as the Pt@Pd core-shell structure is formed via sequential Pt deposition and Pd deposition. It can also be observed that extremely small Pt particles and slightly larger Pd particles are occasionally present in the samples. Considering their proportion in the sample, their contribution to the CO_2 reduction performance is assumed to be negligible. The line-scanning EDX profile also confirms the Pt@Pd core-shell structure (Figure. S2.3). A similar core-shell structure can be seen for Pd@Pt sample in Figure 2.3 (e-h). The corresponding line-scanning EDX profile in Figure S2.3 also demonstrates the Pd core encapsulated in the Pt shell. On the other hand, Figure 2.3 (i-l) reveals a random distribution of Pt and Pd for the Pt-Pd alloy sample, implying a random alloy structure in this sample.

X-ray photoelectron spectroscopy (XPS) of the ALD prepared Pt-Pd bimetallic electrocatalysts was carried out to investigate their surface chemistry. The Pt 4f high-resolution spectra suggest that Pt exists in the studied samples in three oxidation states of Pt^0, Pt^{2+}, and Pt^{4+} (Figure 2.4a-c). The Pt 4f 7/2 peaks are shifted to lower binding energies than pure Pt samples[57]. On the other hand, the Pd 3d spectra indicate that Pd exists in

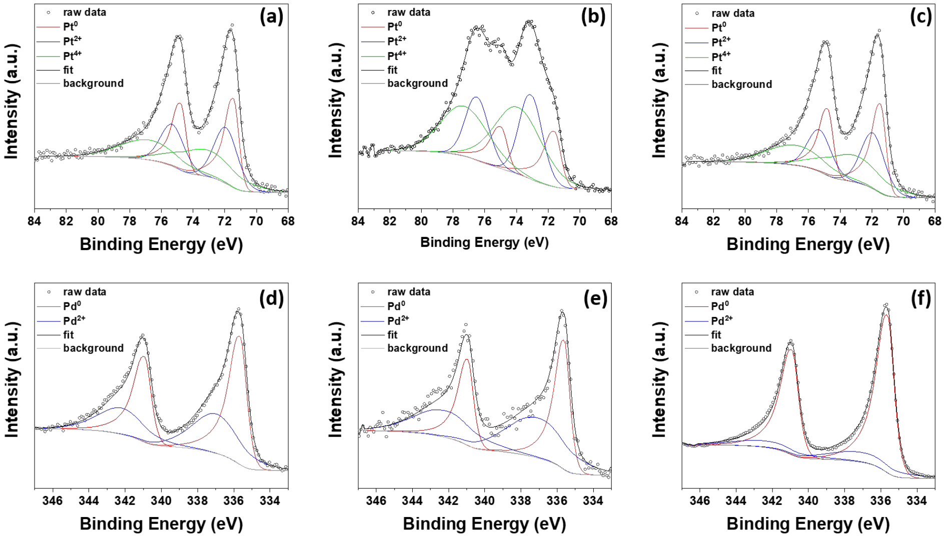

Figure 2.4. XPS spectra of the Pt@Pd core-shell (a,d), Pd@Pt core-shell (b,e), and Pt-Pd alloy (c,f) catalysts.

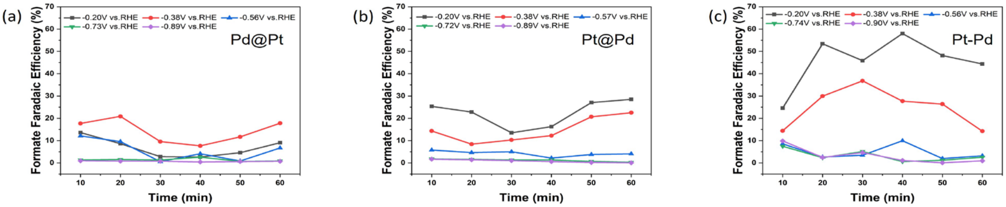

Figure 2.5. The faradaic efficiency for formate as a function of time at different applied potentials for the a) Pt@Pd core-shell, b) Pd@Pt core-shell Catalyst, and c) Pt-Pd alloy structure catalysts.

metallic and Pd^{2+} states in the Pt-Pd samples (Figure 2.4d-f). As demonstrated in Figure 2.4, a considerable amount of Pt and Pd is oxidized to some degree since the catalysts were synthesized in an oxidative environment. The refined Pd 3d spectra indicate that these peaks are shifted to higher binding energies than pure Pd[58]. For example, the 4f 7/2 peak attributed to Pt^{2+} of the Pt@Pd sample is shifted from 72.7 eV to 72.0 eV, and the Pt^{4+} peak is shifted from 74.9 eV to 73.2 eV[59-60]. On the other hand, the 3d 5/2 peak corresponding to Pd^0 is shifted from 335.4 eV to 335.6 eV, and the binding energy of Pd^{2+} shifted from 336.4 eV to 336.9 eV. The variation of different peak positions is different for each structure; however, in general, Pt 4f peaks are shifted to lower binding energies, and Pd 3d peaks are shifted to higher binding energies. The negative binding energy shift of Pt and positive binding energy shift of Pd suggest electron transfer from Pd to Pt due to Pd-Pt interactions, altering the electronic structure of Pt-Pd nanoparticles.

2.2.2 Electrochemical Properties

The electrocatalytic performance of Pt-Pd bimetallic electrocatalysts for CO_2 reduction was investigated in a three-electrode electrochemical H-cell at room temperature, where a cation-exchange Nafion 117 membrane separates the anode and cathode compartments. As shown in Figure 2.5, the Pt-Pd catalyst with the alloy structure displays a better formate faradaic efficiency than the two core-shell catalysts. Moreover, the Pt@Pd core-shell catalyst shows a higher formate faradaic efficiency than the Pd@Pt core-shell structure catalysts. We observed that at -0.2 V vs. RHE, a maximum faradaic efficiency of 46% (averaged over one hour) toward formate was achieved for the Pt-Pd alloy catalysts. However, when the applied potential is higher than -0.38 V vs. RHE, the formate faradaic efficiency decreases drastically. We also observed a trend for the Pt-Pd alloy structure catalyst, where the faradaic efficiency of formate increases in the first half hour and then decreases afterward. This suggests that the Pt-Pd alloy nanoparticles are restructuring during the process, which increases the formate selectivity for a while and, in the end, leads to catalyst deactivation. When it comes to the core-shell structure catalysts, we found that the Pt@Pd catalysts can achieve 22% (averaged over one hour) FE towards formate at -0.2 V vs. RHE. However, the Pd@Pt catalysts only achieve 7% faradaic efficiency (averaged over one hour) towards formate at -0.2 V vs. RHE and reach a 11% faradaic efficiency (averaged over one hour) towards formate at -0.38 V vs. RHE. The slightly higher formate selectivity of the Pt@Pd sample probably stems from its Pd shell since Pd has higher formate selectivity than Pt. The Pt@Pd and Pd@Pt core-shell catalysts have comparable average particle size and metal loading, so this indicates that adjusting the core-shell metal composition of the core-shell structure catalyst can significantly tune the selectivity of the catalysts. The Pt-Pd bimetallic catalyst prepared by ALD or wet chemistry methods can achieve optimal faradaic efficiencies at different potentials. For example: the Pt-Pd nanoparticles prepared by Kortlever et al[50]. via a co-precipitation method reach an optimal faradaic efficiency at -0.5 V vs. RHE, whilst the catalyst prepared by ALD (this study), reach the highest faradaic efficiency at a much lower overpotential. Diercks et al[61]. report that unsupported PdPt aerogels synthesized by a sol-gel method can reach higher faradaic efficiencies by increasing the Pd content. However, since the amount of binder and the catalyst preparation method are both very different from this work, it is hard to make a comparison between the two catalysts. Since the binder has a significant influence on the catalyst performance[62], a fair comparison of the effect of synthesis methods on the electrocatalytic performance remains challenging.

Our other observations for the core-shell structured catalysts suggest that their faradaic efficiencies show a trend to decrease in the first half hour and then increase in the following half hour. This is at variance with the trend shown by the catalysts with an alloy structure. This trend lead us to focus on the structure of the catalysts after being used. We performed a STEM-EDX mapping analysis of the catalysts after electrochemistry tests and, as can be seen in Figure S2.4, we found that the core-shell nanoparticles gradually lost their core-shell structures and formed alloy particles. Similarly, the alloy catalyst became more homogeneous after electrochemistry tests. The instability of the core-shell structured catalysts under the applied potentials explains the trends we observed in Figure 2.5. It indicates that the alloy structure is more favorable than the core-shell structures for the Pt-Pd bimetallic systems when used as an electrocatalyst for CO_2 reduction. Additionally, the core-shell structures seem unstable and gradually restructure to an alloy phase under the applied potential.

In summary, a way of synthesizing well-controlled core-shell and alloy structured catalysts by ALD on the surface of powder substrate material has been demonstrated. This method is easily scalable to produce large amounts of catalyst and can be used to synthesize other core-shell/alloy structure catalysts for customized applications. Different catalyst structures with a controlled metal loading and particle size can be achieved by changing the deposition sequence and the number of cycles during the ALD process.

2.3 Conclusion

Here, Pt-Pd bimetallic catalysts with three different structures have been synthesized, and the effects of the structure of the catalyst nanoparticles on electrocatalytic selectivity for CO_2 reduction to formate have been determined. We find that by controlling the particle size and bimetallic composition, individually changing the structure of the catalyst can have a significant impact on the selectivity. The Pt-Pd alloy catalysts have better selectivity toward formate production than the core-shell structures. Overall, the Pt-Pd alloy catalysts can reach 46% faradaic efficiency at -0.2 V vs. RHE over the course of one hour. The Pd@Pt core-shell structures have lower faradaic efficiencies of 22% and 11%, respectively, at -0.2 V vs. RHE. In addition, we find that the core-shell structures are not stable under electroreduction conditions, irrespective of whether Pd or Pt is the core. During the CO_2 reduction reaction the core-shell catalyst nanoparticles restructure to a thermodynamically more stable alloy form, enhancing their catalytic performance. This re-emphasizes the influence of the catalyst nanostructure on catalyst performance and draws attention to the catalyst stability during the reaction.

2.4 Experimental Section

2.4.1 Materials

(Trimethyl)methylcyclopentadienylplatinum(IV) (($MeCpPtMe_3$), 99%) and Palladium(II) hexafluoroacetylacetonate ($Pd(hfac)_2$, 95%) were purchased from STREM. Potassium bicarbonate ($KHCO_3$, 99.7%), formaldehyde solution (containing 10-15% methanol as stabilizer, 37 wt.% in H_2O), and Nafion perfluorinated resin solution (5 wt.% in lower aliphatic alcohols and 15-20 % water) were purchased from Sigma-Aldrich. Carbon black-Vulcan XC 72R was purchased from the FuelCell store. Glassy carbon rods were purchased from HTW Hochtemperatur-Werkstoffe GmbH (Germany) and used as working electrodes. The electrolyte solution was prepared from ultrapure water (Milli-Q IQ 7000, 18.2 MΩ). All chemicals were received and used without further purification.

2.4.2 Catalyst synthesis

The Pt-Pd bimetallic catalysts with core-shell or alloy structure were synthesized in a vibrated fluidized bed reactor operating at atmospheric pressure, as described elsewhere[63-

[64]. We used 0.5 grams of carbon black for each synthesis batch in the reactor. The ALD procedure of Pt deposition[65] and Pd deposition[66] are modified from the reported literature. In summary, the ALD precursors ($MeCpPtMe_3$ and $Pd(hfac)_2$) were kept at 70 ℃, and the co-reactants (O_3 and formalin) were kept at room temperature during the experiments. N_2 (99.999 vol%) was used as both carrier and purging gas, and a gas flow of 1 L min^{-1} was used. The reactor was heated and maintained at 200 ℃ for all ALD process. 1 min dosing of $MeCpPtMe_3$, 5 min dosing of O_3 and 5 min purging were used for Pt ALD cycle. And 12 min dosing of $Pd(hfac)_2$, 6 min dosing of formalin, and 12 min purging were used for Pd ALD cycle. The detailed information on Pt ALD and Pd ALD operation conditions can be found in Table S2.2. In general, the Pt@Pd core-shell structure catalyst was synthesized by first applying 3 cycles of Pt deposition followed by 12 cycles of Pd deposition with carbon black being fluidized in the reactor. The Pd@Pt core-shell structure catalyst synthesized vice versa, first applied 12 cycles of Pd deposition followed by 3 cycles of Pt deposition. The Pt-Pd alloy structure catalyst was synthesised by first applying 1 cycle of Pt deposition followed by 4 cycles of Pd deposition and repeated the sequence three times to keep the consistency of the Pt-Pd bimetallic catalysts samples. The carbon black powder was pre-treated at 200 ℃ for 30 minutes under ozone flow and 15 minutes N_2 flow to remove the residual ozone in the samples before each experiment. During all experiments, the carbon black substrate was kept fluidized in the reactor with N_2 flow to achieve homogeneous exposure with precursor and co-reactant.

2.4.3 Material Characterization

The microstructures and particle size distribution of different catalysts were characterized using the JEOL JEM1400 transmission electron microscope (TEM) at a voltage of 120 kV. X-ray diffraction (XRD) measurements were carried out to analyze the crystal structure of the catalysts using a Bruker D2 Phaser instrument. It was operated in powder diffraction mode with Cu Kα radiation at 45 kV and 40 mA. STEM-EDX mapping was conducted to obtain the nanostructure information of the samples before and after the electrochemical tests. It was conducted using the FEI cubed titan Cs-corrected 80-300 kV TEM. Bright Field (BF) images were taken for enhanced contrast using an objective aperture blocking most diffracted electron beams, and elemental mapping in STEM mode was done using the super-X in the ChemiSTEM^{TM} configuration.

Elemental analysis of Pt and Pd was carried out by ICP-OES. Approximately 30 mg of each sample was destructed in 1.5 ml 65% HNO_3 and 4.5 ml 30% HCl using the microwave. The destruction time in the microwave was 60 minutes at 1300 W. After the destruction, the samples were diluted to 50 ml with MQ and analyzed with ICP-OES 8000. X-ray photoelectron spectroscopy (XPS) measurements were carried out using a ThermoFisher Kα system (ThermoFisher Scientific) with a photon energy of 1486.7 eV. Survey scans were conducted using 55 eV pass energy and 0.1 eV per step, and 200 µm spot size with charge neutralization. All peak positions were calibrated according to the C1s peak at 284.8 eV using the CasaXPS software for peak deconvolution.

2.4.4 Electrochemical measurements

The electrochemical reduction of CO_2 was performed in a H-cell setup[67]. The working electrodes were prepared by the drop-casting method. First, the catalyst ink was prepared by adding 4mg of catalyst, 800 µL deionized water, 150 µL isopropanol, and 50 µL of Nafion perfluorinated resin solution together and sonication for 1h in the ice bath. Then 30 µL of the catalyst ink was drop cast on the end surface of the glassy carbon rod. The reference electrode used in this paper was Ag/AgCl electrode, and the counter electrode used was Pt foil. A piece of cation-exchange membrane Nafion 117 (FuelCell store) was used to separate the anode and cathode chamber of the H-cell. 0.1 M $KHCO_3$ solution was used as electrolyte on both anode and cathode sides, the cathode chamber was purged by CO_2 for 30 minutes before the experiments. The electrochemical measurements were carried out using a Biologic SP-200 potentiostat (Biologic, France). The applied potential was converted to the reversible hydrogen electrode (RHE) by the formula mentioned in the literature[68], and the Ohmic loss of the cell was compensated for every experiment. The electrolyte in the cathode chamber was taken out every ten minutes during the testing for analysis by high-performance liquid chromatography (HPLC, Agilent 1260 Infinity).

References

1. Kibria, M. G.; Edwards, J. P.; Gabardo, C. M.; Dinh, C. T.; Seifitokaldani, A.; Sinton, D.; Sargent, E. H., Electrochemical CO_2 Reduction into Chemical Feedstocks: From Mechanistic Electrocatalysis Models to System Design. *Adv Mater* **2019,** *31* (31), e1807166.

2. Spurgeon, J. M.; Kumar, B., A comparative technoeconomic analysis of pathways for commercial electrochemical CO_2 reduction to liquid products. *Energy & Environmental Science* **2018,** *11* (6), 1536-1551.

3. BP Statistical Review of World Energy-2018.

4. Zhang, L.; Zhao, Z. J.; Gong, J., Nanostructured Materials for Heterogeneous Electrocatalytic CO_2 Reduction and their Related Reaction Mechanisms. *Angew Chem Int Ed Engl* **2017,** *56* (38), 11326-11353.

5. Wu, J.; Huang, Y.; Ye, W.; Li, Y., CO_2 Reduction: From the Electrochemical to Photochemical Approach. *Adv Sci (Weinh)* **2017,** *4* (11), 1700194.

6. Topuz, F.; Uyar, T., Atomic layer deposition of palladium nanoparticles on a functional electrospun poly-cyclodextrin nanoweb as a flexible and reusable heterogeneous nanocatalyst for the reduction of nitroaromatic compounds. *Nanoscale Advances* **2019,** *1* (10), 4082-4089.

7. Wang, Y.; Marquard, S. L.; Wang, D.; Dares, C.; Meyer, T. J., Single-Site, Heterogeneous Electrocatalytic Reduction of CO_2 in Water as the Solvent. *ACS Energy Letters* **2017,** *2* (6), 1395-1399.

8. Markku Leskela, M. R., Atomic layer deposition (ALD): from precursors to thin film structures. *Thin Solid Films* **2002**.

9. Goulas, A.; van Ommen, J. R., Scalable Production of Nanostructured Particles using Atomic Layer Deposition. *KONA Powder and Particle Journal* **2014,** *31* (0), 234-246.

10. George, S. M., Atomic Layer Deposition: An Overview. *Chem. Rev.* **2010,** *110, 111–131*.

11. Lin, Y.-S.; Kwak, I.; Chung, T.-F.; Yang, J.-R.; Kummel, A. C.; Chen, M.-J., Nucleation engineering for atomic layer deposition of uniform sub-10 nm high-K dielectrics on $MoTe_2$. *Applied Surface Science* **2019,** *492*, 239-244.

12. Liu, J.; Wei, A.; Pan, G.; Xiong, Q.; Chen, F.; Shen, S.; Xia, X., Atomic Layer Deposition-Assisted Construction of Binder-Free Ni@N-Doped Carbon Nanospheres Films as Advanced Host for Sulfur Cathode. *Nano-Micro Letters* **2019,** *11* (1).

13. Chen, Z.; Zhang, G.; Prakash, J.; Zheng, Y.; Sun, S., Rational Design of Novel Catalysts with Atomic Layer Deposition for the Reduction of Carbon Dioxide. *Advanced Energy Materials* **2019,** *9* (37).

14. Kim, H. J.; Jackson, D. H. K.; Lee, J.; Guan, Y.; Kuech, T. F.; Huber, G. W., Enhanced Activity and Stability of TiO_2-Coated Cobalt/Carbon Catalysts for Electrochemical Water Oxidation. *ACS Catalysis* **2015,** *5* (6), 3463-3469.

15. Kennedy, R. M.; Crosby, L. A.; Ding, K.; Canlas, C. P.; Gulec, A.; Marks, L. D.; Elam, J. W.; Marshall, C. L.; Poeppelmeier, K. R.; Stair, P. C., Replication of SMSI via ALD: TiO_2 Overcoats Increase Pt-Catalyzed Acrolein Hydrogenation Selectivity. *Catalysis Letters* **2018,** *148* (8), 2223-2232.

16. Junling Lu, B. F., Mayfair C. Kung, Guomin Xiao, Jeffrey W. Elam, Harold H. Kung, Peter C. Stair, Coking- and Sintering-Resistant Palladium Catalysts Achieved Through Atomic Layer Deposition. *Science* **2012,** *VOL 335*.

17. Duan, H.; You, R.; Xu, S.; Li, Z.; Qian, K.; Cao, T.; Huang, W.; Bao, X., Pentacoordinated Al(3+) -Stabilized Active Pd Structures on Al_2 O_3 -Coated Palladium Catalysts for Methane Combustion. *Angew Chem Int Ed Engl* **2019,** *58* (35), 12043-12048.

18. Cao, K.; Zhu, Q.; Shan, B.; Chen, R., Controlled Synthesis of Pd/Pt Core Shell Nanoparticles Using Area-selective Atomic Layer Deposition. *Sci Rep* **2015,** *5*, 8470.

19. Cheng, N.; Banis, M. N.; Liu, J.; Riese, A.; Li, X.; Li, R.; Ye, S.; Knights, S.; Sun, X., Extremely stable platinum nanoparticles encapsulated in a zirconia nanocage by area-selective atomic layer deposition for the oxygen reduction reaction. *Adv Mater* **2015,** *27* (2), 277-81.

20. Marichy, C.; Ercolano, G.; Caputo, G.; Willinger, M. G.; Jones, D.; Rozière, J.; Pinna, N.; Cavaliere, S., ALD SnO2 protective decoration enhances the durability of a Pt based electrocatalyst. *Journal of Materials Chemistry A* **2016,** *4* (3), 969-975.

21. Cheng, N.; Norouzi Banis, M.; Liu, J.; Riese, A.; Mu, S.; Li, R.; Sham, T.-K.; Sun, X., Atomic scale enhancement of metal–support interactions between Pt and ZrC for highly stable electrocatalysts. *Energy & Environmental Science* **2015,** *8* (5), 1450-1455.

22. Yang, H.; Chen, Y.; Qin, Y., Application of atomic layer deposition in fabricating high-efficiency electrocatalysts. *Chinese Journal of Catalysis* **2020,** *41* (2), 227-241.

23. Zheng, X.; De Luna, P.; García de Arquer, F. P.; Zhang, B.; Becknell, N.; Ross, M. B.; Li, Y.; Banis, M. N.; Li, Y.; Liu, M.; Voznyy, O.; Dinh, C. T.; Zhuang, T.; Stadler, P.; Cui, Y.; Du,

X.; Yang, P.; Sargent, E. H., Sulfur-Modulated Tin Sites Enable Highly Selective Electrochemical Reduction of CO_2 to Formate. *Joule* **2017,** *1* (4), 794-805.

24. Chen, Z.; Chen, C.; Weinberg, D. R.; Kang, P.; Concepcion, J. J.; Harrison, D. P.; Brookhart, M. S.; Meyer, T. J., Electrocatalytic reduction of CO_2 to CO by polypyridyl ruthenium complexes. *Chem Commun (Camb)* **2011,** *47* (47), 12607-9.

25. Chen, Z.; Concepcion, J. J.; Brennaman, M. K.; Kang, P.; Norris, M. R.; Hoertz, P. G.; Meyer, T. J., Splitting CO_2 into CO and O_2 by a single catalyst. *Proc Natl Acad Sci U S A* **2012,** *109* (39), 15606-11.

26. Li, T. T.; Shan, B.; Xu, W.; Meyer, T. J., Electrocatalytic CO_2 Reduction with a Ruthenium Catalyst in Solution and on Nanocrystalline TiO_2. *ChemSusChem* **2019,** *12* (11), 2402-2408.

27. Schreier, M.; Héroguel, F.; Steier, L.; Ahmad, S.; Luterbacher, J. S.; Mayer, M. T.; Luo, J.; Grätzel, M., Solar conversion of CO_2 to CO using Earth-abundant electrocatalysts prepared by atomic layer modification of CuO. *Nature Energy* **2017,** *2* (7).

28. Zhang, Z.; Patterson, M.; Ren, M.; Wang, Y.; Flake, J. C.; Sprunger, P. T.; Kurtz, R. L., Atomic layer deposition of ZnO on Cu-nanoclusters for methanol synthesis. *Journal of Vacuum Science & Technology A: Vacuum, Surfaces, and Films* **2013,** *31* (1).

29. Kornienko, N.; Zhao, Y.; Kley, C. S.; Zhu, C.; Kim, D.; Lin, S.; Chang, C. J.; Yaghi, O. M.; Yang, P., Metal-organic frameworks for electrocatalytic reduction of carbon dioxide. *J Am Chem Soc* **2015,** *137* (44), 14129-35.

30. Yang, F.; Hu, W.; Yang, C.; Patrick, M.; Cooksy, A. L.; Zhang, J.; Aguiar, J. A.; Fang, C.; Zhou, Y.; Meng, Y. S.; Huang, J.; Gu, J., Tuning Internal Strain in Metal-Organic Frameworks via Vapor Phase Infiltration for CO_2 Reduction. *Angew Chem Int Ed Engl* **2020,** *59* (11), 4572-4580.

31. Kung, C.-W.; Audu, C. O.; Peters, A. W.; Noh, H.; Farha, O. K.; Hupp, J. T., Copper Nanoparticles Installed in Metal–Organic Framework Thin Films are Electrocatalytically Competent for CO_2 Reduction. *ACS Energy Letters* **2017,** *2* (10), 2394-2401.

32. Steven M. George, B. Y., Arrelaine A. Dameron, Surface Chemistry for Molecular Layer Deposition of Organic and Hybrid Organic-Inorganic Polymers. *Accounts of chemical research* **2008**.

33. Liang, X.; Yu, M.; Li, J.; Jiang, Y. B.; Weimer, A. W., Ultra-thin microporous-mesoporous metal oxide films prepared by molecular layer deposition (MLD). *Chem Commun (Camb)* **2009,** (46), 7140-2.

34. Gould, T. D.; Izar, A.; Weimer, A. W.; Falconer, J. L.; Medlin, J. W., Stabilizing Ni Catalysts by Molecular Layer Deposition for Harsh, Dry Reforming Conditions. *ACS Catalysis* **2014,** *4* (8), 2714-2717.

35. Zhang, B.; Chen, Y.; Li, J.; Pippel, E.; Yang, H.; Gao, Z.; Qin, Y., High Efficiency Cu-ZnO Hydrogenation Catalyst: The Tailoring of Cu-ZnO Interface Sites by Molecular Layer Deposition. *ACS Catalysis* **2015,** *5* (9), 5567-5573.

36. Zhang, L.; Zhao, Y.; Banis, M. N.; Adair, K.; Song, Z.; Yang, L.; Markiewicz, M.; Li, J.; Wang, S.; Li, R.; Ye, S.; Sun, X., Rational design of porous structures via molecular layer deposition as an effective stabilizer for enhancing Pt ORR performance. *Nano Energy* **2019,** *60*, 111-118.

37. Tong, X.; Yang, P.; Wang, Y.; Qin, Y.; Guo, X., Enhanced photoelectrochemical water splitting performance of TiO_2 nanotube arrays coated with an ultrathin nitrogen-doped carbon film by molecular layer deposition. *Nanoscale* **2014,** *6* (12), 6692-700.

38. Kortlever, R.; Shen, J.; Schouten, K. J.; Calle-Vallejo, F.; Koper, M. T., Catalysts and Reaction Pathways for the Electrochemical Reduction of Carbon Dioxide. *J Phys Chem Lett* **2015,** *6* (20), 4073-82.

39. Chen, C.; Khosrowabadi Kotyk, J. F.; Sheehan, S. W., Progress toward Commercial Application of Electrochemical Carbon Dioxide Reduction. *Chem* **2018,** *4* (11), 2571-2586.

40. Pavesi, D.; Ali, F. S. M.; Anastasiadou, D.; Kallio, T.; Figueiredo, M.; Gruter, G.-J. M.; Koper, M. T. M.; Schouten, K. J. P., CO2 electroreduction on bimetallic Pd–In nanoparticles. *Catalysis Science & Technology* **2020,** *10* (13), 4264-4270.

41. Van Daele, K.; De Mot, B.; Pupo, M.; Daems, N.; Pant, D.; Kortlever, R.; Breugelmans, T., Sn-Based Electrocatalyst Stability: A Crucial Piece to the Puzzle for the Electrochemical CO2 Reduction toward Formic Acid. *ACS Energy Letters* **2021,** *6* (12), 4317-4327.

42. Zhao, C.; Wang, J.; Goodenough, J. B., Comparison of electrocatalytic reduction of CO2 to HCOOH with different tin oxides on carbon nanotubes. *Electrochemistry Communications* **2016,** *65*, 9-13.

43. Vogt, C.; Groeneveld, E.; Kamsma, G.; Nachtegaal, M.; Lu, L.; Kiely, C. J.; Berben, P. H.; Meirer, F.; Weckhuysen, B. M., Unravelling structure sensitivity in CO_2 hydrogenation over nickel. *Nature Catalysis* **2018,** *1* (2), 127-134.

44. O'Neill, B. J.; Jackson, D. H. K.; Lee, J.; Canlas, C.; Stair, P. C.; Marshall, C. L.; Elam, J. W.; Kuech, T. F.; Dumesic, J. A.; Huber, G. W., Catalyst Design with Atomic Layer Deposition. *ACS Catalysis* **2015,** *5* (3), 1804-1825.

45. Singh, J. A.; Yang, N.; Bent, S. F., Nanoengineering Heterogeneous Catalysts by Atomic Layer Deposition. *Annu Rev Chem Biomol Eng* **2017,** *8*, 41-62.

46. Zhao, C.; Wang, J., Electrochemical reduction of CO_2 to formate in aqueous solution using electro-deposited Sn catalysts. *Chemical Engineering Journal* **2016,** *293*, 161-170.

47. Yoshio H, H. H. W., Toshio T and Osamu K, Electrocatalytic process of CO selectivity in electrochemical reduction of CO_2 at metal electrodes in aqueous media. *Electrochemica Acta* **1993**.Yoshio H

48. Min, X.; Kanan, M. W., Pd-catalyzed electrohydrogenation of carbon dioxide to formate: high mass activity at low overpotential and identification of the deactivation pathway. *J Am Chem Soc* **2015,** *137* (14), 4701-8.

49. Chatterjee, S.; Griego, C.; Hart, J. L.; Li, Y.; Taheri, M. L.; Keith, J.; Snyder, J. D., Free Standing Nanoporous Palladium Alloys as CO Poisoning Tolerant Electrocatalysts for the Electrochemical Reduction of CO_2 to Formate. *ACS Catalysis* **2019,** *9* (6), 5290-5301.

50. Kortlever, R.; Peters, I.; Koper, S.; Koper, M. T. M., Electrochemical CO_2 Reduction to Formic Acid at Low Overpotential and with High Faradaic Efficiency on Carbon-Supported Bimetallic Pd–Pt Nanoparticles. *ACS Catalysis* **2015,** *5* (7), 3916-3923.

51. Koper, M. T. M., Thermodynamic theory of multi-electron transfer reactions: Implications for electrocatalysis. *Journal of Electroanalytical Chemistry* **2011,** *660* (2), 254-260.

52. Kortlever, R.; Balemans, C.; Kwon, Y.; Koper, M. T. M., Electrochemical CO_2 reduction to formic acid on a Pd-based formic acid oxidation catalyst. *Catalysis Today* **2015,** *244*, 58-62.

53. Van Bui, H.; Grillo, F.; van Ommen, J. R., Atomic and molecular layer deposition: off the beaten track. *Chem Commun (Camb)* **2016,** *53* (1), 45-71.

54. Beetstra, R.; Lafont, U.; Nijenhuis, J.; Kelder, E. M.; van Ommen, J. R., Atmospheric Pressure Process for Coating Particles Using Atomic Layer Deposition. *Chemical Vapor Deposition* **2009,** *15* (7-9), 227-233.

55. Liang, X.; Lyon, L. B.; Jiang, Y.-B.; Weimer, A. W., Scalable synthesis of palladium nanoparticle catalysts by atomic layer deposition. *Journal of Nanoparticle Research* **2012,** *14* (6).

56. De, A.; Datta, J.; Haldar, I.; Biswas, M., Catalytic Intervention of MoO_3 toward Ethanol Oxidation on PtPd Nanoparticles Decorated MoO_3-Polypyrrole Composite Support. *ACS Appl Mater Interfaces* **2016,** *8* (42), 28574-28584.

57. Vovk, E. I.; Kalinkin, A. V.; Smirnov, M. Y.; Klembovskii, I. O.; Bukhtiyarov, V. I., XPS Study of Stability and Reactivity of Oxidized Pt Nanoparticles Supported on TiO_2. *The Journal of Physical Chemistry C* **2017,** *121* (32), 17297-17304.

58. M. Brun, A. B., J.C. Bertolini, XPS, AES and Auger parameter of Pd and PdO. *Journal of electron spectoscopy and related phenomena* **27 October 1998,** *104 (1999) 55–60*.

59. Long, N. V.; Duy Hien, T.; Asaka, T.; Ohtaki, M.; Nogami, M., Synthesis and characterization of Pt–Pd alloy and core-shell bimetallic nanoparticles for direct methanol fuel cells (DMFCs): Enhanced electrocatalytic properties of well-shaped core-shell morphologies and nanostructures. *International Journal of Hydrogen Energy* **2011,** *36* (14), 8478-8491.

60. Jang, E. J.; Lee, J.; Oh, D. G.; Kwak, J. H., CH4 Oxidation Activity in Pd and Pt–Pd Bimetallic Catalysts: Correlation with Surface PdOx Quantified from the DRIFTS Study. *ACS Catalysis* **2021,** *11* (10), 5894-5905.

61. Diercks, J. S.; Georgi, M.; Herranz, J.; Diklić, N.; Chauhan, P.; Clark, A. H.; Hübner, R.; Faisnel, A.; Chen, Q.; Nachtegaal, M.; Eychmüller, A.; Schmidt, T. J., CO_2 Electroreduction on Unsupported PdPt Aerogels: Effects of Alloying and Surface Composition on Product Selectivity. *ACS Applied Energy Materials* **2022,** *5* (7), 8460-8471.

62. Hong, J.; Park, K. T.; Kim, Y. E.; Tan, D.; Jeon, Y. E.; Park, J. E.; Youn, M. H.; Jeong, S. K.; Park, J.; Ko, Y. N.; Lee, W., Ag/C composite catalysts derived from spray pyrolysis for efficient electrochemical CO_2 reduction. *Chemical Engineering Journal* **2022,** *431*.

63. Zhang, D.; La Zara, D.; Quayle, M. J.; Petersson, G.; van Ommen, J. R.; Folestad, S., Nanoengineering of Crystal and Amorphous Surfaces of Pharmaceutical Particles for Biomedical Applications. *ACS Appl Bio Mater* **2019,** *2* (4), 1518-1530.

64. Zhang, D.; Quayle, M. J.; Petersson, G.; van Ommen, J. R.; Folestad, S., Atomic scale surface engineering of micro- to nano-sized pharmaceutical particles for drug delivery applications. *Nanoscale* **2017,** *9* (32), 11410-11417.

65. Grillo, F.; Van Bui, H.; Moulijn, J. A.; Kreutzer, M. T.; van Ommen, J. R., Understanding and Controlling the Aggregative Growth of Platinum Nanoparticles in Atomic Layer Deposition: An Avenue to Size Selection. *J Phys Chem Lett* **2017,** *8* (5), 975-983.

66. Elam, J. W.; Zinovev, A.; Han, C. Y.; Wang, H. H.; Welp, U.; Hryn, J. N.; Pellin, M. J., Atomic layer deposition of palladium films on Al2O3 surfaces. *Thin Solid Films* **2006,** *515* (4), 1664-1673.

67. Y. Song, P. N. P., The electrochemical synthesis of aminonitrilesI. H-cell studies with adiponitrile and azelanitrile. *Joural of Applied Electrochemistry* **1990,** *21*.

68. Wang, L.; Lee, C.-Y.; Schmuki, P., Solar water splitting: preserving the beneficial small feature size in porous α-Fe_2O_3 photoelectrodes during annealing. *J. Mater. Chem. A* **2013,** *1* (2), 212-215.

Supporting Information for Chapter 2

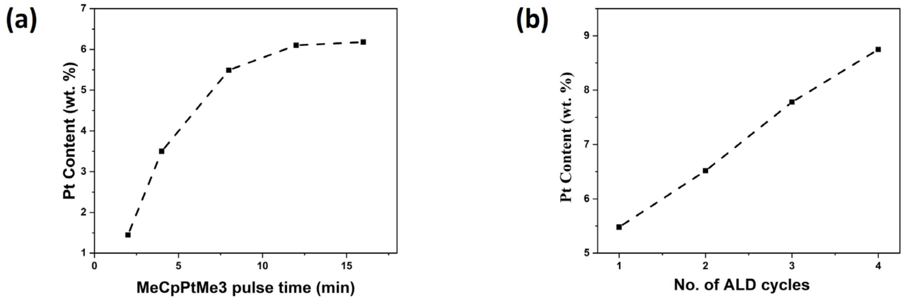

Figure S2.1. MeCpPtMe3 saturation curve (a) and Pt growth per cycle curve (b) during Pt ALD.

Table S2.1: Metal loading and Pd:Pt ratio of bimetallic samples

Sample	Pt content (wt%)	Pd content (wt%)	Overall metal content (wt%)	Pd:Pt ratio
Pt@Pd	2.46	4.21	6.67	63:37
Pd@Pt	2.11	3.88	5.99	65:35
Pt-Pd	2.57	4.98	7.55	66:34

Table S2.2: Experimental conditions. (RT indicates room temperature)

Material	Precursor (T,℃)	Co-reactant (T,℃)	$T_{reaction}$ (℃)	Exposure Time (min) (Precursor-N_2-Co-reactant-N_2)
Pt	($MeCpPtMe_3$) (70)	O_3 (RT)	200	1-5-5-5
Pd	$Pd(hfac)_2$ (70)	Formalin (RT)	200	12-12-6-12

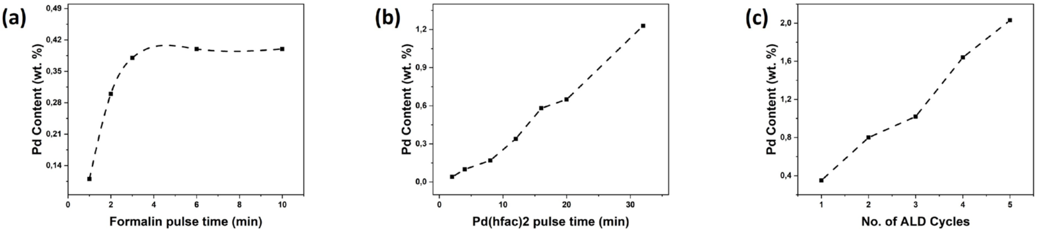

Figure S2.2. Formaline saturation curve (a), Pd(hfac)2 saturation curve, (b), and Pd growth per cycle curve (c) during Pd ALD.

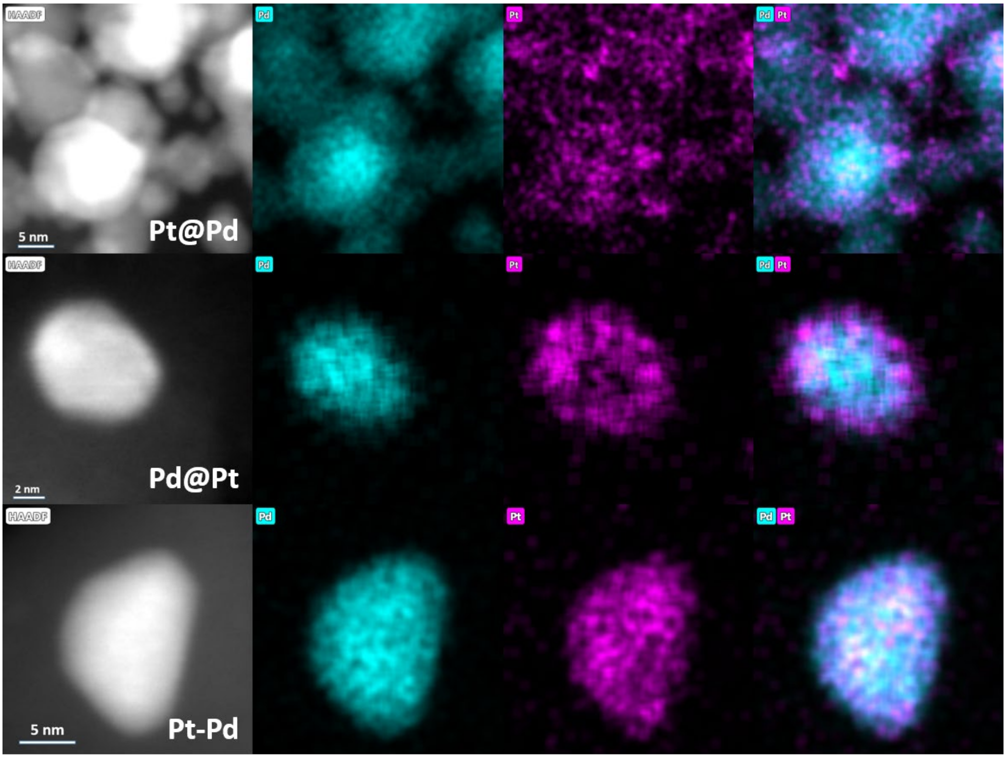

Figure S2.3. STEM-EDX mapping images and line-scanning EDX profiles of the Pt@Pd core-shell catalyst, Pd@Pt core-shell catalyst and Pt-Pd alloy catalyst

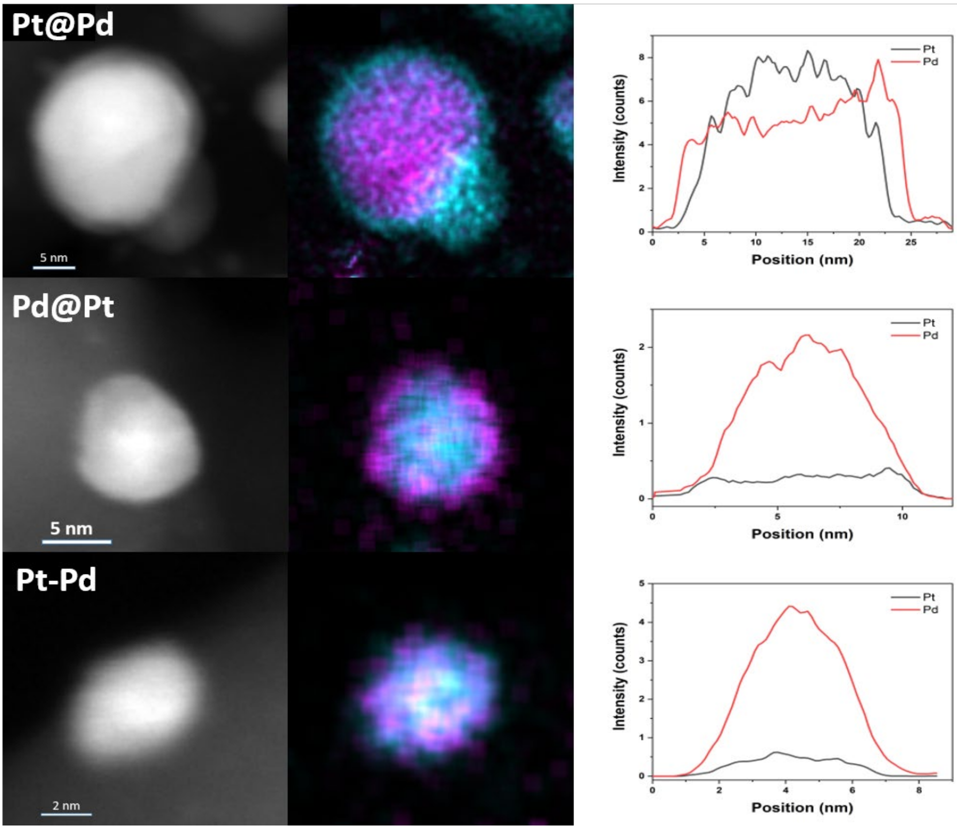

Figure S2.4. STEM-EDX mapping images of the Pt@Pd core-shell catalyst, Pd@Pt core-shell catalyst and Pt-Pd alloy catalyst after electrochemical measurements

3

Enhancing the durability of Pt nanoparticles for water electrolysis using ultrathin SiO_2 layers

This study uses atomic layer deposition (ALD) to coat platinum nanoparticles (Pt/CB) with silicon dioxide (SiO_2) to prevent deactivation during hydrogen evolution

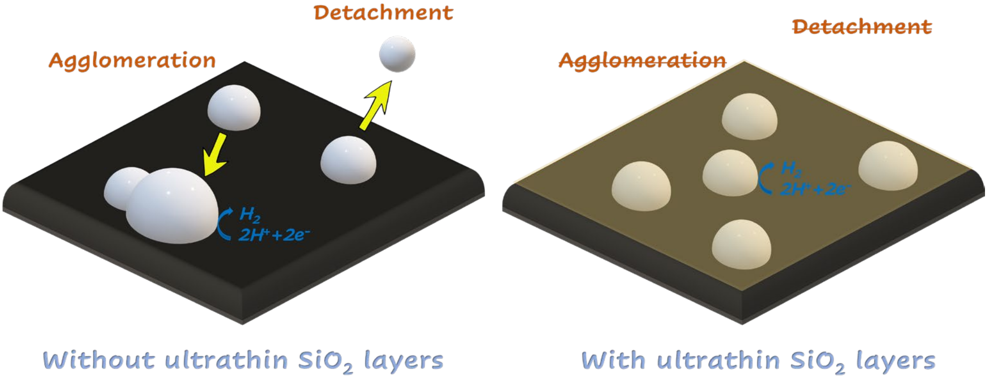

Abstract: Extending the lifetime of electrocatalytic materials is a major challenge in electrocatalysis. Here, we employ atomic layer deposition (ALD) to coat the surface of carbon black supported platinum nanoparticles (Pt/CB) with an ultra-thin layer of silicon dioxide (SiO_2) to prevent deactivation of the catalyst during H_2 evolution. Our results show that after an accelerated durability test (ADT) the current density at -0.2 V vs. reversible hydrogen electrode (RHE) of the unprotected Pt/CB catalyst was reduced by 34%. By contrast, after coating the Pt/CB catalyst with 2 SiO_2 ALD cycles, the current density at the same potential was reduced by 7% after the ADT procedure, whereas when the Pt/CB sample was coated with 5 SiO_2 ALD cycles, the current density was reduced by only 2% after the ADT. Characterization of the Pt particles after electrochemical testing shows that the average particle size of the uncoated Pt/CB catalyst increases by roughly 16% after the ADT, whereas it only increases by 3% for the Pt/CB catalyst coated with 5 cycles of SiO_2 ALD. In addition, the coating also strongly reduces the detachment of Pt nanoparticles, as shown by a strong decrease in the Pt concentration in the electrolyte after the ADT. However, 20 cycles of SiO_2 ALD coating results in an over-thick coating that has an inhibitory effect on the catalytic activity. In summary, we demonstrate that only a few cycles of SiO_2 ALD can strongly improve the stability of Pt catalyst for the hydrogen evolution reaction.

3.1 Introduction

Hydrogen is a pivotal feedstock for the chemical industry and is one of the pillars of the energy transition, as it is a clean and sustainable energy carrier[1]. Currently, the most widely used method for hydrogen production is natural gas reforming, which emits large amounts of CO_2, relies on fossil inputs, and produces blue or grey hydrogen. When integrated with renewable electricity production, water electrolysis yields nearly no CO_2 emissions during operation and produces green hydrogen[2]. Platinum (Pt) is one of the most effective electrocatalysts for both water reduction to hydrogen in polymer electrolyte membrane (PEM) electrolyzers and hydrogen oxidation in PEM fuel cells. However, as a noble metal, its high costs and scarcity limit its application.

To overcome these challenges, most of the research focusses on two potential solutions. The first approach is to decrease the Pt amount in the electrolyzer and improve the Pt utilization efficiency via decreasing the Pt particle size. For instance, Wan et al.[3] confined sub-nanometer Pt clusters in hollow mesoporous carbon spheres to stabilize and immobilize the Pt clusters, enhancing the mass activity of the Pt catalyst. Additionally, Cheng et al.[4] produced isolated single Pt atoms and clusters on a N-doped graphene substrate using atomic layer deposition (ALD) and found that these have a higher activity compared to commercial Pt/C catalysts. This is due to their small sizes and the unique electronic interaction between the adsorbed Pt single atoms and N-doped graphene. The second approach is to protect the Pt catalyst from degradation and prolong its lifetime. The Pt catalysts used for water electrolysis mainly degrade via dissolution, catalyst detachment, and agglomeration processes as deactivation mechanisms[1, 5]. Marichy et al.[6] combined electrospinning, microwave-assisted synthesis, and ALD to synthesize Pt nanoparticles on carbon fibers with a SnO_2 coating. They found that with the SnO_2 coating, the Pt catalyst durability increased remarkably during voltage cycling between 0.6 V and 1.2 V vs. reversible hydrogen electrode (RHE) and that the activity towards the oxygen reduction reaction (ORR) increased slightly. The SnO_2 layer lowered the corrosion of the carbon support and prevented the aggregation of Pt particles. Kim et al.[7] found that a TiO_2 coating can be used to enhance the activity and stability of Co/C catalysts for electrochemical water oxidation. The TiO_2 coating can prevent the catalyst from sintering as it decorates the undercoordinated Co nanoparticles at defects, corners, and edges, protecting those sites. However, the intrinsic instability of these metal oxides coatings remains a concern when they are applied for protection under reductive potentials[8].

SiO_2 is stable under acidic (pH ≥2) as well as moderately alkaline (pH ≤10) conditions, and exhibits outstanding electrochemical stability under both reductive and oxidative potentials[9, 10]. Its high-temperature resistance is also outstanding, allowing it to remain stable up to 650°C[11, 12]. This makes it a suitable material for catalyst protection and therefore it is already used for the protection of catalysts in thermochemical and photochemical processes. For example, Wang et al.[13] used SiO_2 to introduce a strong metal-support interaction with Cu catalysts and to stabilize these catalysts for hydrogenation reactions. Li et al.[14] applied SiO_2 to encapsulate cobalt oxide nanoparticles used as methane combustion catalyst. They found that the embedded $CoOx@SiO_2$ catalyst showed superior performance compared to the bare supported $CoOx@SiO_2$ catalyst. Trompoukis et al.[15] used SiO_2 to protect a Pt photocatalyst and found that the SiO_2 can increase the minority carrier lifetimes and avoids the growth of thin interfacial oxide between the photoactive material and the catalyst. Takenaka et al.[16] used an impregnation method to deposit different amounts of SiO_2 on a Pt/CB electrocatalyst to increase the durability of this catalyst in a polymer electrolyte fuel cell (PEFC). However, due to the impregnation method they used, the lowest SiO_2 coating loading achieved in the catalyst is 12.5 wt%, which, while considered low, still represents a relatively high percentage. While the durability of the catalyst used at the cathode is increased, the relatively thick SiO_2 coating decreases the Pt/CB catalyst activity. Since SiO_2 is more insulating than the metal oxides mentioned before, minimizing the coating thickness is crucial to maintain the electrical conductivity of the catalyst during electrocatalysis to avoid inactivate the catalyst. As such, very thin insulator films (thickness of < 2 nm) are still conductive due to the tunneling effect, while very thick coatings will have a suppressive effect on the catalytic activity[17, 18]. To achieve a uniformly covered surface of the catalyst with an ultrathin coating, a gentle and delicate method with precise control at the nanometer scale is required. ALD is a suitable choice due to its sub-nanometer control over layer thickness, enabling the production of uniform and conformal coatings on various surfaces[19]. Furthermore, investigating the impact of the SiO_2 coating on the water splitting, rather than application in a PEFC, is also necessary.

In this work, we demonstrate the potential of ultrathin SiO_2 coatings made via ALD to enhance the stability of commercial Pt on carbon black (Pt/CB) catalysts for the hydrogen evolution reaction. We find that an ultrathin SiO_2 coating can efficiently provide a strongly protective effect, preventing the catalyst from agglomeration and detachment in accelerated durability tests (ADT). While the thickness of the protective layer has a stronger effect on catalyst performance than was previously recognized.

3.2 Experimental Section

Materials

Silicon tetrachloride ($SiCl_4$, 99%) was purchased from Alfa Aesar, isopropanol (≥98%) was purchased from Honeywell, Nafion^{TM} perfluorinated resin solution (5 wt.% in lower aliphatic alcohols and 15-20 % water) and sulfuric acid (H_2SO_4, 95-97%) were purchased from Sigma-Aldrich. Deionized water with the resistivity of 18 million ohm-cm were used as the co-reactant. 40 wt% of Pt on Carbon black- Vulcan XC 72R catalyst was purchased from the

FuelCell store. Glassy carbon rods and glassy carbon plates were ordered from HTW Hochtemperatur-Werkstoffe GmbH (Germany). The electrolyte solution was prepared from ultrapure water (Milli-Q IQ 7000, 18.2 MΩ). All chemicals were received and used without further purification.

Catalyst synthesis

The SiO_2 coatings on the catalyst were deposited in a custom-built flat substrate ALD reactor[19-21] operating at atmospheric pressure. The reactor chamber consists of a metal cylinder with an inner diameter of 40 mm and a length of 190 mm, along with a substrate holder with dimensions of 30 mm by 125 mm. The deposition temperature was monitored and controlled using two thermocouples installed inside and outside wall of the ALD reactor to ensure an even temperature profile. We employed atmospheric pressure ALD here instead of vacuum ALD since at large scale it will reduce the investment costs and increase the throughput[20, 21]. The ALD procedure of SiO_2 deposition is modified from the reported literature[22]. Nevertheless, the time settings of the reaction and the precursor gas flow rate we used were different. In brief, $SiCl_4$ and H_2O serving as ALD reactants were kept in stainless-steel bubblers and evaporated at room temperature. N_2, with a purity of 99.999%, was utilized as both the carrier and purging gas, and a gas flow of 0.5 L min^{-1} was used throughout the whole process. The gas flowed parallel to the surface of the substrate in the reactor. The samples were pre-treated under air plasma at room temperature and at 4 mbar pressure for 60 seconds using a Harrick plasma machine before each experiment. The ALD reactor was heated and maintained at 100 °C for the entire ALD process. 15 seconds pulses were used to introduce $SiCl_4$ into the reactor, followed by 60 seconds purging with N_2 and 30 seconds dosing of H_2O vapor. After that, 60 seconds purging with N_2 was used to finish a full ALD cycle. More detailed information on SiO_2 ALD operation conditions can be found in Table S3.1. Samples with different numbers of ALD cycles were obtained by repeating the ALD cycles for the required times. At the end of synthesis process, the reactor was purged with N_2 flow for 15 minutes and cooled down to room temperature.

Material Characterization

The JEOL JEM1400 transmission electron microscope (TEM) operating at 120 kV voltage was employed to examine and analyze the microstructures and particle size distribution of various catalysts. To assess the crystal structure of the catalysts, X-ray diffraction (XRD) measurements were conducted utilizing a Bruker D8 advance diffractometer with Bragg-Brentano geometry and a Lynxeye position-sensitive detector. The X-ray was generated using Cu Kα radiation at 45 kV and 40 mA. The Pt concentration in the electrolyte was quantified using the inductively coupled plasma-optical emission spectrometry (ICP-OES) method, employing a PerkinElmer Optima 5300 DV ICP-OES instrument. X-ray photoelectron spectroscopy (XPS) measurements were performed employing a Thermo Scientific™ K-alpha^{TM} (ThermoFisher^{TM} Scientific) utilizing a monochromated X-ray of aluminum Kα radiation (1486.7 eV) with a spot size of 400 µm. For survey scans, a pass energy of 200 eV and a step size of 1 eV were used, while the high-resolution spectra were acquired with a pass energy of 50 eV and a step size of 0.1 eV. All peak positions were analyzed and calibrated, referencing the aliphatic C1s peak at 284.8 eV, using CasaXPS.

Electrochemical measurements

The electrochemical measurements were conducted using a H-cell setup[23]. The preparation of the working electrodes involved a drop-casting technique. Initially, a catalyst ink was created by mixing 4 mg of catalyst with 800 µL of deionized water, 150 µL of isopropanol, and 50 µL of Nafion perfluorinated resin solution. The mixture was sonicated in an ice bath for 1 hour. Subsequently, 50 µL of the catalyst ink was drop cast onto the glassy carbon electrode surface, repeating the process 4 times. The prepared working electrodes were coated with SiO_2 using the ALD process, as described earlier, and subsequently used as working electrode. An Ag/AgCl electrode served as the reference electrode, while a graphite rod was utilized as the counter electrode. All potentials used in this work were converted to the RHE scale according to the equation[24]:

$$E_{RHE} = E_{Ag/AgCl} + 0.197 + 0.059*pH$$

0.5 M H_2SO_4 was used as electrolyte in both chambers. A cation-exchange membrane, Nafion^{TM} 117 (FuelCell store), was utilized to separate the anode and cathode chamber of the H-cell. A Biologic SP-200 potentiostat was employed to conduct the electrochemical measurements. Potentiostatic electrochemical impedance spectroscopy was used to measure the ohmic loss of the cell and was compensated for every experiment. An ADT was carried out by repeating CV scans for 1000 times between -0.2 V- 0.35 V vs RHE at a scan rate of 50 mV/s [23]. Linear sweep voltammetry (LSV) was recorded from -0.3 V to -0 V vs RHE at a scan rate of 2 mV/s.

3.3 Results and Discussion

A series of SiO_2-coated Pt/CB samples was prepared using ALD and compared with the uncoated Pt/CB sample. The deposition procedure used to prepare the coated samples can be found in the experimental section and Table S3.1. In summary, the $SiCl_4$ vapor in a nitrogen stream and a humidified nitrogen stream was alternatingly fed into the home-built tubular flat substrate reactor[25] to initiate the layer by layer growth of SiO_2 on the surface of Pt/CB catalyst. By varying the number of coating cycles of the ALD process, the film thickness was changed accordingly. As can be seen in Figure 3.1, the TEM images of the original Pt/CB catalyst indicate Pt nanoparticles of 3.2 ± 0.5 nm (number-averaged diameter ± standard deviation). Figure 3.1 also shows that the average Pt particle size after SiO_2 ALD does not change considerably. The average Pt size measured through TEM imaging remains 3.2 ± 0.5 nm and 3.2 ± 0.6 for the sample with 5 and 20 ALD cycles, respectively. Considering the reported growth per cycle of SiO_2 using $SiCl_4$ in the employed experimental conditions, which is around 2 Å per cycle[26, 27], a very thin SiO_2 layer is expected even after 20 cycles of ALD coating. We have conducted the TEM characterization towards the outmost layer of the 20 cycles ALD coated sample, as shown in Figure S3.1. The film thickness of this sample is around 5.8 nm after 20 cycles ALD. This leads to an estimated growth per cycle for SiO_2 of 2.9 Å.

X-ray diffraction (XRD) analysis of the original Pt/CB catalyst and of the Pt/CB catalyst after applying a variant number of ALD cycles of SiO_2 coating were carried out to investigate the crystallinity of the catalysts. Figure S3.1 shows that there is no significant distinction between the samples before and after SiO_2 ALD. Two strong carbon peaks are observed in the diffractogram, whereas the Pt signal is relatively weak and only a small peak at 39.8° that represents the Pt (111) plane is observed. SiO_2 peaks were not detected, as is expected since the SiO_2 grown by ALD is mostly amorphous[28].

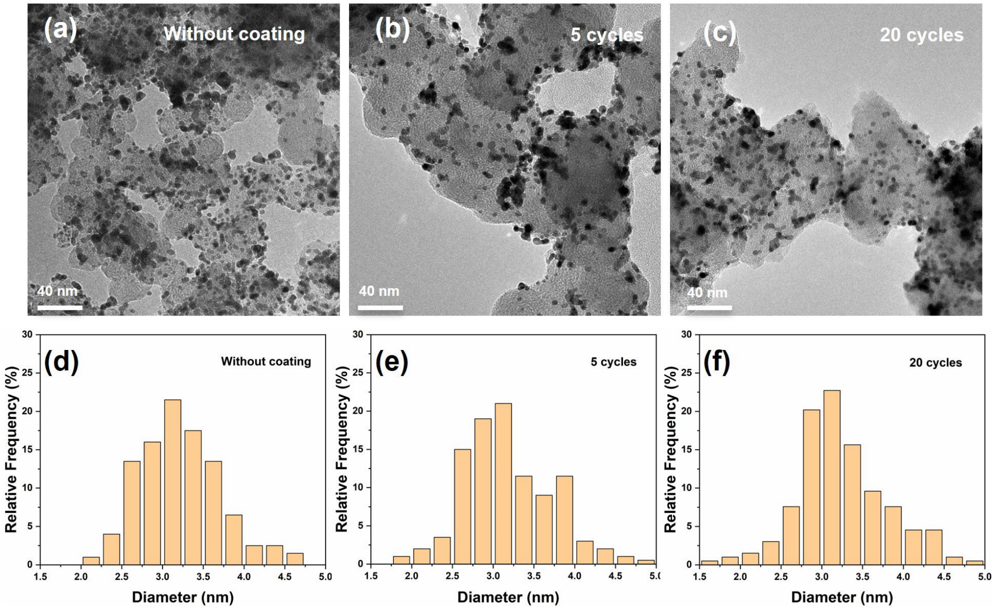

Figure 3.1. TEM images and particle size distribution of Pt/CB catalysts before and after SiO_2 ALD coating: (a,d) original Pt/CB without ALD coating; (b,e) Pt/CB catalyst after 5 cycles of SiO_2 ALD coating, and (c,f) Pt/CB catalyst after 20 cycles of SiO_2 ALD coating.

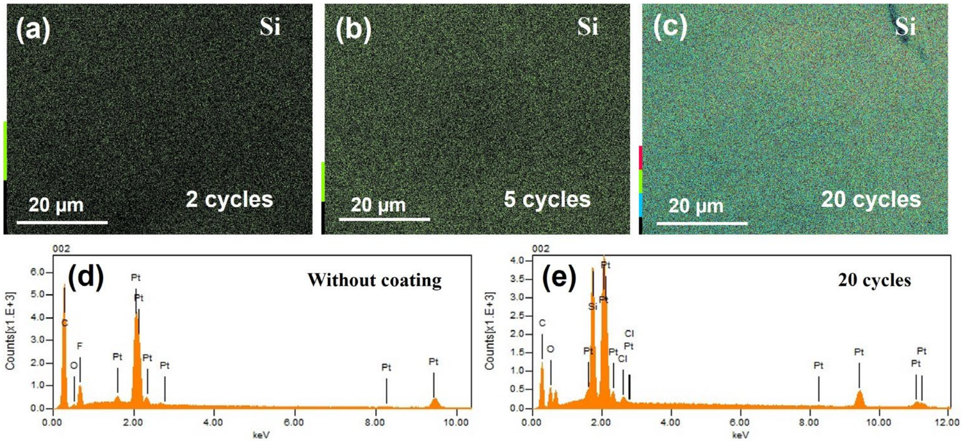

Figure 3.2. SEM-EDS elemental mapping of the Pt/CB catalysts after SiO_2 ALD coating, the color bar indicates the Si K_α signal intensity in each sample: (a-c) SEM images of Pt/CB catalysts after 2, 5, and 20 cycles of SiO_2 ALD coating; (d-e) EDS spectra of Pt/CB catalysts with and without 20 cycles of SiO_2 ALD coating.

The uniform deposition of SiO_2 on the surface of the catalyst is confirmed with SEM-EDS (Figure 3.2). The color bar on the left side of the SEM-EDS maps (Figure 3.2a-c) is an indicator of the Si K_α signal intensity in each sample. The SEM-EDS maps indicate that the surface concentration of Si increases with an increase in ALD cycles. It is worth noting that the EDS spectra also reveal a small peak of fluorine which originates from the Nafion^{TM} polymer used as binder to stabilize the catalyst on the surface of the glassy carbon during the drop-casting process. XPS was employed to investigate the surface chemistry of the ALD coated Pt/CB samples. The Si 2p high-resolution spectra (Figure S3.3) suggest that Si in the studied

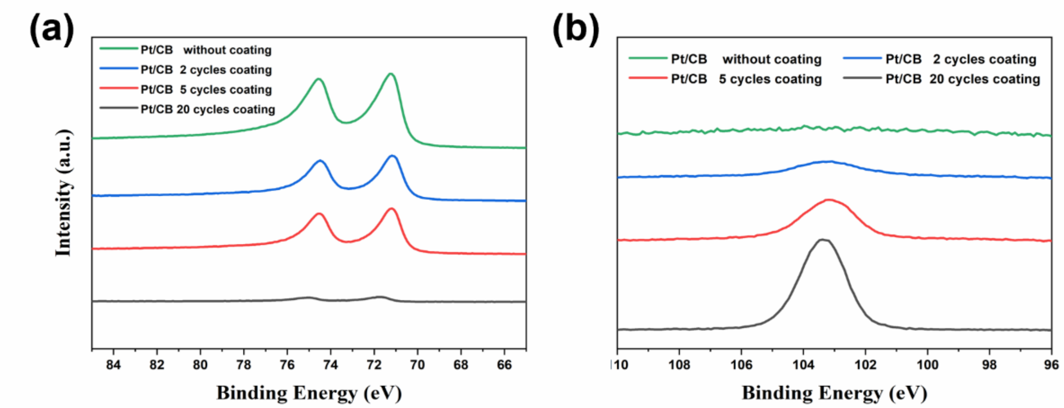

Figure 3.3. The Pt and Si XPS spectra of the Pt/CB catalyst with and without SiO_2 coating: (a) Pt 4f XPS spectra, (b) Si 2p XPS spectra.

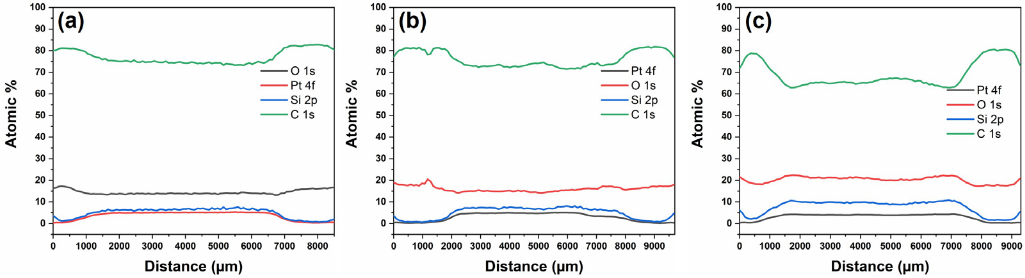

Figure 3.4. XPS line scan profiles of Pt/CB catalyst after SiO_2 ALD coating: (a) 2 ALD cycles, (b) 5 ALD cycles, and (c) 20 ALD cycles of SiO_2 coating.

samples exist in the SiO_2 state and can be deconvoluted into Si $2p_{3/2}$ and Si $2p_{1/2}$. The Pt 4f peak intensity slightly diminishes as the number of ALD cycles increases from 2 to 5 cycles (Figure 3.3a). However, it becomes vanishingly low after 20 cycles. This indicates a significant coating thickness of SiO_2 after 20 cycles of ALD, which is further supported by the peak intensity of Si shown in Figure 3.3b. The Si peak intensity exhibits a slight increase as the number of ALD cycles increases, with a sharp rise after 20 ALD cycles. The analysis depth of XPS is about 4 nm[29, 30], and having a thicker SiO_2 film can strongly attenuate the signal underneath. The very weak Pt 4f peak in the sample coated with 20 ALD cycles compared to the bare sample suggests that the SiO_2 film is above 4 nm. In Figure S3.4, the SiO_2 growth rate was characterized by XPS and EDS, respectively. Due to the detection depth variation of these two techniques[31], Figure S3.4 shows different Si atomic percentages on the surface of the identical sample. However, both characterizations methods show a monotonic increase of the Si atomic percentage as a function of ALD cycles applied.

XPS line scanning was conducted to investigate the SiO_2 uniformity on the catalyst surface. Photoelectron signals were collected from the scanning line through the whole catalyst region, extended to the bare surface of the glassy carbon substrate, and plotted as the function of the horizontal distance. As can be seen from Figure 3.4, the surface concentration of Pt 4f, Si 2p, and O 1s reveals a step increase and decrease, indicating the region where the catalyst is drop casted. The Si 2p and O 1s signals follow the trend of the Pt 4f signal along the line. The C 1s signal shows a trough in the catalyst spot region, stemming from the emerging SiO_2 coverage and the higher Pt atomic percentage in the catalyst region. The Si concentration on the surface of the drop casted catalyst area is significantly higher than on the bare glassy carbon substrate at the edges and increases with the number of ALD cycles. A similar trend can also be seen for the O 1s signal. This observation suggests that the SiO_2 growth rate is much higher on the catalyst surface than on the glassy carbon substrate, and results in selective deposition of SiO_2 on the surface of the Pt/CB catalyst. Two crossover XPS line scans in every sample show comparable results in the X and Y axis, indicating the homogeneity of the catalyst region on the glassy carbon substrate (see Figure S3.5).

To further investigate the SiO_2 distribution on the catalyst area and the glassy carbon substrate, XPS area scans were conducted (Figure S3.6-3.7). The area scan reveals that Pt is homogeneously dispersed over the catalyst region and there is no Si signal detected on the surface of the original Pt/CB catalyst (Figure S3.6). After 5 SiO_2 ALD cycles, the Si 2p signal is clearly visible in Figure S3.7 and aligns with Pt/CB region. This again indicates selective deposition of SiO_2 on the catalyst surface rather than on the glassy carbon substrate.

The effect of different thicknesses of SiO_2 coating on the Pt stability during electrochemical hydrogen evolution was evaluated in a H-cell using a 0.5 M H_2SO_4 electrolyte. ADT of the

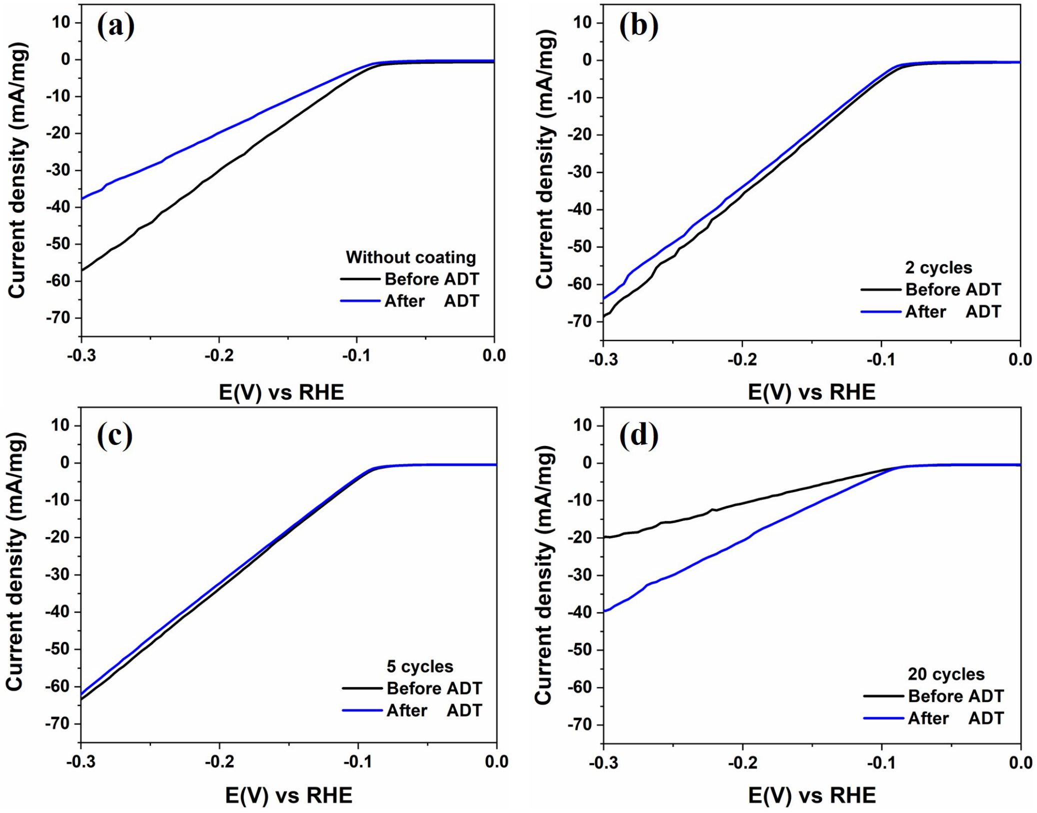

Figure 3.5. Linear sweep voltammogram (LSV) curves of the Pt/CB catalysts before and after accelerated durability tests: (a) original catalyst, Pt/CB catalyst coated with SiO_2 using (b) 2 ALD cycles, (c) 5 ALD cycles, and (d) 20 ALD cycles.

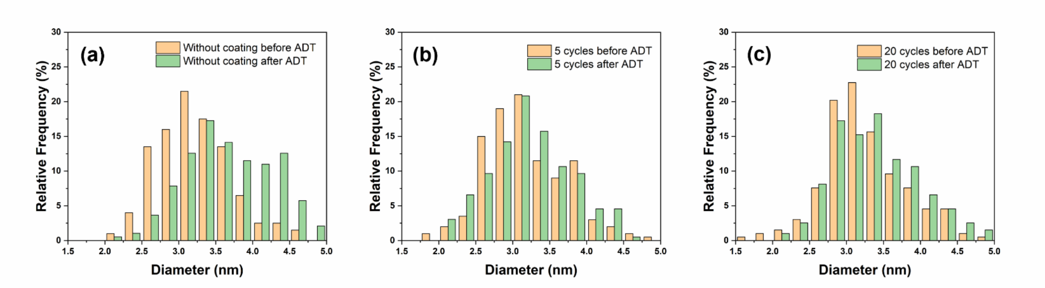

Figure 3.6. Particle size distribution of the Pt/CB catalyst before and after ADT: (a) original catalyst, Pt/CB catalyst coated with SiO_2 using (b) 5 ALD cycles, (c) 20 ALD cycles.

catalysts were conducted similar to literature procedures[32, 33]. In brief, cyclic voltammograms were recorded with a scan rate of 50 mV·s^{-1} from 0.35 V to -0.20 V vs. RHE for 1000 cycles. Linear sweep voltammograms (LSV) were recorded before and after the ADT to measure the catalytic activity of the electrode toward hydrogen evolution (Figure 3.5). For the Pt/CB catalyst without ALD coating, the current density at -0.20 V vs. RHE was reduced by 34% in the water reduction potential range after the ADT. By contrast, the catalyst coated with 2 ALD cycles of SiO_2 showed a current density reduction at the same voltage of only 7% after the same ADT procedure. After applying 5 cycles of SiO_2 ALD, the catalyst current density was merely reduced by 2% after the ADT. The Nyquist plots shown in Figure S3.8 indicate that the charge transfer resistance between the catalysts with and without 5 cycles of ALD coating is comparable. This means that the SiO_2 coating didn't hinder the proton transfer to the Pt catalyst within 5 cycles of ALD coating. However, 20 cycles of SiO_2 deposition showed an inhibitory effect on the catalytic activity, with a 65% decrease in the HER activity compared to the uncoated sample. This indicates that 20 cycles of ALD results in a too thick SiO_2 layer, possibly hindering the electron transfer and suppressing the HER. However, the HER activity of the sample coated with 20 ALD cycles of SiO_2 increased 94% post ADT. Zhuravlev[34] summarized that the surface hydroxyl groups in SiO_2 can form due to the rehydroxylation of SiO_2 in aqueous solutions, and the surface SiO_2 atoms' free valence tend to become saturated with hydroxyl groups in aqueous medium. This process can also happen on our SiO_2 layer, especially during the ADT process. Moon-Sung Kang et al.[35] reported that the silicon hydroxide deposited on the surface of anion-exchange membrane can drastically increase the proton transport number in the membrane. We hypothesize that the increase of silanol groups on the surface of SiO_2 during ADT helps to improve proton transfer in relatively thick SiO_2 layers. Consequently, this process partially restores the HER activity and increases the current density of the 20 cycles coated sample after the ADT procedure.

The particle size distribution (PSD) analysis (shown in Figure 3.6) of Pt/CB catalysts before and after the ADT tests demonstrates that the average particle size of the Pt/CB catalyst without ALD coating increased from 3.2 ± 0.5 nm to 3.7 ± 0.7 nm after the ADT, an increase of 16%. In comparison, the particle size of the Pt particles only increased from 3.2 ± 0.5 nm to 3.3 ± 0.6 nm after being protected by 5 cycles of SiO_2 ALD coating, an increase of 3% after the ADT. This proves that the SiO_2 coating prevents catalyst growth/agglomeration during the ADT, which is one of the main deactivation mechanisms of Pt electrocatalysts during water electrolysis. Figure S3.9 further displays the Pt particle size evolution from TEM imaging after the ADT. Also, Figures S3.10 and S3.11 show that without SiO_2 ALD coating, the bare Pt/CB catalyst surface becomes rougher, and cavities can be seen on the catalyst surface. However, with SiO_2 ALD, the surface of the catalyst before and after the ADT remains nearly similar. The electrolyte after the ADT was collected and analyzed by ICP-OES to measure the Pt concentration in the electrolyte before and after the ADT, and the resulting data is summarized in Table 3.1. Before the ADT, the Pt concentration in the electrolyte is near 0 mg/L. During the ADT, the Pt/CB catalyst gradually degrades, and we observed an increase in Pt concentration to 8.9 mg/L in the Pt/CB sample without ALD coating after ADT. However, after applying 2 cycles of SiO_2 ALD, the Pt concentration in the electrolyte reduced to 4.1 mg/L post ADT. Applying 5 cycles of SiO_2 coating further decreased the Pt concentration in the electrolyte to 1.9 mg/L. Nevertheless, continuing to increase the ALD coating to 20 cycles only caused a minor decrease in Pt concentration and did not significantly enhance the protection effect. This might be due to the crack formation on the relatively thick coating during the ADT process decreasing its protection ability[36]. This process can take place since the flexibility of SiO_2 decreases as the thickness increases and it has very low coefficient of expansion[37]. This implies that simply increasing ALD cycles to further reduce the Pt detachment after ADT is very challenging. The electrochemical oxidation potential of Pt is above 1.2 V vs. RHE[38]. Hence, Pt leaching during the ADT process should be negligible. The main mechanism for the Pt concentration increase after the ADT process should therefore be Pt detachment from the Pt/CB catalyst or catalyst peel off from the electrode. Overall, we show that the ultrathin SiO_2 layers deposited via ALD can be used to strongly reduce the Pt catalyst agglomeration and detachment during water splitting reaction.

Table 3.1. Pt concentration in the electrolyte after ADT, tested by ICP-OES

Sample	Pt concentration (mg/L)
Fresh 0.5M H_2SO_4 electrolyte	<0,02
Pt/CB without ALD coating	8.94
Pt/CB with 2 cycles coating	4.11
Pt/CB with 5 cycles coating	1.94
Pt/CB with 20 cycles coating	1.48

3.4 Conclusions

ALD was employed to coat the surface of Pt/CB electrocatalysts with an ultrathin layer of SiO_2 to prevent deactivation during water electrolysis. Our findings show that without SiO_2 coating, the current density of the untreated Pt/CB catalyst was reduced by 34% at -0.2 V vs. RHE after an ADT. However, after coating the Pt/CB catalyst with 2 SiO_2 ALD cycles, the current density was only reduced by 7% under the same conditions. With 5 SiO_2 ALD cycles, the current density decrease was 2%. The Pt particle size increased by 16% after ADT without SiO_2 coating, but only by 3% after being protected by 5 cycles of SiO_2 deposition. Additionally, we observed severe Pt detachment after the ADT in the Pt/CB catalyst without ALD coating, with the Pt concentration in the electrolyte increasing to 8.9 mg/L after ADT. The Pt detachment can be alleviated by the ultrathin SiO_2 coating synthesized by ALD. After applying 5 cycles of SiO_2 ALD, the Pt detachment/dissolution was reduced to one-fifth compared to the sample without ALD coating. In summary, a nanoscale SiO_2 protective layer strongly reduces Pt agglomeration and detachment during the hydrogen evolution reaction in acidic conditions. By performing just a few ALD cycles, keeping this coating ultrathin, an inhibitory effect on the electrocatalytic activity is avoided.

References

1. H. Jin, B. Ruqia, Y. Park, H. J. Kim, H. S. Oh, S. I. Choi and K. Lee, *Advanced Energy Materials*, 2020, **11**.
2. D. Merki and X. Hu, *Energy & Environmental Science*, 2011, **4**.
3. X. K. Wan, H. B. Wu, B. Y. Guan, D. Luan and X. W. D. Lou, *Adv Mater*, 2020, **32**, e1901349.
4. N. Cheng, S. Stambula, D. Wang, M. N. Banis, J. Liu, A. Riese, B. Xiao, R. Li, T. K. Sham, L. M. Liu, G. A. Botton and X. Sun, *Nat Commun*, 2016, **7**, 13638.
5. S. Cherevko, N. Kulyk and K. J. J. Mayrhofer, *Nano Energy*, 2016, **29**, 275-298.
6. C. Marichy, G. Ercolano, G. Caputo, M. G. Willinger, D. Jones, J. Rozière, N. Pinna and S. Cavaliere, *Journal of Materials Chemistry A*, 2016, **4**, 969-975.
7. H. J. Kim, D. H. K. Jackson, J. Lee, Y. Guan, T. F. Kuech and G. W. Huber, *ACS Catalysis*, 2015, **5**, 3463-3469.
8. Y. Shao, J. Liu, Y. Wang and Y. Lin, *J. Mater. Chem.*, 2009, **19**, 46-59.
9. Z. Liu, V. Bode, P. Hadayati, H. Onay and E. J. R. Sudhölter, *Fuel*, 2020, **280**.
10. S. Ghanbari, E. Kazemzadeh, M. Soleymani and A. Naderifar, *Colloid and Polymer Science*, 2015, **294**, 381-388.
11. Z. W. Liwei Wang, Hua Yang, Guangli Yang, *Materials Science Commuication*, 1998, **57**.
12. M. Liehr, J. E. Lewis and G. W. Rubloff, *Journal of Vacuum Science & Technology A: Vacuum, Surfaces, and Films*, 1987, **5**, 1559-1562.
13. S. Wang, K. Feng, D. Zhang, D. Yang, M. Xiao, C. Zhang, L. He, B. Yan, G. A. Ozin and W. Sun, *Adv Sci (Weinh)*, 2022, **9**, e2104972.
14. L. Li, H. Chen, C. Zhang and Z. Fei, *Molecular Catalysis*, 2019, **469**, 155-160.
15. C. Trompoukis, J.-Y. Feng, T. Bosserez, J. Rongé, J. Dendooven, C. Detavernier, R. Baets and J. A. Martens, *Sustainable Energy & Fuels*, 2021, **5**, 3115-3123.
16. S. Takenaka, H. Matsumori, H. Matsune and M. Kishida, *Applied Catalysis A: General*, 2011, **409-410**, 248-256.

17. W. C.-Y. Ma, H.-S. Hsu, C.-C. Fang, C.-Y. Jao and T.-H. Liao, *Thin Solid Films*, 2018, **660**, 926-930.

18. K. Kato, T. Mori, Y. Morita, T. Matsukawa, M. Takenaka and S. Takagi, *Applied Physics Express*, 2020, **13**.

19. H. Van Bui, F. Grillo and J. R. van Ommen, *Chem Commun (Camb)*, 2016, **53**, 45-71.

20. K. S. Yoo, D.-G. Kim, S. Lee, W.-B. Lee and J.-S. Park, *Ceramics International*, 2022, **48**, 18803-18810.

21. D. H. Levy, D. Freeman, S. F. Nelson, P. J. Cowdery-Corvan and L. M. Irving, *Applied Physics Letters*, 2008, **92**.

22. D. La Zara, F. Sun, F. Zhang, F. Franek, K. Balogh Sivars, J. Horndahl, S. Bates, M. Brannstrom, P. Ewing, M. J. Quayle, G. Petersson, S. Folestad and J. R. van Ommen, *ACS Nano*, 2021, **15**, 6684-6698.

23. P. N. P. Y. Song, *Joural of Applied Electrochemistry*, 1990, **21**.

24. L. Wang, C.-Y. Lee and P. Schmuki, *J. Mater. Chem. A*, 2013, **1**, 212-215.

25. A. Santoso, A. Damen, J. R. van Ommen and V. van Steijn, *Chem Commun (Camb)*, 2022, **58**, 10805-10808.

26. Y. Du, X. Du and S. M. George, *Thin Solid Films*, 2005, **491**, 43-53.

27. O. S. Jason W. Klaus, Steven M. George, *Science*, 1997, **278**.

28. J. Guo, D. Benz, T.-T. Doan Nguyen, P.-H. Nguyen, T.-L. Thi Le, H.-H. Nguyen, D. La Zara, B. Liang, H. T. Hintzen, J. R. van Ommen and H. Van Bui, *Applied Surface Science*, 2020, **530**.

29. G. E. M. Thomas A. Carlson, *Journal of electron spectoscopy and related phenomena*, 1972, **73**.

30. B. R. Strohmeier, *Surface and Interface Analysis*, 1990, **15**.

31. K. Rokosz, T. Hryniewicz, D. Matysek, S. Raaen, J. Valicek, L. Dudek and M. Harnicarova, *Materials (Basel)*, 2016, **9**.

32. M. Smiljanić, M. Bele, F. Ruiz-Zepeda, M. Šala, A. Kroflič and N. Hodnik, *Electrochimica Acta*, 2021, **400**.

33. Y. Lai, Z. Zhang, Z. Zhang, Y. Tan, L. Yu, W. Wu, Z. Wang, T. Jiang, S. Gao and N. Cheng, *Chemical Engineering Journal*, 2022, **435**.

34. L. T. Zhuravlev, *Colloids and Surfaces A: Physicochemical and Engineering Aspects*, 1999, **173 (2000) 1-38**.

35. M. S. Kang, Y. J. Choi, H. J. Lee and S. H. Moon, *J Colloid Interface Sci*, 2004, **273**, 523-532.

36. M. Putkonen, M. Bosund, O. M. E. Ylivaara, R. L. Puurunen, L. Kilpi, H. Ronkainen, S. Sintonen, S. Ali, H. Lipsanen, X. Liu, E. Haimi, S.-P. Hannula, T. Sajavaara, I. Buchanan, E. Karwacki and M. Vähä-Nissi, *Thin Solid Films*, 2014, **558**, 93-98.

37. H. Shan, X. Wang, F. Shi, J. Yan, J. Yu and B. Ding, *ACS Appl Mater Interfaces*, 2017, **9**, 18966-18976.

38. S. Bawari, T. N. Narayanan and J. Mondal, *Electrochemistry Communications*, 2023, **147**.

Supporting information for chapter 3

Table S3.1: ALD experimental conditions. (RT indicates room temperature)

Material	Precursor (T,°C)	Co-reactant (T,°C)	$T_{reaction}$ (°C)	Pulse Time (s) (Precursor-N_2-Co-reactant-N_2)	Flow rate(L/min)
SiO_2	$SiCl_4$ (RT)	H_2O vapor (RT)	100	15-60-30-60	0,5-0,5-0,5-0,5

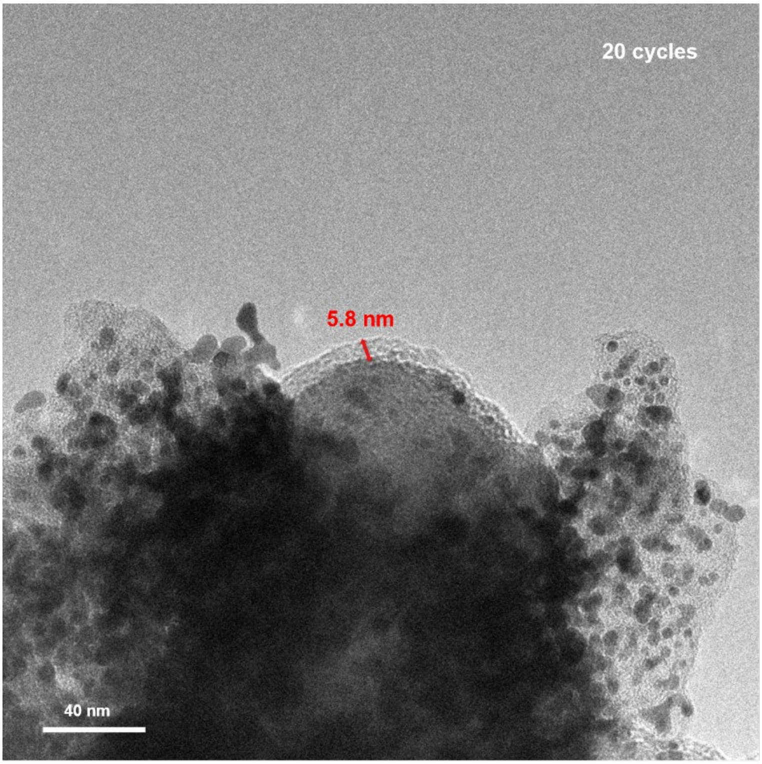

Figure S3.1. Film thickness determination, TEM image of the Pt/CB catalyst after 20 ALD cycles. Sampling from the outermost surface of the catalyst ink spot.

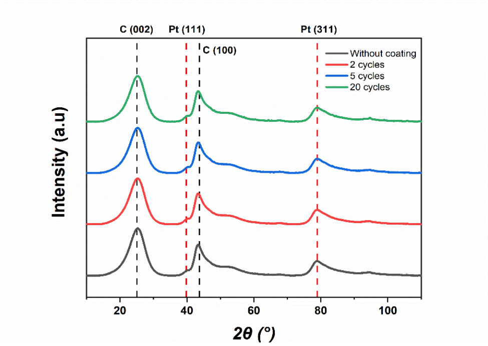

Figure S3.2. X-ray diffraction patterns of the original Pt/CB catalyst and the Pt/CB catalyst after applying variant numbers of ALD cycles.

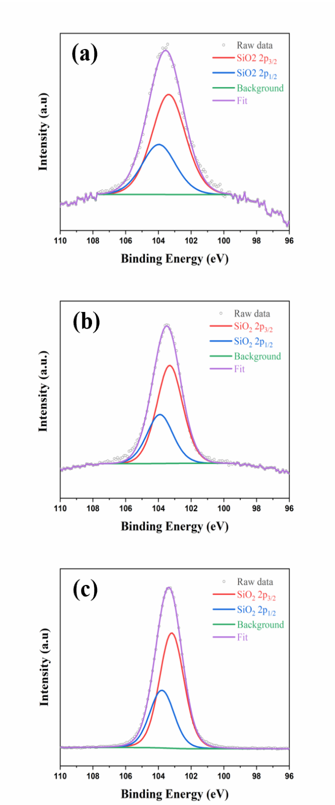

Figure S3.3. The Si 2p XPS spectra of the Pt/CB catalyst with SiO_2 coating: (a) 2 ALD cycles, (b) 5 ALD cycles, and (c) 20 ALD cycles of SiO_2 ALD coating.

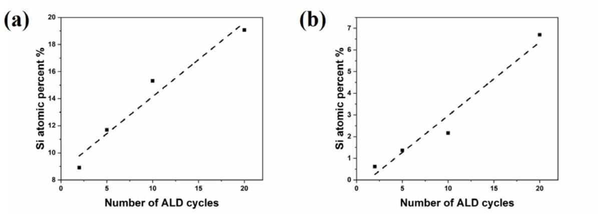

Figure S3.4. Growth per ALD cycle of SiO_2 deposition on the surface of Pt/CB catalyst, based on (a) XPS and (b) EDS characterization, respectively.

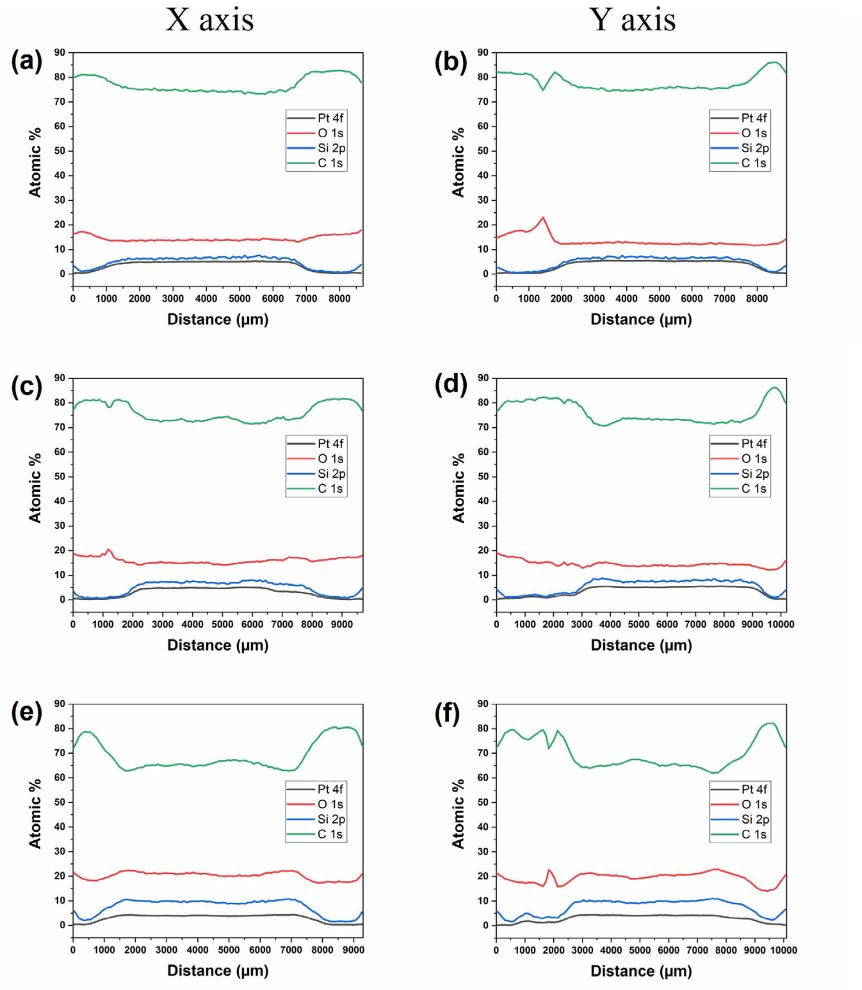

Figure S3.5. Crossover XPS line scan of the Pt/CB catalyst drop casted on the glassy carbon substrate after applying variant numbers of SiO2 ALD cycles: (a, b) 2 ALD cycles, (c, d) 5 ALD cycles, and (e, f) 20 ALD cycles scanning from X and Y axis.

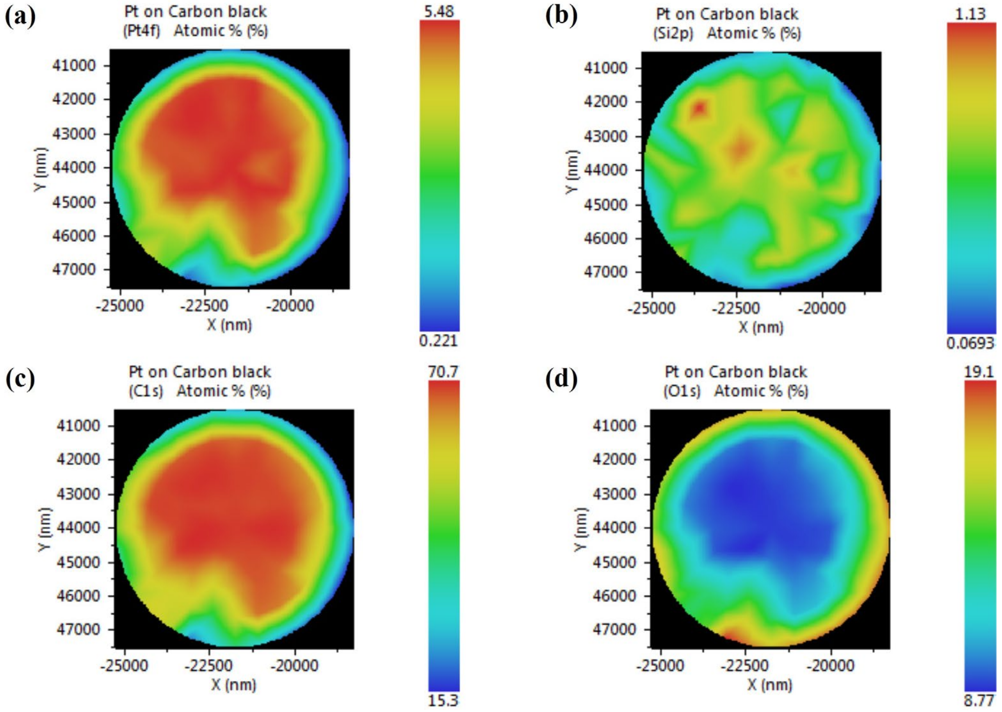

Figure S3.6. XPS area scans of the original Pt/CB catalyst on glassy carbon electrode; (a) Pt 4f signal; (b) Si 2p signal; (c) C 1s signal; (d) O 1s signal scanned from the catalyst spot and its margin region.

Two red spots shown in Figure S5b represent one atomic percent of Si on the surface of the sample and this might come from contamination from the lab environment, like small flakes of glass wool.

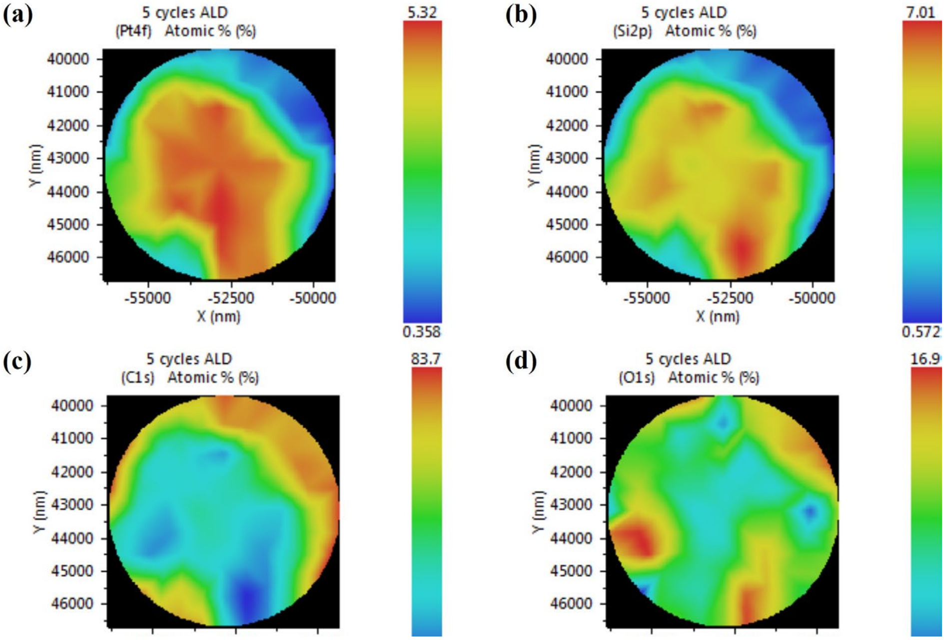

Figure S3.7. XPS area scans of the Pt/CB catalyst after 5 cycles of SiO_2 ALD on glassy carbon electrode; (a) Pt 4f signal; (b) Si 2p signal; (c) C 1s signal; (d) O 1s signal scanned from the catalyst spot and its margin region.

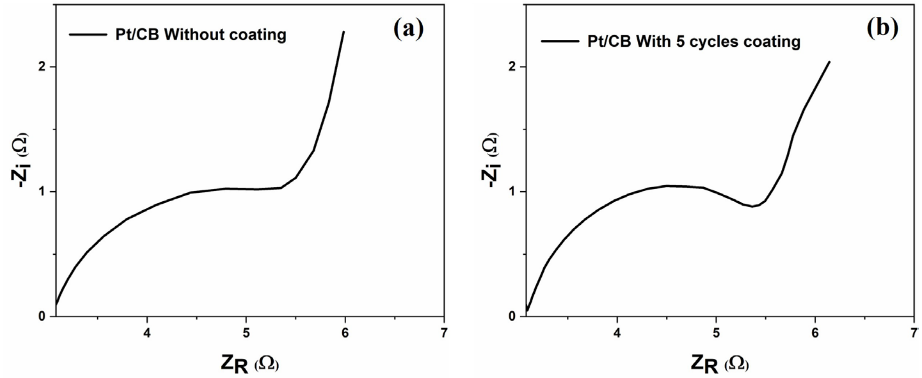

Figure S3.8. The Nyquist plots of Pt/CB catalyst with and without 5 cycles ALD coating.

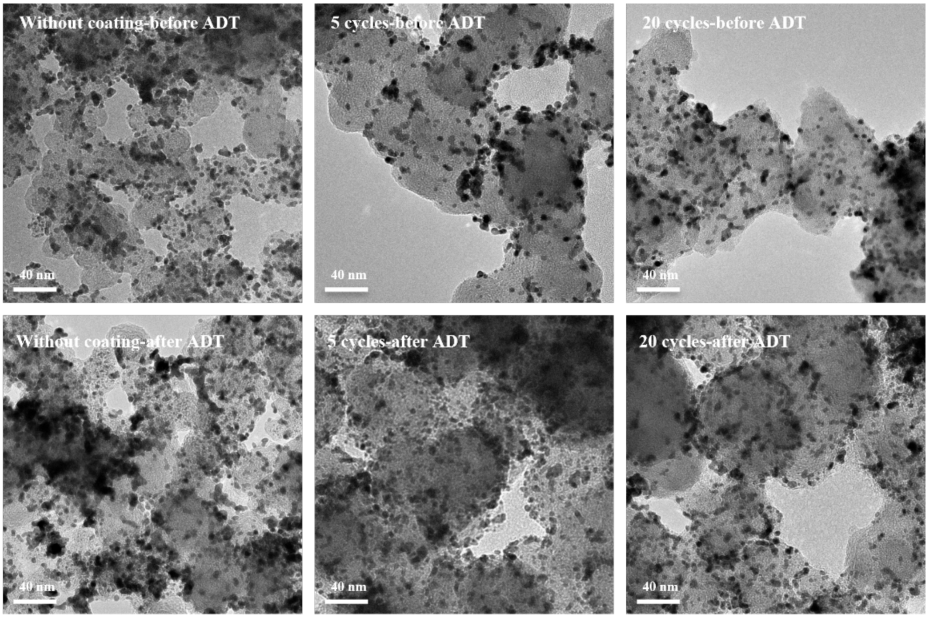

Figure S3.9. TEM images of the Pt/CB catalyst before (top row) and after (bottom row) accelerated durability tests.

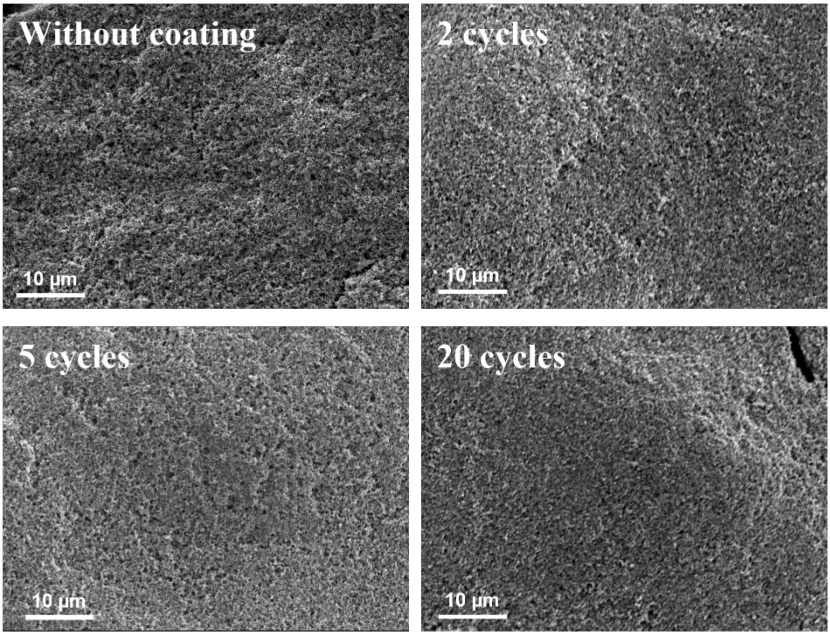

Figure S3.10. SEM images of the Pt/CB catalyst before accelerated durability tests.

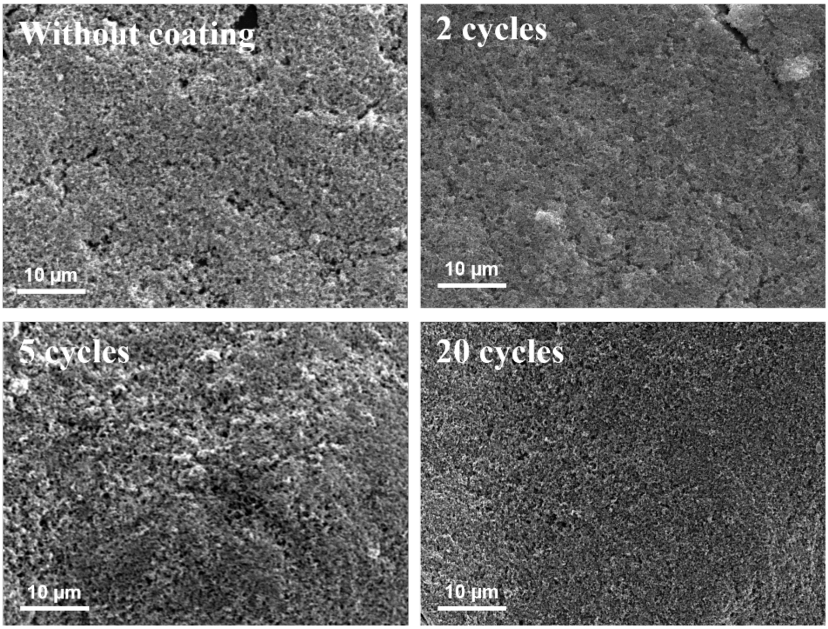

Figure S3.11. SEM images of the Pt/CB catalyst after accelerated durability tests.

4

The effects of SO_2 impurities on CO_2 electroreduction on bare silver and SiO_2 coated silver in different cell geometries

This chapter examines the impact of SO_2 impurities on CO_2 electroreduction in H-cell and membrane electrode assembly (MEA) reactor systems.

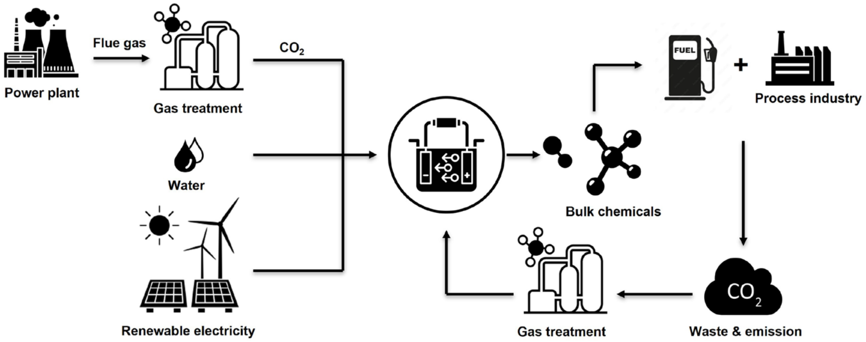

Abstract: Electrochemical CO_2 reduction presents an opportunity to transform waste flue gas with water and renewable electricity into chemicals or fuels. However, the energy-intensive nature of purification of flue gas underscores the appeal of directly utilizing the flue gas streams containing impurities. In this study, we investigate the impact of SO_2 impurities on CO_2 electroreduction in two electrochemical cell geometries: an H-cell and a membrane electrode assembly (MEA) cell. We observe distinctly different behavior of the Ag on carbon black (Ag/CB) catalyst under SO_2 impurities in the H-cell compared to the MEA cell, where SO_2 impurities exhibit a more pronounced effect on Ag/CB catalysts in the H-cell than in the MEA system. This difference is attributed to the higher solubility of SO_2 in the electrolyte compared to CO_2, resulting in an accumulation effect and causing differences in the SO_2 concentration near the electrode between the H-cell and the MEA system. By depositing a very thin SiO_2 coating on the outermost surface of the Ag/CB catalyst using atomic layer deposition (ALD), the impact of SO_2 on the catalyst's selectivity is diminished. This is attributed to the permeability difference between CO_2 and SO_2 through the SiO_2 coatings and results in a local SO_2 concentration difference between samples with and without SiO_2 coatings.

4.1 Introduction

With the ongoing rise in global CO_2 emissions, there is an urgent need to develop sustainable technologies for capturing and utilizing CO_2. The electrochemical reduction of CO_2 offers an appealing method for transforming surplus CO_2, along with water and renewable electricity, into bulk chemicals that can be directly used in the process industry or as fuels, as depicted in Figure 4.1. The electrochemical reduction of CO_2 to CO is particularly intriguing as this is a two-electron reduction product, resulting in significant yields from each mole of electron transfer[1]. Silver (Ag) is one of the best catalysts for the electroreduction of CO_2 to CO because of its high selectivity for CO during CO_2 reduction and its high stability over prolonged periods of operation[2-5]. However, the Ag catalyst is susceptible to poisoning and subsequent loss of activity during the reaction due to the presence of impurities in the reactants[6-9]. Nevertheless, the CO_2 streams from industry often contain a variety of pollutants, and the CO_2 concentration typically is relatively low. The anticipated costs of capturing CO_2 from a biomass-fueled combustion power plant range from \$150 to \$400 per metric ton of CO_2[10]. Furthermore, purification expenses for this procedure are projected to be between \$70 and \$275 per metric ton of CO_2[10]. Despite purification procedures, the purity of the obtained CO_2 gas still remains uncertain. Contaminants can pose a significant challenge to the long-term operation of Ag catalysts in industrial application. Hence, it is crucial to study the CO_2 reduction reaction (CO_2RR) on Ag catalysts in the presence of varying concentrations of impurities. Furthermore, it is also important to develop strategies for protecting the catalysts from exposure to impurities and alleviating the poisoning issue.

Unprocessed flue gas emissions contain various gaseous impurities, the concentration of each impurity significantly depends on the emission source and hence the type of industry. Typically, flue gas emitted from power plants contains impurities such as sulfur oxides (SO_X), nitrogen oxides (NO_X), oxygen, and volatile organic compounds (VOC)[11-12]. Hee Ko et al. have studied the impact of nitrogen oxides on electrochemical CO_2RR[13]. They used various NO_x (including NO, NO_2, and N_2O) on Cu, Ag, and Sn catalysts in a flow cell and found that the presence of NO_x (up to 0.83 vol%) in the CO_2 feed results in a notable reduction in Faradaic efficiency (FE) during CO_2 electroreduction. This reduction is attributed to the preferential electroreduction of NO_x over CO_2. However, despite the decrease in FE, when the pure CO_2 feed is restored, the electrocatalyst maintains similar CO_2 reduction capabilities. This indicates that the enduring impact of NO_x on the catalytic performance of the modeled catalysts is negligible over the long term. Xu et al. found that when O_2 impurities are present at typical concentrations (4 vol% of O_2), most of the current was redirected from CO_2RR towards the oxygen reduction reaction (ORR)[14]. This poses more serious issues when

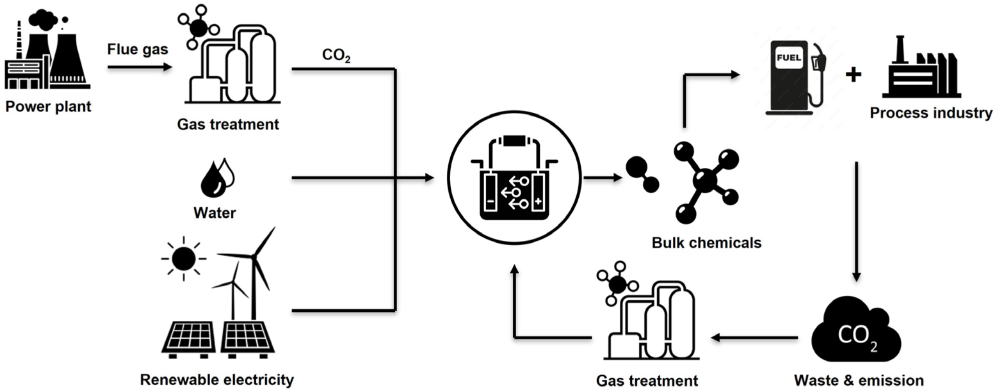

Figure 4.1. Schematic illustration of the idea CO_2 electroreduction industry.

operating at elevated pressures. For example, 99% of the current was redirected to ORR at 15 bar. Van Daele et al. studied the stability of Ag and Bi_2O_3 catalysts with 198 ppm SO_2 in CO_2 and 213 ppm NO in CO_2 over the course of 20h[15]. They found that the studied catalysts have a stable performance and high Faradaic efficiencies towards the target products over 20h. Therefore, it seems that operating with 200 ppm of NO and SO_2 in the gas feed will not have much effect on the catalyst during CO_2RR. However, the presence of oxygen will significantly suppress the FE towards target products during CO_2RR, with 1 vol% of O_2 added to the stream, 23% of the FE towards CO_2RR was lost. This likely is due to the fact that the oxygen impurity has a higher concentration than NO and SO_2, and the preferential reduction of O_2 compared to CO_2 during the reaction. Based on the aforementioned reports, we may infer that the impurities primarily affect the CO_2RR through competing reactions, rather than the poisoning effects that will lead to a long-term influence on the catalysts. Moreover, these studies are all carried out in flow cell reactors, while an H-cell system may give additional insights.

The objective of this paper is to determine the effect of SO_2 impurities on the Ag catalyst for the electrochemical reduction of CO_2 in two different cell geometries: an H-cell and a membrane electrode assembly (MEA) cell. We select SO_2 as the impurity for this study since it is found in most flue gases and sulfur has a pronounced poisoning effect on Ag catalysts[7-9]. We find that SO_2 has a more pronounced impact on Ag on carbon black (Ag/CB) catalysts in the H-cell compared to in the MEA reactor. This is attributed to the higher solubility of SO_2 in the electrolyte compared to CO_2, leading to an accumulation effect in the H-cell. This causes a higher SO_2 concentration near the electrode surface in the H-cell system than in the MEA reactor system. We use atomic layer deposition (ALD) to deposit SiO_2 on Ag/CB catalyst to protect it from SO_2 impurities. ALD is a gas phase coating technique based on the alternating use of two reactants, depositing a thin film on a substrate. It provides sub-nanometer precision in coating thickness, controlled by the number of deposition cycles[16]. After applying a few cycles of SiO_2 ALD providing a nanocoating on the outer surface of the Ag/CB catalyst, the effect of SO_2 on the selectivity of the catalyst is diminished at less negative potentials. This is attributed to the permeability difference between CO_2 and SO_2 through SiO_2 coatings.

4.2 Results and discussion

4.2.1 SO_2 impurities effects on CO_2 electroreduction in H-cell reactor

We first examined the effect of SO_2 impurities on the Ag/CB catalyst for CO_2 electroreduction in the H-cell system. A series of Ag/CB samples coated with SiO_2 were synthesized using ALD with a flat substrate reactor and compared with an uncoated Ag/CB sample. To determine the actual Ag weight percentage in the original Ag/CB nanoparticles, the sample underwent characterization through thermogravimetry differential thermal analysis (TG/DTA). The TG/DTA analysis (Figure S4.1) showed that roughly 22 wt% of Ag_2O residues were presented

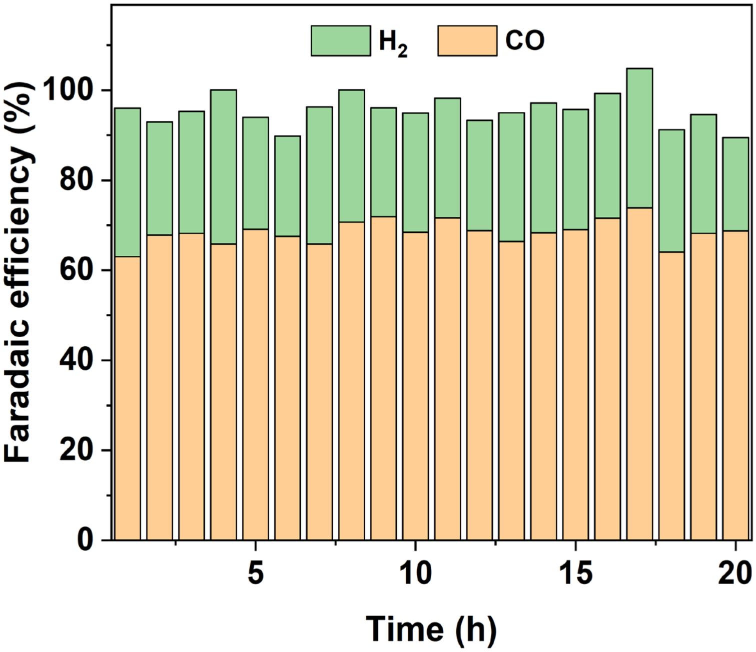

Figure 4.2. Faradaic efficiency of the uncoated Ag/CB catalyst during 20h H-cell testing at -1.0 V vs RHE using pure CO_2 gas feed in a 0.1 M $KHCO_3$ electrolyte.

after the analysis and revealed approximately 20 wt% of Ag in the original Ag/CB samples. The rate of SiO_2 deposition was characterized via X-ray photoelectron spectroscopy (XPS), with Figure S4.2 illustrating a monotonic increase in Si atomic percentage with the number of ALD cycles. High-resolution Si 2p spectra indicated that the Si in the coated samples predominantly exists in the SiO_2 state, which can be deconvoluted into Si 2p3/2 and Si 2p1/2 peaks. This demonstrated successful SiO_2 deposition on the surface of Ag/CB samples, with the Si content increasing proportionally with the number of coating cycles.

The stability of the original Ag/CB catalyst was assessed in an H-cell at -1.0 V vs RHE over a 20-hour period. Figure 4.2 shows that the Faradaic efficiency (FE) of the original Ag/CB catalyst towards CO remained relatively constant at around 70% throughout the 20-hour test, with minor fluctuations. This underscores the stability of the original Ag/CB catalyst in H-cell environments, consistent with previous research indicating the robustness of Ag catalysts under similar testing conditions[2-5]. Notably, the Ag catalyst exhibited no significant deterioration in performance under neutral pH conditions. However, the selectivity of the original Ag catalyst was found to be lower than that reported in some papers[2, 17-18]. To further investigate the selectivity of the Ag catalyst, we also evaluated pure Ag nanoparticles drop-casted onto a glassy carbon electrode while maintaining consistent metal loading (80 $\mu g/cm^2$) with our Ag/CB catalyst. As depicted in Figure S4.3, an optimal FE_{CO} of the pure Ag nanoparticles was achieved at -0.8 V vs RHE, with a similar selectivity towards CO of around 70%. Upon mixing the Ag nanoparticles with carbon black to mimic our Ag/CB catalyst while keep the same Ag loading on the electrode, we observed that the optimal FE was achieved at -1.0 V vs RHE, demonstrating a FE_{CO} of approximately 72%. This indicates that the low FE of the Ag catalyst is not inherent to the catalyst itself but is more associated with the used H-cell configuration. While the partial current density of the Ag nanoparticles with or without mixing with carbon black towards CO appeared comparable at all three potentials, there was a notable disparity in the H_2 partial current density between the Ag nanoparticles drop casted directly on the glassy carbon electrode and those mixed with carbon black. The Ag nanoparticles mixed with carbon black consistently exhibited a lower H_2 partial current density at all three potentials.

SO_2 concentrations of 10 ppm, 100 ppm, and 1000 ppm were tested in this study, considering that the majority of flue gas emissions from power plants typically fall within a SO_2 concentration range from 100 to 400 ppm[15]. The feed gas flow rate used in H-cell testing was 8 sccm. The gas compositions employed for the SO_2 impurity experiments are listed in Table S4.1. Three different gas cylinders containing 0-10000 ppm SO_2 were utilized, and a gas mixer was employed to ensure thorough mixing of various gas streams to achieve a homogeneous gas stream flowing into the H-cell cathode chamber. The original Ag/CB catalyst (i.e., 0 cycle) and catalysts with 2, 4 and 8 cycles of SiO_2 ALD coating were tested at three potentials using chronoamperometry (CA) under different gas feed compositions. As is seen from Figure 4.3, the catalyst performance was first benchmarked with a pure CO_2 feed and a similar selectivity toward CO was observed with and without SiO_2 coating, reaching the highest FE_{CO} of 70% at -1.0 V vs RHE. Nevertheless, when SO_2 impurities were introduced into the gas stream, the FE_{CO} of the uncoated Ag/CB catalyst showed a significant decrease. A decrease in FE_{CO} to 57% with 10 ppm SO_2 and 56% with 100 ppm SO_2, at -1.0 V vs RHE was observed. At the highest concentration of SO_2 (1000 ppm SO_2), the FE_{CO} decreased by 23%, 24%, and 14% at -0.8 V vs RHE, -1.0 V vs RHE, and -1.2 V vs RHE, respectively. The SO_2 poisoning effect on the Ag catalyst appears to be potential dependent, with a greater impact observed at lower potentials. This is expected due to the more favorable reduction of SO_2 over CO_2, since SO_2 reduction has a significantly less negative reduction potential compared to CO_2 reduction[19]. When we calculate the loss in FE_{CO} and attribute it to SO_2 reduction, we find that approximately 50 ppm SO_2 is required to account for the missing FE when 1000 ppm SO_2 is introduced at -0.8 V vs RHE. This suggests that there is sufficient SO_2 in the gas stream during the reaction for the indicated SO_2 reduction (detailed calculation method can be found in SI, the required SO_2 concentration method section). Additionally, the potential poisoning of the Ag/CB catalyst during the reaction can also contribute to the performance degradation when SO_2 is introduced to the gas stream

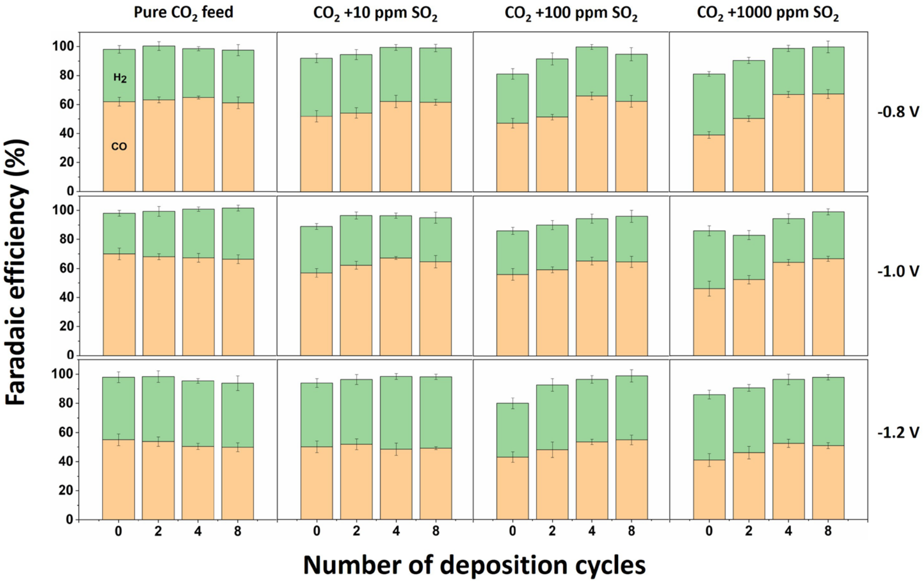

Figure 4.3. Faradaic efficiency of the Ag/CB catalyst with or without SiO_2 coating during 1h H-cell CA testing in a 0.1 M $KHCO_3$ electrolyte at 3 potentials using CO_2 gas feed with different concentrations of SO_2 impurities. The data was collected from two independent measurements and the error bars represent the arithmetic mean.

as we detected the formation of Ag_2S species on the surface of the catalyst after the reaction, as shown in Figure 4.4. All of these factors combined together contribute to the decrease in FE_{CO} for the CO_2 electrolysis. The decrease in CO selectivity of the Ag/CB catalyst at a high concentration of SO_2 impurities was more pronounced at less negative potential (-0.8 V vs RHE) compared to more negative potential (-1.2 V vs RHE) indicating that the competition between SO_2 reduction and CO_2 reduction is potential dependent. SO_2 reduction is more favored compared to CO_2 reduction at less negative potentials. As the potential becomes more negative, the effectiveness of CO_2 reduction increases, with the loss in FE_{CO} decreasing. The Ag/CB catalysts protected with 2-8 ALD cycles of SiO_2 coating were much less affected by the SO_2 contaminant. At -0.8 V vs RHE, the FE_{CO} of the uncoated Ag/CB catalyst was 52%, 47%, and 39% with 10 ppm SO_2, 100 ppm SO_2, and 1000 ppm SO_2, respectively. After

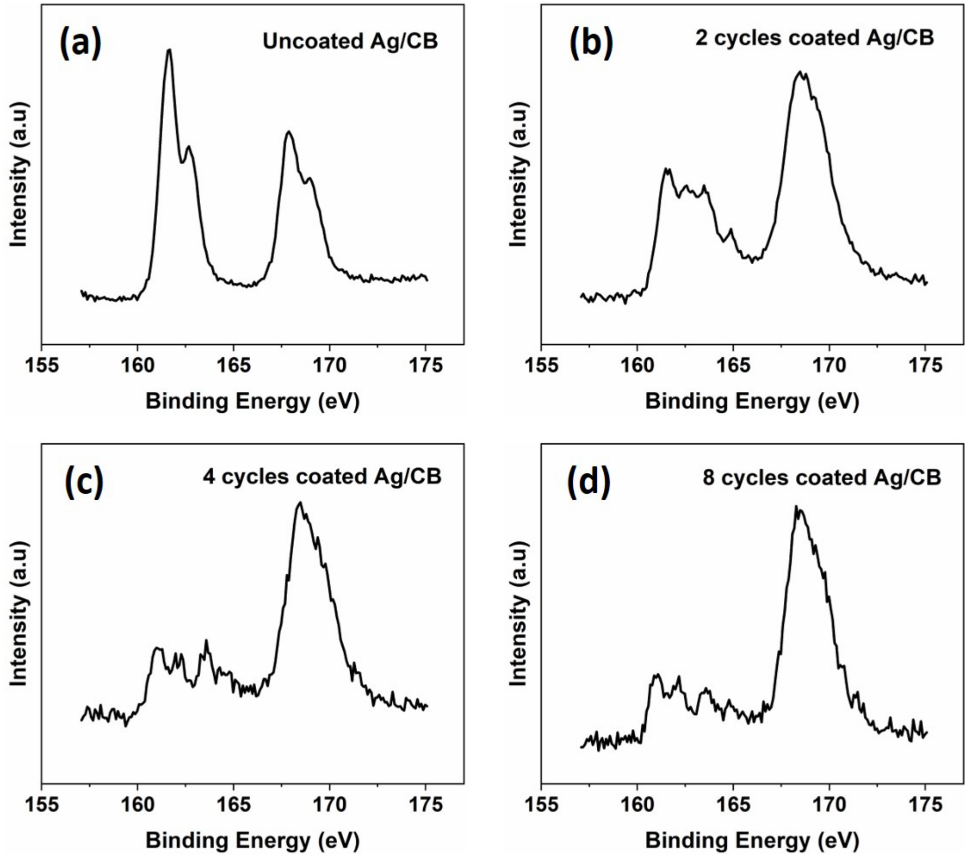

Figure 4.4. S 2p XPS spectrum of the Ag/CB catalyst with or without SiO_2 coating after CO_2 electrolysis with 1000 ppm SO_2 tested at H-cell at -1.0 V vs. RHE

applying 2 cycles of SiO_2 coating on the surface of the catalyst, the FE_{CO} improved to 54%, 51%, and 50%, respectively. When we further increased the coating cycles to 4 cycles, the FE_{CO} of the ALD coated catalyst increased to 62%, 65%, and 66%. After 8 cycles of SiO2 coating, the FECO reached 62%, 62%, and 67%. The SiO_2 coating thereby effectively reduced the SO_2 poisoning effect on the Ag catalyst. When the applied potential became more negative, the SO_2 effects on Ag catalyst decreased, and the coating effectiveness decreased as well. The FE_{CO} of the uncoated Ag/CB catalyst at -1.2 V vs RHE was 50%, 43%, and 41% under 10 ppm SO_2, 100 ppm SO_2, and 1000 ppm SO_2, respectively. After 2 cycles of coating, the FE_{CO} improved to 51%, 48%, and 46%. And after 4 cycles coating, it increased to 48%, 53%, and 52%. With 8 cycles coating, the FECO improved to 49%, 54%, and 50%. The decreased FE_{CO}, especially for the uncoated and 2 cycles coated samples under SO_2 impurity, can likely be attributed to the SO_2 reduction and the poisoning of the catalysts. However, due to the high solubility of the sulfur-containing anions in the electrolyte and its cross-over through the anion-exchange membrane to the anolyte and directly released to the atmosphere afterwards, we cannot accurately detect the SO_2 reduction products and quantify their Faradaic efficiency.

Figure 4.4 presents the XPS characterization of the Ag/CB catalyst without and with SiO_2 coating following a 1-hour CA test at -1.0 V vs RHE with 1000 ppm SO_2. In all samples, an intense peak at 168.7 eV was observed in the S 2p spectrum, attributed to the sulfur-containing functional groups within the Nafion binder utilized for drop-casting the catalyst on the surface of the glassy carbon electrode, and serving as the ionomer in the catalyst. Peaks at 161.1 eV and 162.2 eV are attributed to silver sulfide (Ag_2S) formation during the reaction[20]. Notably, the intensity of the Ag_2S peaks was notably higher in the uncoated catalyst. Upon applying 2-8 cycles of SiO_2 coating, a decrease in the intensity of the Ag_2S peak was observed, suggesting that SiO_2 coating mitigated Ag_2S formation during the reaction under high concentrations of SO_2 (1000 ppm SO_2) gas feed. An XPS area scan was conducted after 1h CO_2 electrolysis at -1.0 V vs RHE with 2 kinds of gas feed. Figure S4.5 shows that the uncoated Ag/CB catalyst after 1h CO_2 electrolysis with pure CO_2 gas feed only has a low intensity of S peak on the electrode. For a gas feed of CO_2 with 1000 ppm SO_2, the uncoated Ag/CB catalyst shows a much stronger S peak on the electrode. Nevertheless, for the catalyst treated with 8 cycles of SiO_2 coating, the S peak is significantly decreased on the electrode after CO_2 electrolysis with 1000 ppm SO_2.

In summary, we found that the Ag/CB catalyst was significantly affected by SO_2 impurities in the H-cell geometry, especially for a high SO_2 concentration and at a less negative potential. The SiO_2 coating can be used to protect the Ag/CB catalyst from SO_2 impurities and maintain the catalyst selectivity for all investigated potentials.

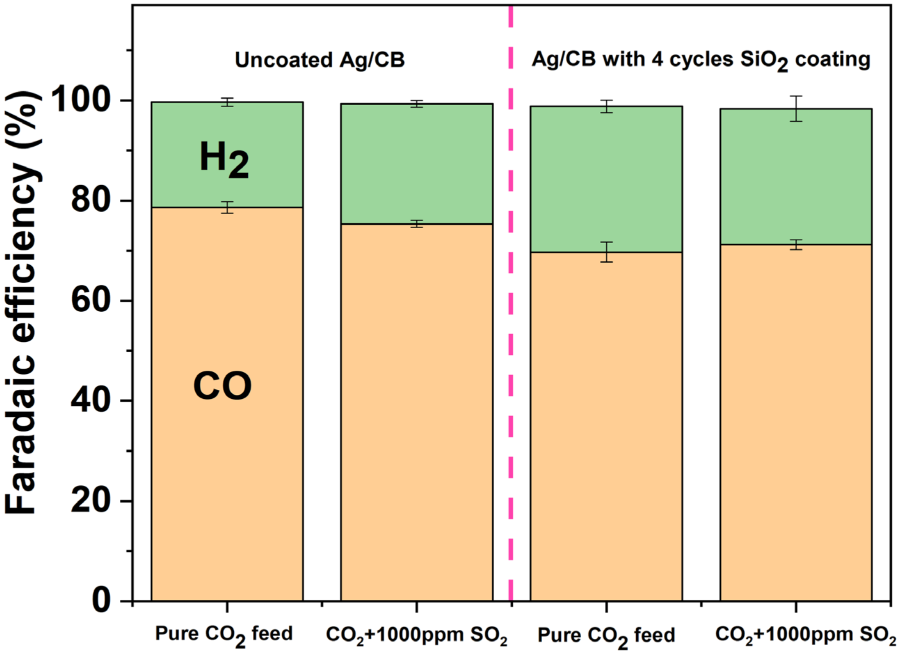

Figure 4.5. Faradaic efficiency of the Ag/CB catalyst with or without SiO_2 coating tested at MEA reactor at 100mA/cm^2 current density in a 1 M $KHCO_3$ electrolyte with pure CO_2 feed or CO_2 mixed with 1000 ppm SO_2. The data was collected from two independent measurements and the error bars represent the arithmetic mean.

4.2.2 SO_2 and CO_2 permeability differences through SiO_2 coating

To further illustrate the protection mechanism of SiO_2 on Ag/CB catalysts against SO_2 impurities, we investigated the permeability differences of SO_2 and CO_2 through SiO_2 coatings based on existing papers. Mohd Nor et al. found that CO_2 has high permeability through SiO_2 modified polymer matrix membranes[21]. After adding 5 wt% of SiO_2 nanoparticles to the polymer matrix membranes (ENR/PVC), the CO_2 gas permeability increased to approximately 6 times higher than the original membranes without SiO_2 modification. Wahab et al. also found a similar phenomena[22]. They reported that CO_2 gas exhibits strong interaction with SiO_2 due to the presence of hydroxyl functional groups (–OH) on the SiO_2 particles. This interaction enhances the solubility of CO_2 within the membrane, thereby improving CO_2 diffusivity and resulting in high permeability of CO_2 through SiO_2 filled fiber mixed matrix membrane. Meng et al. tested that the organic-inorganic hybrid SiO_2 membranes exhibited a high O_2 permeance that was 2.87×10^{-8} mol

m^{-2} s^{-1} Pa^{-1} and a poor SO_2 permeance of 3.9 × 10^{-9} mol m^{-2} s^{-1} Pa^{-1}. The O_2 permeance was 7.4 times higher than the SO_2 permeance through the membranes[23]. This indicates that the SO_2 permeability through this organic-inorganic hybrid SiO_2 membranes is very low. Yoshiura et al. also found that the 3,3,3-trifluoropropyltrimethoxysilane derived SiO_2 membranes have very high SO_4^{2-} ions rejection rates[24]. The $NaSO_4$ and $MgSO_4$ rejection percentage after the liquid permeation tests was 91.0% and 98.2%, respectively. This is attributed to the dissociation of the –OH groups on the silica surface during testing and produce a negatively charged surface. The SiO_2 coating on the Ag/CB catalyst was negatively charged during CO_2RR as well. Hence, it can also have a repulsive effect on SO_2 derived ions. Yu et al. discovered that silica-zirconia membranes with a high Si/Zr molar ratio (Si/Zr = 7/3) exhibit excellent resistance to SO_3 and demonstrate gas separation of O_2/SO_3 selectivity ranging from 13 to 10, surpassing the Knudsen selectivity of 1.58[25]. This suggests promising potential for their application in O_2/SO_3 separation processes and indicates that O_2 has more than 10 times higher permeability through silica-zirconia membranes with a high Si/Zr molar ratio compared to SO_3. Based on the preceding discussion, it can be inferred that there is a notable difference in the permeability of CO_2 and SO_2 through SiO_2, with CO_2 showing significantly higher permeability compared to SO_2 or SO_2 derived ions present in the

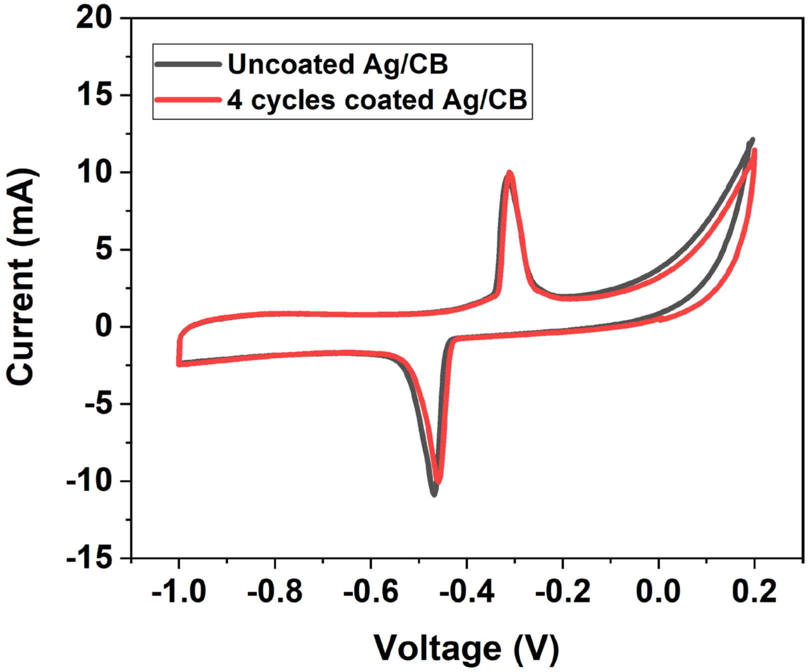

Figure 4.6. CV testing of the uncoated Ag/CB catalyst and the catalyst with 4 cycles of SiO_2 coating, tested at MEA reactor.

electrolyte. The variation in permeability between CO_2 and SO_2 indicates that the concentrations of these gases outside and inside the SiO_2 coating, which directly interact with the Ag/CB catalyst, are also likely to differ. The lower SO_2 concentration on the inside of the coating may account for the observation that after applying 2-8 cycles of SiO_2 coating, the formation of Ag_2S on the electrode surface is considerably less than without SiO_2 coating after CO_2 electrolysis with 1000 ppm SO_2 feed at -1.0V vs RHE. It also explains why SO_2 has much less effect on the catalyst's selectivity after it has been coated with SiO_2 films. The SO_2 concentration near the electrode surface decreases, so the competition between the SO_2 reduction and CO_2 reduction is reduced, and the potential poisoning of the Ag/CB catalyst is minimized.

4.2.3 SO_2 impurities effects on CO_2 electroreduction in MEA reactor

Based on the findings from our investigation using the H-cell reactor, we proceeded to evaluate the performance of SiO_2 coated Ag/CB samples in a MEA reactor to understand their behavior in the flow cell system. Given that the current density in the H-cell is relatively low and cannot meet industrially relevant requirements, assessing the SiO_2 coated Ag/CB catalyst in a flow cell geometry such as a MEA is needed.

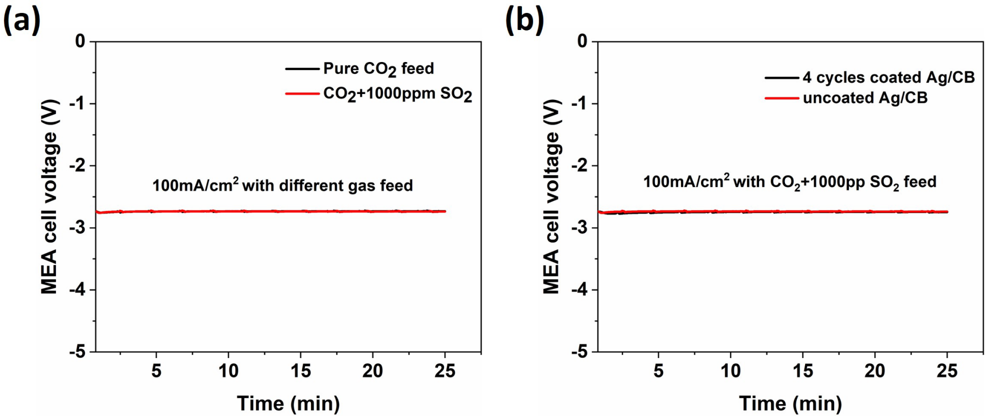

Figure 4.7. CP testing of the Ag/CB catalyst at MEA reactor. (a) Original Ag/CB catalyst tested with pure CO_2 or CO_2 with 1000 ppm SO_2 impurities at 100mA/cm^2 current density. (b) Ag/CB catalyst with or without 4 cycles of SiO_2 coating tested using CO_2 with 1000 ppm SO_2 impurities as gas feed at 100mA/cm^2 current density.

We applied 4 cycles of SiO_2 coating on Ag/CB powders using a fluidized bed ALD reactor. This is different from the samples used in H-cell tests, in which we used a flat substrate ALD reactor and only coated the very outermost surface of the Ag/CB catalyst on the glassy carbon electrode. For these experiments, we fluidized the Ag/CB powder in a dedicated ALD reactor and coated the entire surface of the Ag/CB particles. The coated Ag/CB catalyst was airbrushed on the gas diffusion electrode and assembled in the MEA electrolyzer for the electrochemistry tests. The uncoated Ag/CB catalyst tested in MEA showed a FE_{CO} of 79% at 100mA/cm^2 with a pure CO_2 gas feed (as shown in Figure 4.5). When the gas feed shifted to CO_2 with 1000 ppm SO_2, the FE_{CO} did not decrease significantly as in the experiments in the H-cell, but remained at a FE_{CO} of 75%. When the Ag/CB catalyst was coated with 4 cycles of SiO_2, we observed that the catalyst's selectivity was inhibited to some extent. The 4 cycles SiO_2 coated sample showed a FE_{CO} of 70% with pure CO_2 feed, and a FE_{CO} of 71% when the

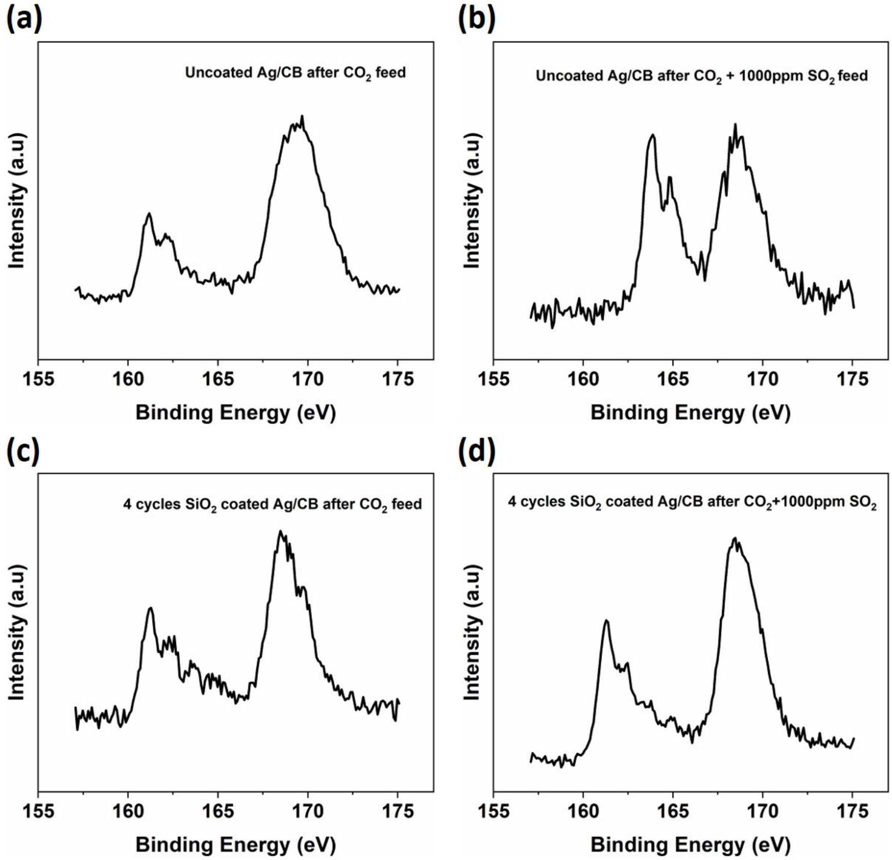

Figure 4.8. S 2p XPS spectrum of the Ag/CB catalyst with or without SiO_2 coating after CO_2 electrolysis with or without 1000 ppm SO_2 tested at MEA reactor at 100mA/cm^2.

gas feed was changed to CO_2 combined with 1000 ppm SO_2. The slight inhibition effect of the coating may stem from the reduction in the electrical conductivity of the catalyst. Furthermore, we hypothesize that this reduction is due to the complete coating of the entire catalyst nanoparticle with non-conductive SiO_2 in the fluidized bed reactor, rather than just the outermost surface of the catalyst that interacts with the electrolyte, as applied in the H-cell. Nevertheless, Figure 4.6 shows that the CV scan of the uncoated Ag/CB catalyst and the catalyst with 4 cycles of SiO_2 coating do not have notable differences. The oxidation and reduction peaks of Ag are well defined with 4 cycles of SiO_2 coating and nearly coincide with the catalyst without coating. This indicates that the obstruction caused by the SiO_2 coating on the catalyst's outmost surface active sites is minimal. Figure 4.7 shows the chronopotentiometry (CP) results of the Ag/CB catalyst tested at 100 mA/cm^2. It indicates that adding 1000 ppm SO_2 to the feeding gas does not change the cell potential under the same current density. Applying an SiO_2 coating also did not alter the cell potential for the same current density. The XPS characterization of the catalyst before and after the CO_2 electrolysis with or without SO_2 impurities are shown in Figure 4.8. From the figure we

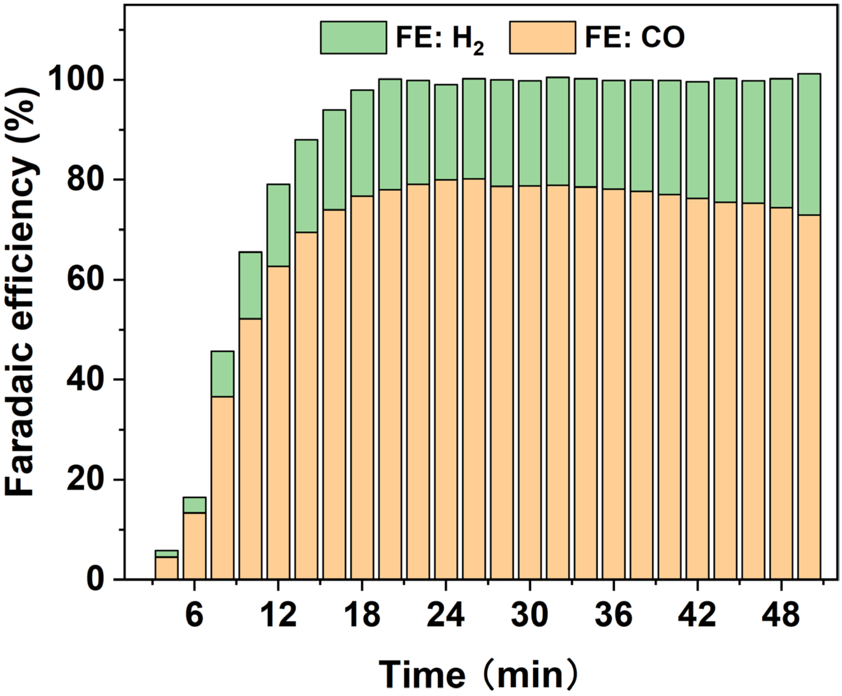

Figure 4.9. Faradaic efficiency of the original Ag/CB catalyst tested at MEA reactor at 100mA/cm^2 current density with pure CO_2 feed for 50 minutes.

observe that peaks at 161.1 eV and 162.2 eV, which are attributed to Ag_2S, are present in all samples, even with pure CO_2 feed. This is likely due to the higher Nafion loading on the GDE (218.5 µg/cm^2) compared to the H-cell electrode (87.4µg/cm^2), and more importantly, the higher current density in MEA caused more reduction of sulfonic acid ($-SO_3H$) groups in the Nafion binder during CO_2 electrolysis. We can observe that the Ag_2S peak becomes stronger after shifting the feed gas from pure CO_2 to CO_2 combined with 1000 ppm SO_2 for the catalyst without SiO_2 coating. Nevertheless, for the catalyst coated with 4 cycles of SiO_2, the Ag_2S peak remains almost identical with or without 1000 ppm SO_2 in the feed gas stream. This suggests that inhibition of SO_2 penetration by SiO_2 is also present in the MEA experiments.

SO_2 impurities in the CO_2 feed had a stronger influence on Ag/CB catalysts within the H-cell system than in the MEA reactor under the conditions used here. We attribute this difference in behaviour to the higher solubility of SO_2 in the liquid electrolyte compared to CO_2, resulting in an accumulation of SO_2 in the batchwise operated H-cell. The solubility of CO_2 in water at 20 °C is 1.7 g/L. Under the same conditions, the solubility of SO_2 is 110 g/L, nearly 65 times higher than that of CO_2 in the electrolyte. This will lead to a continuous increase of SO_2 concentration in the electrolyte within the H-cell during the experiments until it reaches saturation. However, due to the high solubility of SO_2 in the electrolyte and the relatively low concentration of SO_2 in the feed gas stream, even with the highest concentration of SO_2 used in the experiments (CO_2 with 1000 ppm SO_2, which means 0.1 vol% of SO_2 in the CO_2 stream), it would require 6.6 days of continuous dosing to reach SO_2 saturation in the electrolyte. This implies that the electrolyte will never reach saturation during the H-cell experiments and the SO_2 concentration in the electrolyte will keep on increasing during the experiments. Consequently, the SO_2 concentration near the surface of the electrode will be much higher than in the feed gas for the H-cell experiments. On the contrary, in the MEA reactor system, the cathode is in direct contact with the feed gas, without the presence of electrolyte in the cathode serpentine channel. Therefore, the SO_2 concentration near the cathode in the MEA geometry is the same as in the feed gas, which is much lower than the concentration near the cathode in the H-cell system with the same feed gas composition. This explains why the Ag/CB catalyst in the MEA system is not significantly affected by SO_2 impurities and it shows that the Ag/CB catalyst can maintain its performance with 1000 ppm SO_2 impurities in the MEA system within our 25 minutes testing timeframe. The long-term stability of the Ag/CB catalyst in the MEA reactor under SO_2 impurities is worth investigating as well. However, after 50 minutes of CP testing, we encountered significant salt precipitation in the MEA system, resulting in a subsequent decrease in Faradaic efficiency. The FE_{CO} started to decrease after 35 minutes during CP testing with pure CO_2 gas feed at 100 mA/cm^2, as shown in Figure 4.9. Very obvious $KHCO_3$ salt precipitation can be seen on the cathode serpentine channel and gas diffusion electrode after 50 minutes CP testing (as shown in Figure S4.5). Nevertheless, the cell potential was relatively stable during 50 minutes CP testing, as can be seen in Figure S4.6. The minor fluctuation was due to the gas chromatography (GC) injection during the CP testing. The salt precipitation issue prevented us from further investigating the stability of Ag/CB catalyst in the MEA system, especially in the presence of SO_2 impurities. Therefore, this research question awaits further investigation in subsequent studies.

4.3 Conclusions

We have explored the performance of the Ag/CB catalyst under SO_2 impurities for CO_2 electrolysis in two electrochemical cell geometries: an H-cell and a MEA cell. Both systems behave differently with respect to SO_2 contamination in the CO_2 feed. The impact of SO_2 on Ag/CB catalysts was large in the H-cell, while it was nearly absent in the MEA geometry under the relatively short testing time used in this study. This difference can be attributed to the greater solubility of SO_2 in the electrolyte compared to CO_2, leading to an accumulation effect and a much higher liquid phase concentration of SO_2 in the H-cell. This led to a greater performance decrease of the Ag/CB catalyst in the H-cell compared to the MEA geometry, when exposed to the same concentration of SO_2 impurities. An ultrathin SiO_2 coating synthesized via ALD protected the Ag/CB catalyst in the H-cell against SO_2 impurities under relatively less negative potentials. This is due to the SO_2 and CO_2 permeability differences through the SiO_2 coatings. CO_2 has much higher permeability compared to SO_2 (or SO_2 derived ions) through SiO_2. This leads to a significant obstruction in the interaction of SO_2 with the catalyst and might decrease the SO_2 concentration after the SiO_2 coatings.

4.4 Experimental Section

4.4.1 Materials

Silicon tetrachloride ($SiCl_4$, 99%) and Iridium oxide (IrO_2) were purchased from Alfa Aesar, isopropanol (≥98%) was purchased from Honeywell, Nafion^{TM} perfluorinated resin solution (5 wt.% in lower aliphatic alcohols and 15-20 % water) was purchased from Sigma-Aldrich. Deionized water with a resistivity of 18 MΩ-cm was used as the co-reactant for ALD. 20 wt% of Ag on Carbon black- Vulcan XC 72R catalyst, Carbon Black Vulcan XC 72R, and Sigracet 39BB carbon paper gas diffusion layers (GDL) pretreated with PTFE in microporous layer were purchased from FuelCell store. Glassy carbon plates were ordered from HTW Hochtemperatur-Werkstoffe GmbH (Germany). The electrolyte solution was prepared from ultrapure water (Milli-Q IQ 7000, 18.2 MΩ). PiperION® Anion Exchange Membrane, 20 microns, was purchased from FuelCell store and submerged in the electrolyte overnight prior to MEA experiments. Potassium bicarbonate ($KHCO_3$, 99.95%) was purchased from Sigma-Aldrich. Anion exchange membrane (Selemion AMV) was purchased from AGC Engineering and kept in deionized water after receiving, and used for H-cell experiments. Ag nanopowder with a particle size from 20-40 nm and without oxide layer was purchased from Thermo Fisher Scientific. All chemicals were received and used without further purification.

4.4.2 Electrode preparation

Electrode used in H-cell experiments

The Ag/CB catalyst was first drop casted on the glassy carbon electrode before the ALD coating. The catalyst ink was prepared by combining 4 mg of catalyst with 800 µL of deionized water, 180 µL of isopropanol, and 20 µL of Nafion perfluorinated resin solution in a vial. The mixture was then sonicated in an ice bath for 1 hour. Following this, 25 µL of the catalyst ink was drop-cast onto the surface of the glassy carbon electrode each time and this process was repeated four times to achieve a homogeneous deposition on the electrode. The SiO_2 coatings on the catalyst were then deposited in a custom-built flat substrate ALD reactor[16, 26-27] operating at atmospheric pressure. The reactor chamber comprises a metal cylinder with an inner diameter of 40 mm and a length of 190 mm, accompanied by a substrate holder with dimensions of 30 mm by 125 mm. To ensure a uniform temperature profile, the deposition temperature was monitored and regulated using two thermocouples positioned inside and outside the ALD reactor. We opted for atmospheric pressure ALD over vacuum ALD as it reduces investment costs and enhances throughput at a larger scale[26-27]. Our SiO_2 deposition process was adapted from literature[28], but the reaction time and precursor gas flow rate were adjusted based on our own requirements. In summary, the $SiCl_4$ and H_2O, the ALD reactants, were filled in stainless steel bubblers and kept at room temperature. Nitrogen gas, with a purity of 99.999%, served as both carrier and purging gas, flowing at a rate of 0.5 L min^{-1} throughout the process, parallel to the substrate surface in the reactor. Before each experiment, samples underwent air plasma pre-treatment at room temperature and 4 mbar pressure for 60 seconds using a Harrick plasma machine. The ALD reactor was heated to and maintained at 100°C throughout the process. $SiCl_4$ was introduced into the reactor for 15 second pulses, followed by 60 second purging with N_2 and 30 second dosing of H_2O vapor. A final 60-second purging with N_2 completed one ALD cycle. Detailed SiO_2 ALD operation conditions are available in Table S4.2. Samples with varying numbers of ALD cycles were obtained by repeating the ALD cycles as needed. Upon completion of the synthesis process, the reactor was purged with N_2 flow for 15 minutes and cooled to room temperature.

Electrodes used in MEA experiments

The catalyst used during the MEA experiments was synthesized using a vibrated fluidized bed reactor[29-31] operating at atmospheric pressure. A vibrating table was used at a frequency of 60 Hz to fluidize the powders and create uniform fluidization inside the reactor during the reaction. A glass column with an inner diameter of 2.5 cm was used as the reactor. 0.5 g of Ag/CB catalyst (pre-dried at 80 °C for 3 hours before the experiment, to remove the moisture) was used for each synthesis batch in the reactor. The $SiCl_4$ and H_2O, the ALD reactants, were filled in stainless steel bubblers and kept at room temperature. Nitrogen gas, with a purity of 99.999%, served as both carrier and purging gas throughout the reaction. A compensation N_2 stream with a flow rate of 1.5 L min^{-1} was employed during the $SiCl_4$ dosing period to maintain an equal gas flow of 2 L min^{-1} throughout the whole ALD process and keep the fluidization of the powders inside the reactor. The ALD reactor was heated to and maintained at 100°C throughout the process. $SiCl_4$ was introduced into the reactor for 60 second pulses, followed by 150 second purging with N_2 and 60 second dosing of H_2O vapor. A final 150 second purging with N_2 completed one ALD cycle. By repeating the same ALD cycles for 4 times, 4 cycles coated sample was achieved. After the synthesis procedure, the fluidized bed reactor was purged for 15 minutes with N_2 flow to remove the residual reactants. Detailed SiO_2 ALD operation conditions were shown in Table S4.2. The 4 cycles SiO_2 coated Ag/CB powders synthesized using the aforementioned method was utilized to prepare the ink that can be airbrushed on the GDL for the MEA experiments. The ink formula is very similar to the previously mentioned ink formula used for the H-cell experiments. In general, 4 mg of catalyst with 800 µL of isopropanol, 180 µL of deionized water, and 20 µL of Nafion perfluorinated resin solution were mixed in a vial. The mixture was then sonicated in an ice bath for 1 hour. After that, the ink solution was airbrushed onto the GDL using an airbrush gun and N_2 flow to reach a catalyst loading of 0.2 mg/cm^{-1}.

4.4.3 Gas Mixing steps for SO_2 impurities experiments

A gas mixing apparatus (Environics® Series 4000) was employed to mix the feed gas and ensure precise control over gas proportions for the electrochemical tests. To protect against the potential corrosion induced by SO_2, a precautionary measure was taken by coating the mass flow controllers and gas tubing within the testing system with SilcoNert® and sealing them with Kalrez®. The generation of varied concentrations of SO_2 gas was achieved by using two standard gas cylinders containing SO_2 with concentration of 100 ppm and 10000 ppm, balanced with CO_2 from Linde Gas. The pure CO_2 gas used in the experiments was also from Linde Gas with a purity of 99.999%. Detailed information regarding the gas recipes used for the electrochemical tests can be found in Table S4.1.

4.4.4 Material Characterization

X-ray photoelectron spectroscopy (XPS) analyses were conducted utilizing the Thermo Scientific™ K-alpha™ instrument from ThermoFisher™ Scientific. The instrument employed monochromatic X-ray beams of aluminum Kα radiation (1486.7 eV) with a spot size of 400 µm. For the survey scans, a pass energy of 200 eV and a step size of 1 eV were employed, while higher-resolution spectra were obtained using a pass energy of 50 eV and a step size of 0.1 eV. All peak positions were analyzed and calibrated with reference to the aliphatic C 1s peak at 284.8 eV, utilizing CasaXPS software.

XPS area scan was performed with a Thermo Scientific™ K-alpha™ (ThermoFisher™ Scientific) utilizing a monochromatic X-ray of aluminum Kα radiation (1486.7 eV) and a circular area was chosen with a diameter of 12 mm. 121 points were selected and evenly distributed within the circular area. A pass energy of 153 eV and a dwell time of 0.5 s were used. The data was analyzed and plotted using the Avantage software.

4.4.5 Electrochemical measurements

Electrochemical measurements in H-cell

The electrochemical measurements were conducted using a H-cell setup[32]. A leak-free Ag/AgCl reference electrode was employed, alongside a counter electrode consisting of IrO_2-coated glassy carbon electrode. All potentials employed in this study were adjusted to the RHE scale using the following equation[33].

$$E_{RHE} = E_{Ag/AgCl} + 0.197 + 0.059*pH$$

A 0.1 M solution of $KHCO_3$ served as the electrolyte in both chambers and each chamber contains 1.8 mL of electrolyte. An anion-exchange membrane, Selemion AMV, was utilized to separate the anode and cathode chambers of the H-cell. Electrochemical measurements were conducted using a Biologic SP-200 potentiostat. Potentiostatic electrochemical impedance spectroscopy was utilized to evaluate the ohmic loss of the cell and was compensated for each experiment. Chronoamperometric measurements were carried out at different applied potentials from -0.8 to -1.2 V vs. RHE and were used to determine the FE of the catalysts. Before each experiment, the cathode electrolyte was purged with feeding gas for 15 minutes. The gas products were analyzed by an in-line gas chromatography (GC) (Compact GC4.0, Global Analyzer Solutions). Every 2 minutes the products were analyzed by the GC for quantification. The gas flow rate used during the experiments was kept at 8 sccm for every tests.

Electrochemical measurements in MEA

The electrochemical measurements were conducted using a MEA reactor purchased from Dioxide Materials. It is a 5 cm^2 CO_2 MEA electrolyzer cell coupled with a stainless steel flowfield plate with a serpentine channel in contact with the cathode GDE and a titanium flowfield plate with a serpentine channel in contact with the anode GDE. The reactor was assembled with 2 N*m Torque to ensure a leak-free assembly. The working electrode was prepared using the aforementioned method. The counter electrode was an IrO_2 airbrushed GDE. The anion-exchange membrane used in the MEA was PiperION® Anion Exchange Membrane. 40 ml of 1 M $KHCO_3$ solution was used and circulated with a flow rate of 5 ml/min in the anode serpentine channel. Chronopotentiometry measurements were carried out at different current densities and were used to determine the FE of the catalysts. And the current density was calculated by dividing the applied current by the geometric area of the working electrode. The CV measurements were carried out from 0.2 V to -1.0 V at a scan rate of 10 mV/s. The gas products were analyzed using the same in-line GC as described in the H-cell experiments; the gas flow rate used during the experiments was 20 sccm for every test.

Reference

1. Chen, C.; Khosrowabadi Kotyk, J. F.; Sheehan, S. W., Progress toward Commercial Application of Electrochemical Carbon Dioxide Reduction. *Chem* **2018,** *4* (11), 2571-2586.

2. Ma, M.; Liu, K.; Shen, J.; Kas, R.; Smith, W. A., In Situ Fabrication and Reactivation of Highly Selective and Stable Ag Catalysts for Electrochemical CO_2 Conversion. *ACS Energy Lett* **2018,** *3* (6), 1301-1306.

3. Zhang, N.; Zhang, X.; Tao, L.; Jiang, P.; Ye, C.; Lin, R.; Huang, Z.; Li, A.; Pang, D.; Yan, H.; Wang, Y.; Xu, P.; An, S.; Zhang, Q.; Liu, L.; Du, S.; Han, X.; Wang, D.; Li, Y., Silver Single-Atom Catalyst for Efficient Electrochemical CO_2 Reduction Synthesized from Thermal Transformation and Surface Reconstruction. *Angew Chem Int Ed Engl* **2021,** *60* (11), 6170-6176.

4. Wang, H.; Han, Z.; Zhang, L.; Cui, C.; Zhu, X.; Liu, X.; Han, J.; Ge, Q., Enhanced CO selectivity and stability for electrocatalytic reduction of CO_2 on electrodeposited nanostructured porous Ag electrode. *Journal of CO2 Utilization* **2016,** *15*, 41-49.

5. Liu, S.-Q.; Wu, S.-W.; Gao, M.-R.; Li, M.-S.; Fu, X.-Z.; Luo, J.-L., Hollow Porous Ag Spherical Catalysts for Highly Efficient and Selective Electrocatalytic Reduction of CO_2 to CO. *ACS Sustainable Chemistry & Engineering* **2019,** *7* (17), 14443-14450.

6. Osiewacz, J.; Löffelholz, M.; Weseler, L.; Turek, T., CO poisoning of silver gas diffusion electrodes in electrochemical CO_2 reduction. *Electrochimica Acta* **2023,** *445*.

7. Doronkin, D. E.; Khan, T. S.; Bligaard, T.; Fogel, S.; Gabrielsson, P.; Dahl, S., Sulfur poisoning and regeneration of the Ag/γ-Al_2O_3 catalyst for H_2-assisted SCR of NO_x by ammonia. *Applied Catalysis B: Environmental* **2012,** *117-118*, 49-58.

8. Gobal, F.; Majari Kasmaee, L., Polysulfide Poisoning of Ag Electrocatalyst during L-Ascorbate Ion Electro-oxidation in Alkaline Solution. *Chinese Journal of Catalysis* **2012,** *33* (2-3), 267-274.

9. Houel, V.; Millington, P.; Pollington, S.; Poulston, S.; Rajaram, R. R.; Tsolakis, A., Chemical deactivation of Ag/Al_2O_3 by sulphur for the selective reduction of NO_x using hydrocarbons. *Catalysis Today* **2006,** *114* (4), 334-339.

10. Al-Attas, T.; Nabil, S. K.; Zeraati, A. S.; Shiran, H. S.; Alkayyali, T.; Zargartalebi, M.; Tran, T.; Marei, N. N.; Al Bari, M. A.; Lin, H.; Roy, S.; Ajayan, P. M.; Sinton, D.; Shimizu, G.; Kibria, M. G., Permselective MOF-Based Gas Diffusion Electrode for Direct Conversion of CO_2 from Quasi Flue Gas. *ACS Energy Letters* **2022,** *8* (1), 107-115.

11. D'Alessandro, D. M.; Smit, B.; Long, J. R., Carbon dioxide capture: prospects for new materials. *Angew Chem Int Ed Engl* **2010,** *49* (35), 6058-82.

12. Kim, C.; Eom, T.; Jee, M. S.; Jung, H.; Kim, H.; Min, B. K.; Hwang, Y. J., Insight into Electrochemical CO_2 Reduction on Surface-Molecule-Mediated Ag Nanoparticles. *ACS Catalysis* **2016,** *7* (1), 779-785.

13. Ko, B. H.; Hasa, B.; Shin, H.; Jeng, E.; Overa, S.; Chen, W.; Jiao, F., The impact of nitrogen oxides on electrochemical carbon dioxide reduction. *Nat Commun* **2020,** *11* (1), 5856.

14. Xu, Y.; Edwards, J. P.; Zhong, J.; O’Brien, C. P.; Gabardo, C. M.; McCallum, C.; Li, J.; Dinh, C.-T.; Sargent, E. H.; Sinton, D., Oxygen-tolerant electroproduction of C_2 products from simulated flue gas. *Energy & Environmental Science* **2020,** *13* (2), 554-561.

15. Van Daele, S.; Hintjens, L.; Hoekx, S.; Bohlen, B.; Neukermans, S.; Daems, N.; Hereijgers, J.; Breugelmans, T., How flue gas impurities affect the electrochemical reduction of CO_2 to CO and formate. *Applied Catalysis B: Environmental* **2024,** *341*.

16. Van Bui, H.; Grillo, F.; van Ommen, J. R., Atomic and molecular layer deposition: off the beaten track. *Chem Commun (Camb)* **2016,** *53* (1), 45-71.

17. Yun, H.; Kim, J.; Choi, W.; Han, M. H.; Park, J. H.; Oh, H.-s.; Won, D. H.; Kwak, K.; Hwang, Y. J., Understanding morphological degradation of Ag nanoparticle during electrochemical CO_2 reduction reaction by identical location observation. *Electrochimica Acta* **2021,** *371*.

18. Kim, C.; Eom, T.; Jee, M. S.; Jung, H.; Kim, H.; Min, B. K.; Hwang, Y. J., Insight into Electrochemical CO_2 Reduction on Surface-Molecule-Mediated Ag Nanoparticles. *ACS Catalysis* **2016,** *7* (1), 779-785.

19. Harmon, N. J.; Wang, H., Electrochemical CO_2 Reduction in the Presence of Impurities: Influences and Mitigation Strategies. *Angew Chem Int Ed Engl* **2022,** *61* (52), e202213782.

20. Ghafoor, S.; Ata, S.; Mahmood, N.; Arshad, S. N., Photosensitization of TiO_2 nanofibers by Ag_2S with the synergistic effect of excess surface Ti(3+) states for enhanced photocatalytic activity under simulated sunlight. *Sci Rep* **2017,** *7* (1), 255.

21. Nor, F. M.; Karim, N. H. A.; Abdullah, I.; Othaman, R., Permeability of carbon dioxide and nitrogen gases through SiO_2 and MgO incorporated ENR/PVC membranes. *Journal of Elastomers & Plastics* **2016,** *48* (6), 483-498.

22. Wahab, M. F. A.; Ismail, A. F.; Shilton, S. J., Studies on gas permeation performance of asymmetric polysulfone hollow fiber mixed matrix membranes using nanosized fumed silica as fillers. *Separation and Purification Technology* **2012,** *86*, 41-48.

23. Meng, L.; Kanezashi, M.; Wang, J.; Tsuru, T., Permeation properties of BTESE–TEOS organosilica membranes and application to O_2/SO_2 gas separation. *Journal of Membrane Science* **2015,** *496*, 211-218.

24. Yoshiura, J.; Ishii, K.; Saito, Y.; Nagataki, T.; Nagataki, Y.; Ikeda, A.; Nomura, M., Permeation Properties of Ions through Inorganic Silica-Based Membranes. *Membranes (Basel)* **2020,** *10* (2).

25. Yu, X.; Meng, L.; Nagasawa, H.; Kanezashi, M.; Machida, M.; Tsuru, T., Evaluating the chemical stability of metal oxides in SO_3 and applications of SiO_2‐based membranes to O_2/SO_3 separation. *Journal of the American Ceramic Society* **2019,** *102* (11), 6946-6956.

26. Yoo, K. S.; Kim, D.-G.; Lee, S.; Lee, W.-B.; Park, J.-S., Atmospheric pressure spatial ALD of Al_2O_3 thin films for flexible PEALD IGZO TFT application. *Ceramics International* **2022,** *48* (13), 18803-18810.

27. Levy, D. H.; Freeman, D.; Nelson, S. F.; Cowdery-Corvan, P. J.; Irving, L. M., Stable ZnO thin film transistors by fast open air atomic layer deposition. *Applied Physics Letters* **2008,** *92* (19).

28. La Zara, D.; Sun, F.; Zhang, F.; Franek, F.; Balogh Sivars, K.; Horndahl, J.; Bates, S.; Brannstrom, M.; Ewing, P.; Quayle, M. J.; Petersson, G.; Folestad, S.; van Ommen, J. R., Controlled Pulmonary Delivery of Carrier-Free Budesonide Dry Powder by Atomic Layer Deposition. *ACS Nano* **2021,** *15* (4), 6684-6698.

29. Grillo, F.; Van Bui, H.; Moulijn, J. A.; Kreutzer, M. T.; van Ommen, J. R., Understanding and Controlling the Aggregative Growth of Platinum Nanoparticles in Atomic Layer Deposition: An Avenue to Size Selection. *J Phys Chem Lett* **2017,** *8* (5), 975-983.

30. Li, M.; Fu, S.; Saedy, S.; Rajendrakumar, A.; Tichelaar, F. D.; Kortlever, R.; van Ommen, J. R., Nanostructuring Pt‐Pd Bimetallic Electrocatalysts for CO_2 Reduction Using Atmospheric Pressure Atomic Layer Deposition. *ChemCatChem* **2022**.

31. Kamphorst, R.; Wanjari, P.; Saedy, S.; van Dam, J. F. K.; Thijssen, A.; Brüner, P.; Grehl, T.; Meesters, G. M. H.; van Ommen, J. R., Enhancing colloid stability of polymer microspheres in water through SiO2 coating: Effects of coating cycles and surface coverage. *Surfaces and Interfaces* **2024,** *45*.

32. Y. Song, P. N. P., The electrochemical synthesis of aminonitrilesI. H-cell studies with adiponitrile and azelanitrile. *Joural of Applied Electrochemistry* **1990,** *21*.

33. Wang, L.; Lee, C.-Y.; Schmuki, P., Solar water splitting: preserving the beneficial small feature size in porous α-Fe2O3photoelectrodes during annealing. *J. Mater. Chem. A* **2013,** *1* (2), 212-215.

Supporting information for chapter 4

Table of contents

Figure S4.1. TG/DTA analysis of the original Ag/CB catalyst.

Figure S4.2. Growth per ALD cycle of SiO_2 deposition and Si 2p XPS spectra of the Ag/CB catalyst.

Figure S4.3. Pure Ag nanoparticles FE

Figure S4.4. XPS area scan of the Ag/CB catalyst tested at H-cell.

Required SO_2 concentration calculation method

Figure S4.5. Salt formation after 50 minutes CP testing

Figure S4.6. CP testing of the uncoated Ag/CB catalyst with pure CO_2 gas feed.

Table S4.1. Gas recipes for H-cell testing and MEA testing

Table S4.2. ALD experimental conditions.

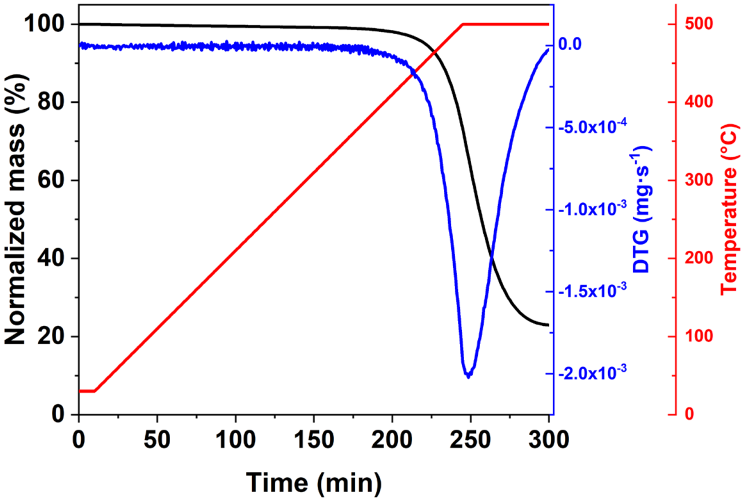

Figure S4.1. TG/DTA analysis of the original Ag/CB catalyst.

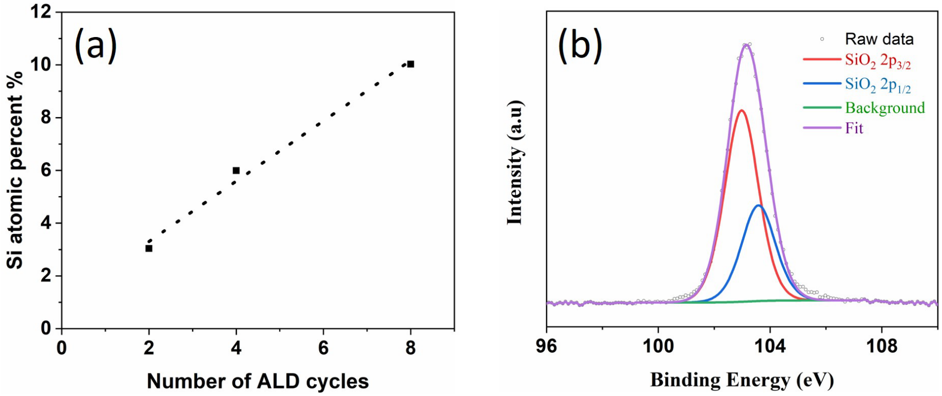

Figure S4.2. (a) Growth per ALD cycle of SiO_2 deposition on the surface of Ag/CB catalyst. (b) Si 2p XPS spectra of the Ag/CB catalyst with 8 cycles of SiO_2 coating.

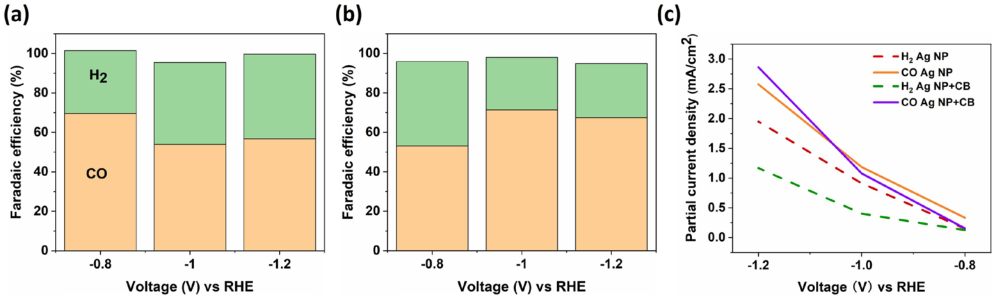

Figure S4.3. (a) Pure Ag nanoparticles drop casted on glassy carbon electrode tested at H-cell. (b) Ag nanoparticles mixed with carbon black to mimic the Ag/CB catalyst drop casted on glassy carbon electrode tested at H-cell. (c) Partial current density of CO and H_2 from pure Ag nanoparticles and Ag nanoparticles mixed with carbon black.

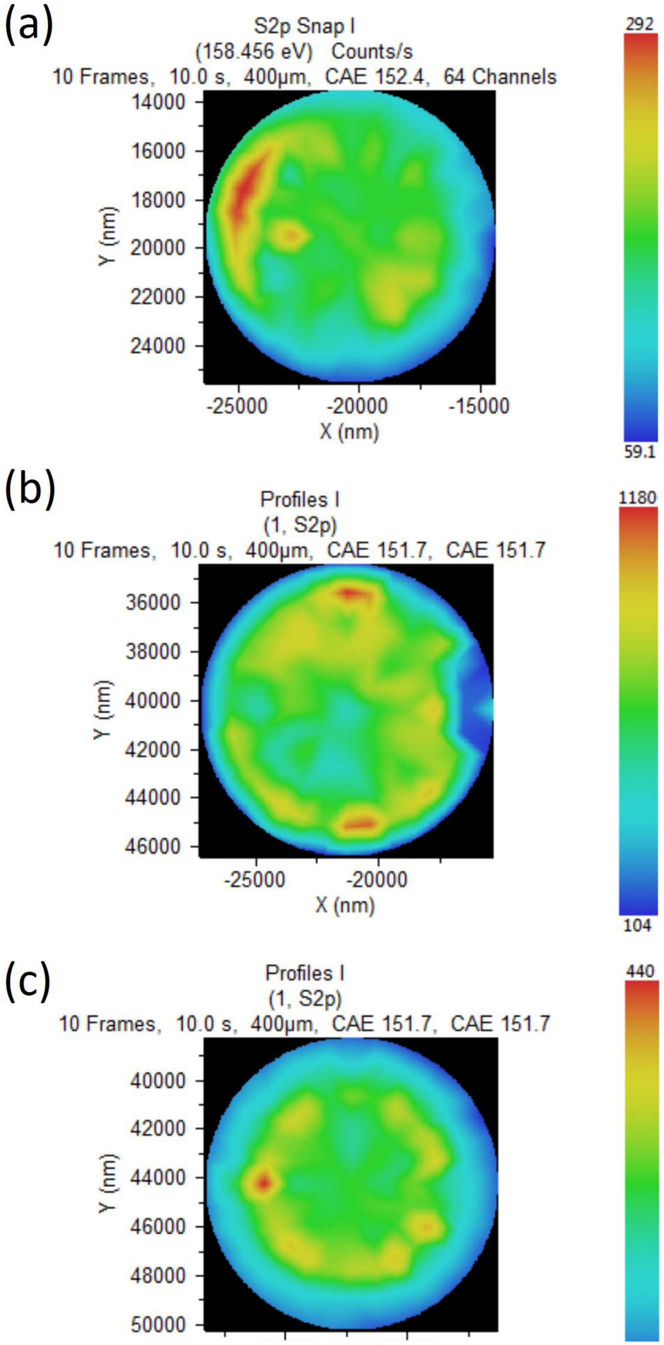

Figure S4.4. XPS area scan of the Ag/CB catalyst tested at H-cell. (a) uncoated Ag/CB catalyst after 1h CO_2 electrolysis at H-cell with pure CO_2. (b) uncoated Ag/CB catalyst after 1h CO_2 electrolysis at H-cell with 1000 ppm SO_2. (c) 8 cycles SiO_2 coated Ag/CB catalyst after 1h CO_2 electrolysis at H-cell with 1000 ppm SO_2.

Required SO₂ concentration calculation method

$$FE_{missing} = FE_{in\ total\ (Ag/CB\ with\ pure\ CO_2\ feed\ )} - FE_{in\ total\ (Ag/CB\ with\ CO_2 + SO_2\ feed)}$$

$$FE_{in\ total} = FE_{H_2} + FE_{CO}$$

$$I_{missing} = FE_{missing} \times I_{in\ total}$$

$$I_{SO_2\ RR\ partial\ current} = I_{missing}$$

$$Required\ flow\ rate\ _{SO_2} = \frac{I_{SO_2\ RR\ partial\ current} \times 6.242 \times 10^{18}}{N_{number\ of\ electrons} \times N_A} \times V_{25°C}$$

$$V_{25°C} = \frac{nRT_{25°C}}{P} = 24.465\ L/mol$$

$$N_A = 6.02 \times 10^{23}\ mol^{-1}$$

$$N_{number\ of\ electrons} = 6$$

$$Required\ C_{concentration}\ SO_2 = \frac{Required\ flow\ rate\ _{SO_2}}{Flow\ rate_{\text{in total}}} \times 100\% \times \frac{1 \times 10^6\ ppm}{\%}$$

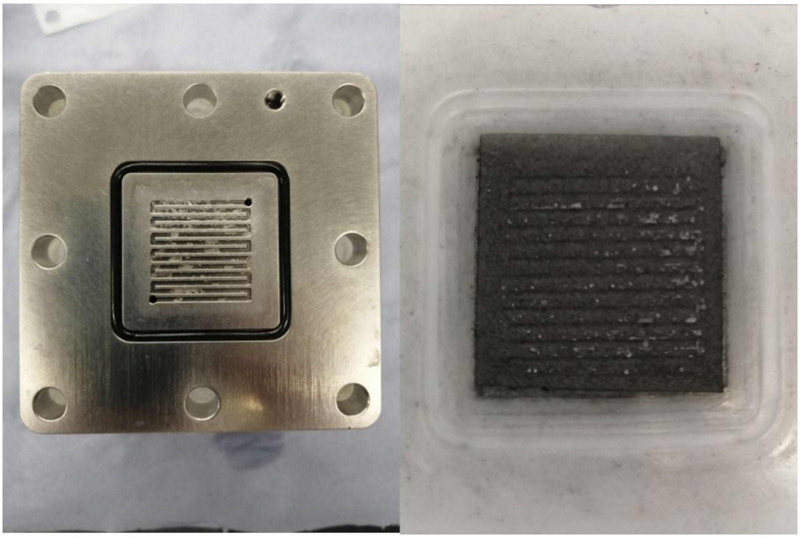

Figure S4.5. Salt formation after 50 minutes CP testing of the uncoated Ag/CB catalyst at 100 mA/cm^2.

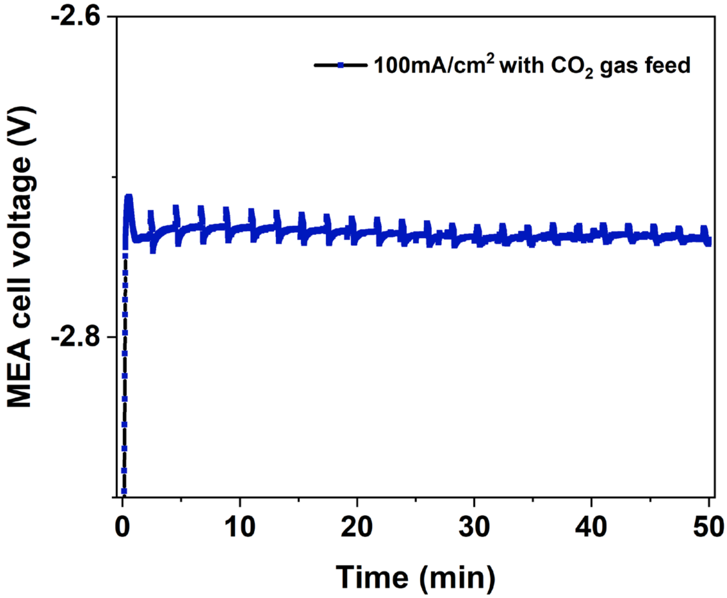

Figure S4.6. CP testing of the uncoated Ag/CB catalyst with pure CO$_2$ gas feed at 100mA/cm^2.

Table S4.1. Gas recipes for H-cell testing and MEA testing

Gas composition	Types of reactors	Gas flow rate (sccm)		
		CO_2	CO_2 + 100 ppm SO_2	CO_2 + 1000 ppm SO_2
CO_2	H-cell	8	0	0
CO_2 + 10 ppm SO_2	H-cell	7.2	0	0.8
CO_2 + 100 ppm SO_2	H-cell	0	8	0
CO_2 + 1000 ppm SO_2	H-cell	7.2	0	0.8
CO_2	MEA cell	20	0	0
CO_2 + 1000 ppm SO_2	MEA cell	18	0	2

Table S4.2. ALD experimental conditions. (RT indicates room temperature)

Material	Precursor (T,℃)	Co-reactant (T,℃)	Type of reactor	$T_{reaction}$ (℃)	Pulse and Purge Time (s) ($SiCl_4$-N_2-H_2O-N_2)	Flow rate(L/min)
SiO_2	$SiCl_4$ (RT)	H_2O vapor (RT)	Flat substrate reactor	100	15-60-30-60	0.5-0.5-0.5-0.5
SiO_2	$SiCl_4$ (RT)	H_2O vapor (RT)	Fluidized bed reactor	100	60-150-60-150	0.5-2-2-2

5

Tuning the wettability of a Ag electrocatalyst by Atomic and Molecular Layer Deposition

Adjusting catalyst wettability shows promise to improve the catalyst performance. Atomic Layer Deposition (ALD) and Molecular Layer Deposition (MLD) offer precise control over coating thickness, but their application for modifying catalyst wettability is not well-explored. This exploratory study aims to use ALD to create hydrophilic SiO_2 and MLD for hydrophobic PET coatings, evaluating their impact on catalyst surface properties and electrochemical performance.

Abstract: CO_2 is the primary contributor to the greenhouse effect and climate change, and therefore there is a urgent need to reduce its atmospheric concentration and emissions. Among various Carbon Capture and Utilization (CCU) processes, electrochemical CO_2 reduction stands out as a promising solution. It can serve as a medium for renewable energy storage and an alternative for sustainable production of carbon-based products. However, this process faces significant challenges such as a low product selectivity, conversion rate, catalyst stability, and the reliance on expensive noble metal electrocatalysts (except copper). These issues are partly due to competing reduction reactions and mass transfer limitations, which are influenced by the interaction between the electrocatalyst and the electrolyte. Adjusting the electrocatalyst wettability is a promising strategy to solve these issues. Studies have shown that tunning the wettability can enhance product selectivity and CO_2 reduction reaction performance. Atomic Layer Deposition (ALD) and Molecular Layer Deposition (MLD) offer precise control over the coating thickness, making them ideal for modifying electrocatalyst surfaces. Despite their potential, the use of ALD and MLD for wettability modification for electrocatalysts is not well-explored. This chapter aims to fabricate hydrophilic SiO_2 and hydrophobic polyethylene terephthalate (PET) coatings using ALD and MLD, respectively. The objective is to investigate the effectiveness of these coatings in tuning the wettability of electrocatalyst surfaces and enhancing their electrochemical performance.

5.1 Introduction

Wettability determines how liquids interact with solid surfaces and can influence the distribution, diffusion, and accessibility of reactants at the catalyst interface. The gas-liquid-solid three-phase microenvironment near the electrodes often plays a crucial role in determining the catalytic process and kinetics, as it can affect the local pH near the catalyst and the stability of catalysts active sites[1]. A hydrophilic surface can enhance water adsorption in for the hydrogen evolution reaction, which is the competing reaction for CO_2 reduction, while a hydrophobic surface can change the gas products release rate and increase the bubble residence time on the electrode[2]. Enhancing the performance of electrocatalysts by adjusting their wettability is a promising approach to improving the efficiency and effectiveness of energy conversion processes. Some studies have already reported on the control of electrocatalyst wettability for various electrochemical processes, including the CO_2 reduction reaction (CO_2RR) and water splitting. Wakerley et al. treated hierarchically structured Cu dendrites with 1-octadecanethiol to create a hydrophobic surface[3]. This surface can trap gases, increasing the CO_2 concentration near the electrode and thereby enhancing ethanol selectivity. However, the stability of the hydrophobic structure of their catalyst during electrochemical processes remains problematic. Chang et al. used different polymetric as binder in ink solution to create a hydrophilic Cu surface (with poly(acrylic acid) as binder) and a hydrophobic Cu surface (with polyvinylidene difluoride as binder)[4]. They found that the hydrophobic Cu surface increased CH_4 selectivity, while the hydrophilic Cu surface increased HCOOH selectivity. Subsequent DFT calculations revealed that the different binding energies of reaction intermediates determined the product distribution. Li et al. immobilized Au nanoparticles on a superhydrophobic porous carbon substrate to create a hydrophobic electrode that works under a solid-liquid-gas three-phase interface microenvironment[1]. They observed a significant increase in the partial current density of CO compared to the Au nanoparticles on a non-hydrophobic surface. Their mathematical model indicated that the interfacial CO_2 concentration of the hydrophobic electrode is approximately 26.2 times higher than the hydrophilic one. The higher CO_2 concentration at the three-phase electrode interface microenvironment led to an increased CO yield. Meng et al. used octadecyltrimethoxysilane (OTS) molecules to increase the hydrophobicity of Pt electrodes and then photocatalytically decomposed the OTS molecules to create hydrophilic Pt electrodes[5]. They found that hydrophilic Pt electrodes have a larger electrochemical active area and a lower adhesion force to gas bubbles compared to hydrophobic electrodes. The hydrophilic surface allows more protons to react on the electrode at a low overpotential, thus producing a larger current. Tuning the electrode surface to be more hydrophilic can promote the hydrogen evolution reaction.

Atomic layer deposition (ALD) and Molecular layer deposition (MLD), which can precisely control coating thickness on the substrate to sub-nanometer scale through layer-by-layer film growth, have been employed as synthesis methods for electrocatalysts[6-7] and for modifying the wettability of surfaces[8-10]. However, using ALD for wettability modification of electrocatalysts for CO_2 reduction remains underexplored. The objective of this chapter is to fabricate two distinct coatings using Atomic Layer Deposition (ALD) and Molecular Layer Deposition (MLD): silica oxide (SiO_2) to impart hydrophilic properties and polyethylene terephthalate (PET) to confer hydrophobic properties.

5.2 Wettability

As discussed in previous sections, wettability can significantly influence electrocatalytic performance by describing the multi-phase balance between gas, liquid, and solid on the electrode surface. Wettability is determined by adhesive forces between the solid and liquid, and cohesive forces within the liquid. Cohesive forces are the attraction between similar molecules, causing them to pull toward each other in a liquid or solid. Adhesive forces are interactions between dissimilar molecules. The balance of these forces defines the degree of wettability.

Thomas Young introduced a method to quantify wettability, known as the water contact angle (WCA). The WCA describes the degree of wettability for a liquid on a surface using Young's equation:

$$\gamma\ SG = \gamma\ SL + \gamma\ LG \cos(\theta\ C)$$

where γ represents interfacial tension (mN/m), SG denotes the solid/gas interface, SL the solid/liquid interface, LG the liquid/gas interface, and θ is the contact angle. The scheme of interfacial tensions and contact angle is shown in Figure 5.1

WCA values determine the surface wettability characteristics: surfaces with a WCA below 90° are hydrophilic, and above 90° are hydrophobic. A superhydrophilic surface has a WCA below 10°, while a superhydrophobic surface has a WCA above 150°[11]. Water interaction with a surface depends on chemical composition (e.g., concentration of polar and nonpolar molecules) and physical surface morphology (e.g., smoothness or roughness). Young's equation assumes an ideal surface, which is not applicable to real surfaces. Therefore, other wettability models were developed: Wenzel, Cassie-Baxter, and the Wenzel-Cassie Coexistent State[11].

Tuning the wettability of electrocatalysts can affect the diffusion layer thickness by influencing gas bubble adhesion and the diffusion coefficient of bulk species to the active site, thereby impacting the catalysts' activity and selectivity.

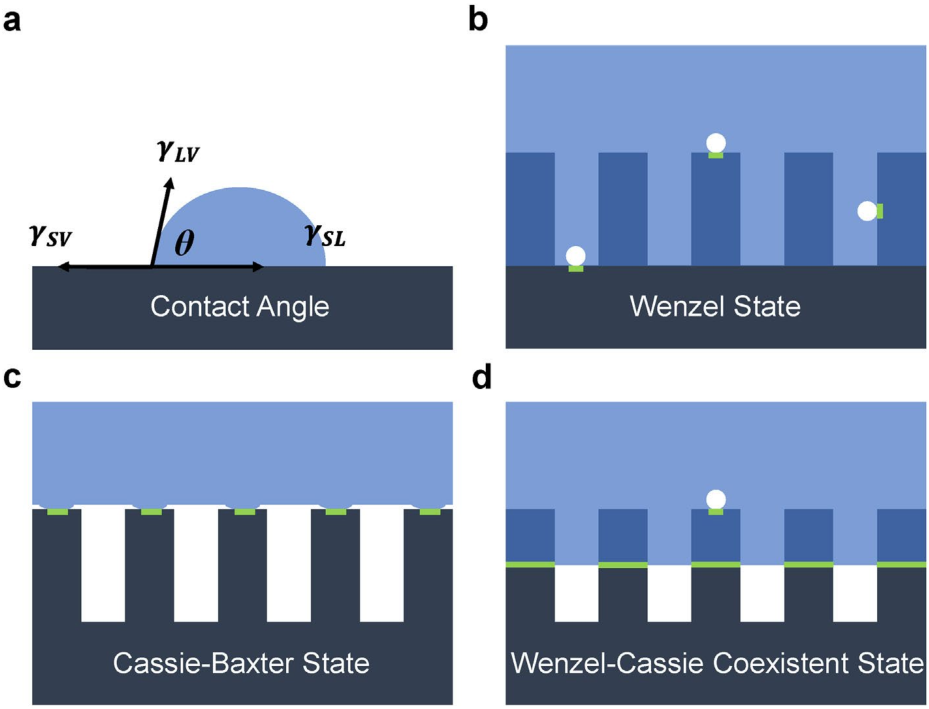

Figure 5.1. Scheme of (a) Contact angle, (b) Wenzel state, (c) Cassi-Baxter state, (d) Wenzel-Cassie Coexistent State[11]. Reprinted with permission from Elsevier.

5.3 The interaction of wetting on different surfaces

The nature of the solid surface interacting with a liquid significantly affects wettability, making it important to understand the type of surface involved. Solid surfaces can be broadly classified into high-energy and low-energy types.

High-energy solid surfaces: These surfaces include materials like metals, ceramics, and glasses, which have strong chemical bonds such as covalent or ionic bonds. When liquids interact with these surfaces, substantial forces are needed to form complete wetting.

Low-energy solid surfaces: These surfaces consist of materials with weaker molecular bonds, such as hydrocarbons or fluorocarbons, where molecules are held together by van der Waals forces or hydrogen bonds. Wetting on these surfaces depends on the type of liquid and can be either partial or complete wetting.

5.4 Wettability measuring methods

5.4.1 Static contact angle

The static contact angle, also known as the sessile drop contact angle, is the simplest and most common method for measuring contact angles. This technique involves placing a drop of liquid on a surface using an optical tensiometer and capturing images of the droplet. These images are then analyzed with an algorithm, usually using Young’s equation, to determine the contact angle between the droplet and the solid surface.

5.4.2 Advancing and receding contact angle-dynamic contact angle

While static contact angle measurements are quick and straightforward, they provide limited information about the surface. To gain more detailed insights, dynamic contact angle measurements are used, including advancing and receding contact angles. Young’s angle theoretically represents the lowest energy equilibrium state between the solid, liquid, and gas phases of a droplet on a surface. However, real surfaces often do not apply to the assumptions underlying Young’s equation due to factors such as surface roughness or chemical heterogeneity, resulting in a range of measurable contact angles.

Dynamic contact angles offer more context for real surfaces by measuring advancing and receding contact angles. These measurements, also known as quasi-static contact angles, can be performed using either optical or force tensiometry, depending on the sample's size, shape, and properties. Additionally, contact angle hysteresis, which is the difference between advancing and receding contact angles, also provides valuable information. For samples suitable for mounting on an optical tensiometer stage, the needle-in method can be used to measure advancing and receding contact angles. In this method, a droplet of liquid is placed on the surface, and a needle is inserted into the droplet to steadily inject more liquid, increasing the droplet's volume. As the volume increases, the contact angle initially increases while the baseline remains stable. When the contact angle stabilizes and the baseline starts to advance, the advancing contact angle (ACA) is reached. Conversely, the receding contact angle (RCA) is measured by gradually removing liquid from a static droplet. Initially, the volume and contact angle decrease while the baseline remains stable. When the contact angle stabilizes again and the baseline begins to recede, the RCA is reached. The difference between the ACA and RCA is referred to as contact angle hysteresis[14].

5.5 Electrowetting

Electrowetting refers to the modification of a surface's wettability through the application of an external electric field. This phenomenon is based on the principle that an electric field can alter the contact angle between a liquid droplet and a solid surface, thereby influencing the extent to which the liquid spreads or contracts on the surface. Consequently, this phenomenon also impacts the wettability of catalysts during electrochemical reactions[15].

5.6 Experimental methods

Materials

Silicon tetrachloride ($SiCl_4$, 99%) was purchased from Alfa Aesar, isopropanol (≥98%) was purchased from Honeywell, NafionTM perfluorinated resin solution (5 wt.% in lower aliphatic alcohols and 15-20 % water), terephthaloyl chloride (TC) and ethylene glycol (EG) were purchased from Sigma-Aldrich. Deionized water with a resistivity of 18 million ohm-cm was used as the co-reactant for ALD. All ALD/MLD precursors and co-reactant were stored in stainless steel bubblers and under inert atmosphere. 20 wt% of Ag on Carbon black- Vulcan XC 72R catalyst, Carbon Black Vulcan XC 72R, and Sigracet 39BB carbon paper gas diffusion electrode pretreated with PTFE in microporous layer were purchased from FuelCell store. Glassy carbon plates were ordered from HTW Hochtemperatur-Werkstoffe GmbH (Germany). All chemicals were received and used without further purification.

Electrocatalyst preparation

Ink preparation: 8 mg of 20% silver on carbon black nanopowder was combined with 800 µL of deionized water, 150 µL of isopropanol, and 50 µL of 5 wt% Nafion in a small glass bottle. This mixture was placed in a nano powder fume hood and subsequently immersed in an ice bath to maintain the temperature at 0°C. Then, the mixture underwent sonication for 30 minutes, with shaking of the glass bottle every 10 minutes.

Drop casting: Drop casting involves placing a small drop of liquid containing suspended particles onto the surface of the electrode to be modified. For this project, the prepared ink is applied to carbon paper. The interaction of the liquid's surface tension with the substrate can cause a coffee ring effect, which alters the distribution of nanoparticles on the electrode. The drop casting procedure were repeated for four times in one electrode to make a homogeneous dispersion of catalyst on the electrode.

Plasma treatment: The reaction mechanism of atomic layer deposition (ALD) relies on functional hydroxyl groups present on the substrate surface. Plasma treatment has been demonstrated to increase the number of hydroxyl groups on the surface. To enhance the quantity of functional groups, the samples underwent plasma treatment by being placed in an air plasma machine for 1 minute. Importantly, we found that ALD experiments need to be performed within half an hour (estimated time, based on the experience of repeated experiments) after plasma treatment of the samples.

ALD-SiO_2 deposition: For the ALD process in this experiment, SiO_2 deposition was conducted using a home-built flat substrate ALD reactor, operated at atmospheric pressure. The pulse sequence for each SiO_2 deposition cycle was $SiCl_4/N_2/H_2O/N_2$. Both precursor bubblers were maintained at room temperature. The temperature for precursor line was set at 80 °C, while the co-reactant line was set at 90 °C. The reactor temperature was maintained at 100 °C. The flow rates for both precursors were set at 0.5 L/min, diluted with 0.5 L/min of N_2, and the purge flow rate was also 0.5 L/min. For each ALD cycle, the pulse time sequence was 10 s/60 s/30 s/60 s.

MLD-PET deposition: The PET deposition pulse sequence for each MLD cycle was $TC/N_2/EG/N_2$. A home-built flat substrate reactor, operated at atmospheric pressure, was employed for MLD experiments. Both precursor bubblers were maintained at 100 °C. The lines were kept at 130 °C, and the reactor temperature was set at 150 °C. The flow rates for both precursors and purges were set at 0.5 L/min. For each ALD cycle, the pulse time sequence was 10 s/2 min/10 s/2 min. The differences in setups, temperatures, and purge times are due to the higher viscosity and handling difficulties of organic chemicals.

5.7 Results and discussion

5.7.1 ALD modification-hydrophobic surface

Before tuning the wettability of Ag/CB electrocatalysts via ALD/MLD modification, we first measured the water contact angle of carbon paper (without plasma treatment) and carbon paper drop casted with the original Ag/CB catalyst. The water contact angle of the carbon paper was 125° ± 5°(with standard deviation), indicating a hydrophobic surface. This result was expected since the carbon paper can be used as gas diffusion electrode and has been treated by PTFE. After drop casting Ag/CB catalysts onto the surface, the water contact angle decreased to 114° ± 7°: a small, not significant decrease of hydrophobicity. This is likely due to the Nafion used in the catalyst ink as an ionomer and catalyst binder. The fluorine and oxygen atoms in this molecular have a high affinity with water due to the hydrogen bonds. The Ag/CB loaded carbon paper electrodes remained hydrophobic with a water contact angle of around 114° before any ALD/MLD modification.

In order to systematically change the wettability of the electrodes, we applied 1-8 cycles of SiO_2 coating via ALD on the surface of Ag/CB catalysts, expecting a proportional change in wettability with the number of deposition cycles. The experimental details are provided in the electrocatalyst preparation sub-section in Section 5.6. Prior to ALD coating, we

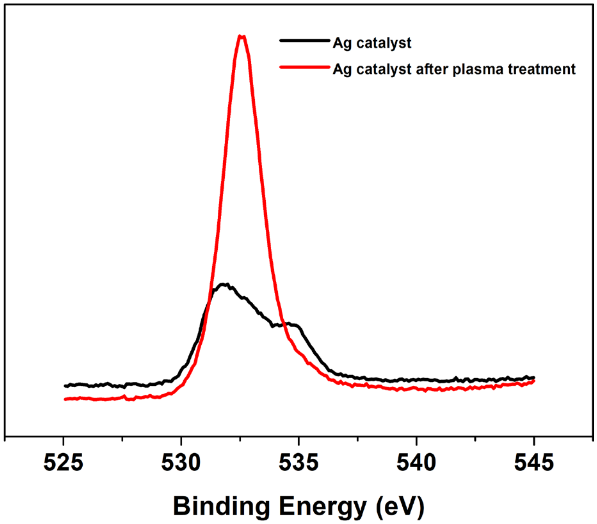

Figure 5.2. XPS oxygen scan for the Ag/CB catalyst deposited on carbon paper before (red) and after plasma treatment (green).

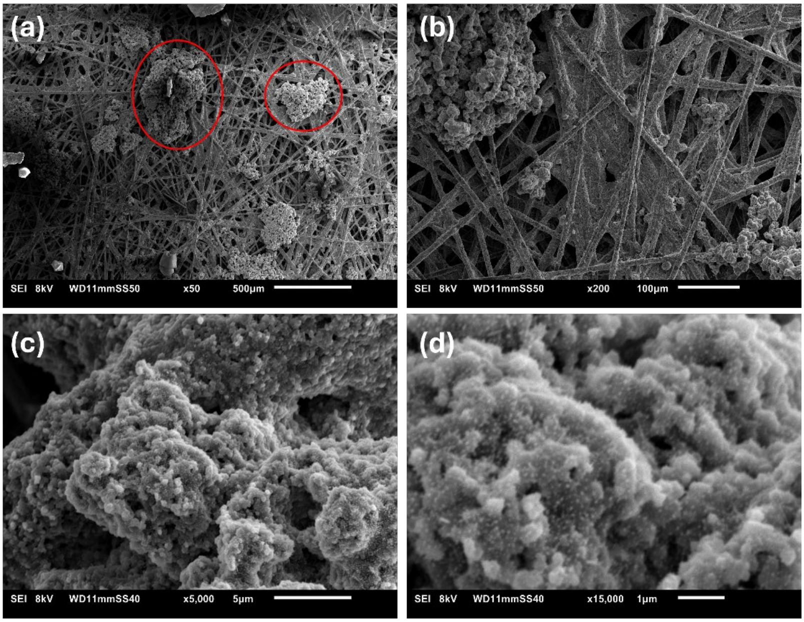

Figure 5.3. SEM images of 4 cycles SiO_2 deposited Ag/CB on carbon paper. The left and right red ellipses in figure (a) indicate the zoomed-in regions shown in figures (c) and (d), respectively.

performed plasma treatment on the samples to increase the concentration of functional

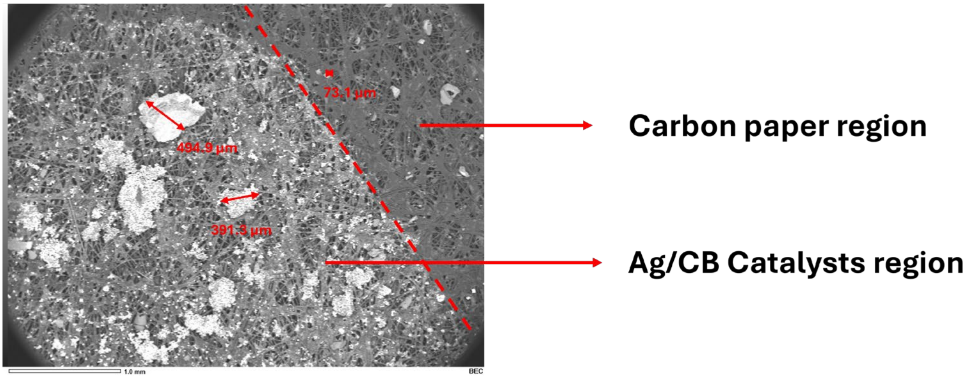

Figure 5.4. SEM image of 4 cycles coated Ag/CB and the measured agglomerates size.

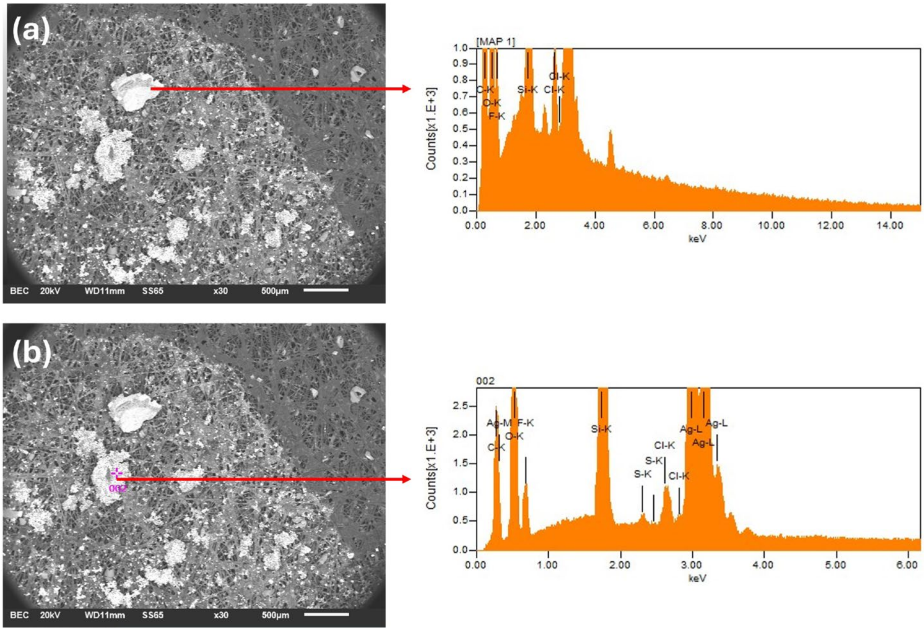

Figure 5.5. SEM image of 4 cycles coated Ag/CB and EDS point detection.

groups on the electrodes to facilitate SiO_2 deposition. As shown in Figure 5.2, the XPS oxygen peak increased significantly after plasma treatment, indicating a higher hydroxy groups concentration, which are essential for SiO_2 deposition[12]. SEM characterization (Figure 5.3) of the Ag/CB catalysts on carbon paper after 4 cycles of SiO_2 coating showed catalysts aggregation over the carbon fibers, with particle diameters varies from 400 µm to 70 µm. Figure 5.4 shows the brightness difference between the drop-casted catalysts region and the surrounding carbon paper. The Ag/CB catalyst region appears much brighter than the surrounding carbon paper region and indicates micron-scale silver particles on the electrode.

We applied EDS to analyze the elemental composition of these large particles. Figure 5.5a shows a particle with peaks of carbon, silicon, chlorine, and fluoride, but no metal elements, suggesting it might be an environmental contaminant or debris from the ALD reactor. Figure 5.5b, however, shows a particle with intense Ag and Si peaks, indicating an aggregated Ag catalyst. In general, we observed extra-large particles on the drop-casted carbon paper, comprising both aggregated Ag catalysts and environmental contaminants. EDS mapping of the same region (Figure 5.6) showed a lower carbon concentration in the catalyst ink region compared to the carbon paper region, while oxygen and Si concentrations were higher in the catalyst region, indicating preferential growth of SiO_2 on the catalyst surface. The intensity of the green colour in the picture indicates the element concentration on the sample surface. The chloride concentration showed no clear difference between catalyst region and carbon paper region. This selective growth was also observed in our previous work with SiO_2 deposition on Pt/CB catalysts, where SiO_2 preferentially grew on the catalyst rather than the glassy carbon region[13]. Further results are shown in Figure 5.7, which characterizes the sample after 8 cycles of SiO_2 coating. In this sample, no extra-large particles

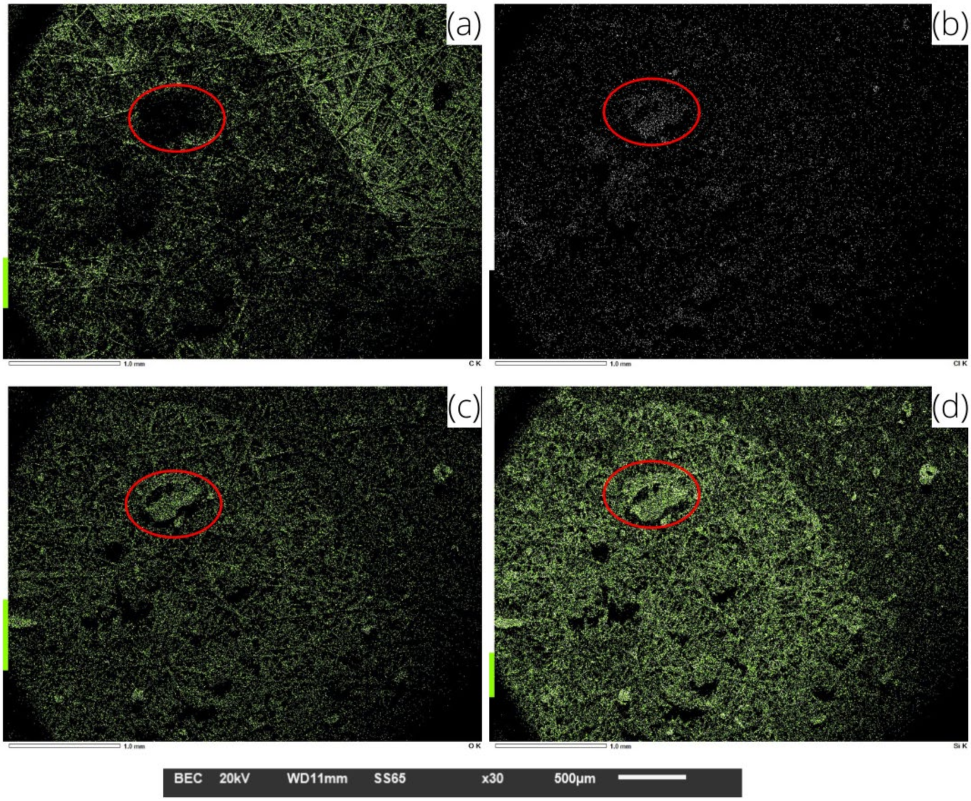

Figure 5.6. EDS maps of 4 cycles coated Ag/CB for each element: (a) carbon map, (b) chloride map, (c) oxygen map, (d) silicon map. The colour bar indicates element concentration. The red ellipses indicate the agglomerate covered by SiO_2.

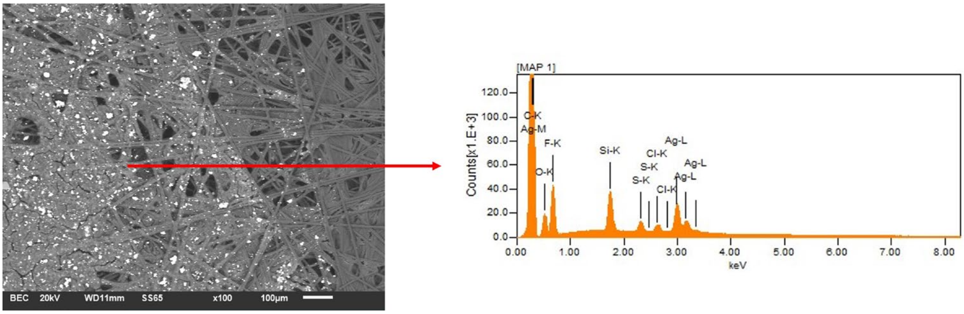

Figure 5.7. SEM image of 8 cycles coated Ag/CB and EDS point detection.

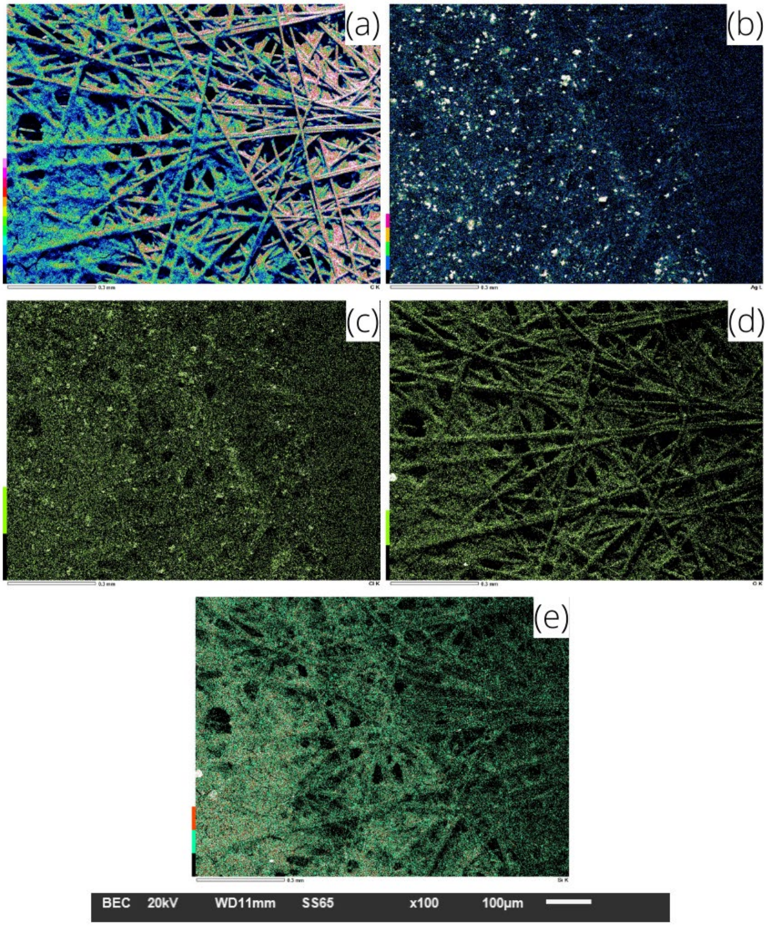

Figure 5.8. EDS maps of 8 cycles coated Ag/CB for each element: (a) carbon map, (b) silver map, (c) chloride map, (d) oxygen map, (e) silicon map. The colour bar indicates element concentration.

were observed on the carbon fibers, and the catalysts were more evenly distributed on the carbon fiber compared to the 4 cycles coated sample. Figure 5.8 also shows preferential growth of SiO_2 on the catalyst region. The XPS survey scan (Figure 5.9) was conducted to investigate the element composition of the sample surface. Si, O, F, Cl, and Ag peaks were detected in the XPS survey scan.

The static water conduct angle WCA test results are shown in Figure 5.10. It consists of data from two batches of repeated experiments. The data for the first batch of samples coated with 2-5 cycles are not shown in this figure, as these samples were superhydrophilic, causing the water droplet to be immediately absorbed upon contact, making the WCA testing results unreadable. The WCA data for these two sets of samples were different than we expected, and we can only conclude that the contact angle of the Ag/CB catalysts tended to decrease as the number of deposited cycles increased. Except for that, almost all measurements had very high standard deviations, indicating that the WCA is sensitive to the specific region where the water droplet lands. This suggests variations in composition or topography across the surface. It contradicts the expected uniformity benefits of the ALD coating method and differs from our results on powder coatings[10]. We speculate that the high standard deviation in the contact angle measurements is due to the carbon paper's composition of woven carbon fibers. SEM images reveal a multilayered mesh structure, resulting in poor uniformity of the sample surface. ALD deposition does not form a complete film on the sample surface to completely change the uniformity of the samples, which leads to significant variability in the contact angle tests.

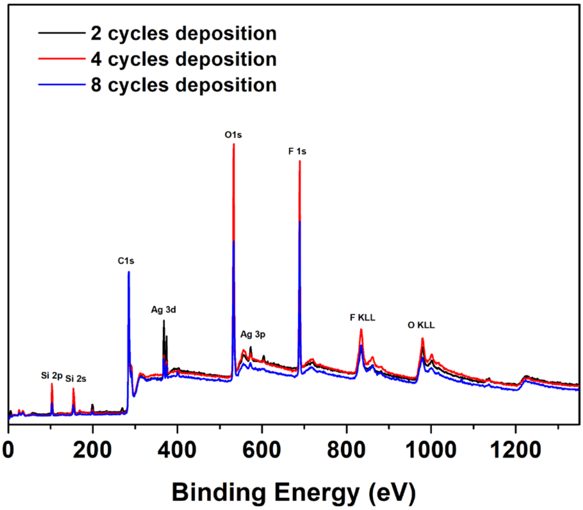

Figure 5.9. XPS data comparison of 2,4,8 cycles coated Ag/CB catalysts.

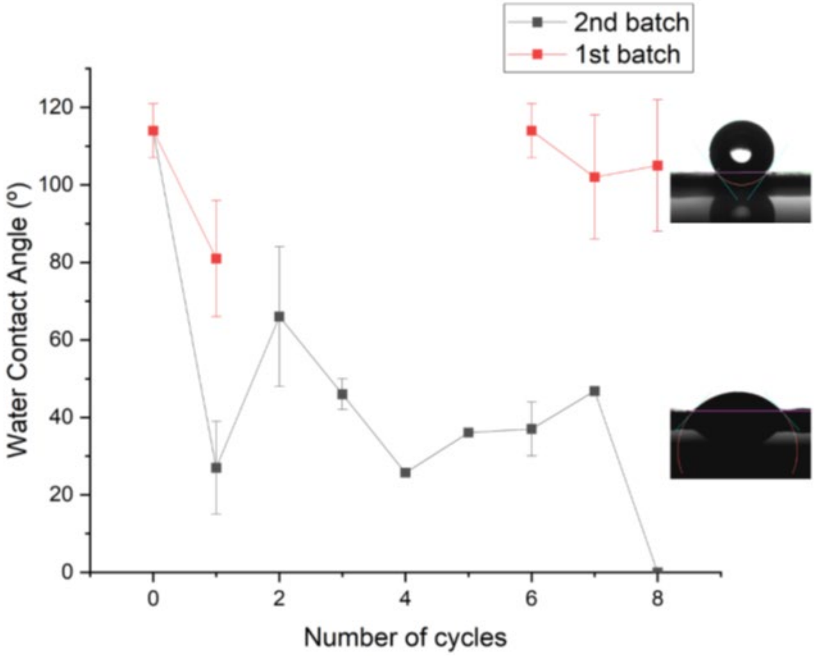

Figure 5.10. WCA as a function of SiO_2 deposition cycles.

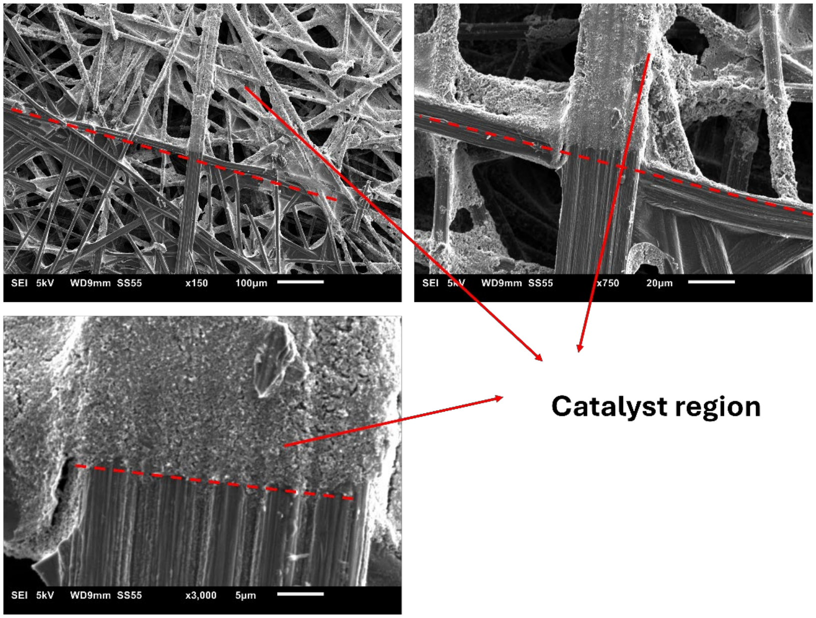

Figure 5.11. SEM images of 1 cycle PET coated Ag/CB catalyst.

5.7.2 MLD modification-hydrophilic surface

PET deposition (MLD modification) was applied to increase the hydrophobicity of the catalysts. SEM characterization was performed on 8 cycles PET coated sample and shown in Figure 5.11. It shows a distinct boundary between the catalyst region and the carbon fiber region, similar to the SiO_2 coated samples. Nevertheless, unlike the ALD samples, we can see a clear film formation, especially in Figure 5.12. In terms of topography, the deposition seemed uniform in certain areas. The XPS survey scan (Figure 5.13) shows O, F, Cl, and Ag peaks, no other contaminants can be found in the sample. The WCA test results showed an increase in hydrophobicity with the number of deposition cycles, exhibiting a liner trend after the first cycle. It increased from 119 ± 2° to 137 ± 2° after 8 PET cycles, representing

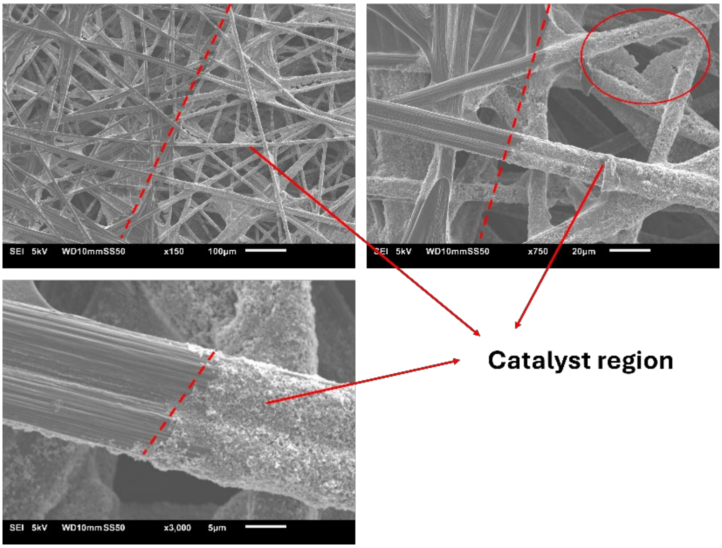

Figure 5.12. SEM images of 8 cycle PET coated Ag/CB catalyst. The red ellipse indicates the coated PET membrane.

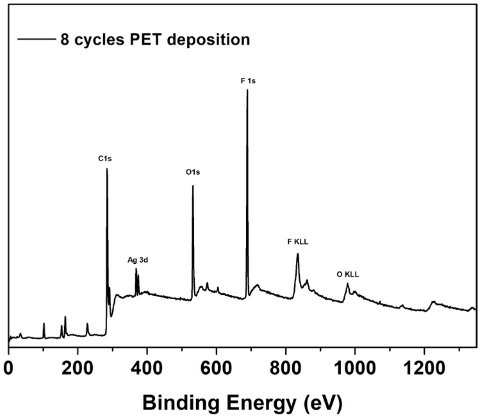

Figure 5.13. XPS survey scan of 8 cycles PET coated Ag/CB catalyst

an approximate 15% increase after coating. A linear fit after the first data point can be established using the following equation:

$$\theta = 1.4 \times number\ of\ cycles + 125.8$$

with R^2 equal to 0.94, as shown by the red line in Figure 5.14. The standard deviation for PET MLD deposition is much smaller than for SiO_2 deposition. We speculate that this is because PET deposition forms a more complete film on the sample surface compared to SiO_2 deposition, resulting in a more homogeneous and less rough surface, thereby reducing the standard deviation of the tests.

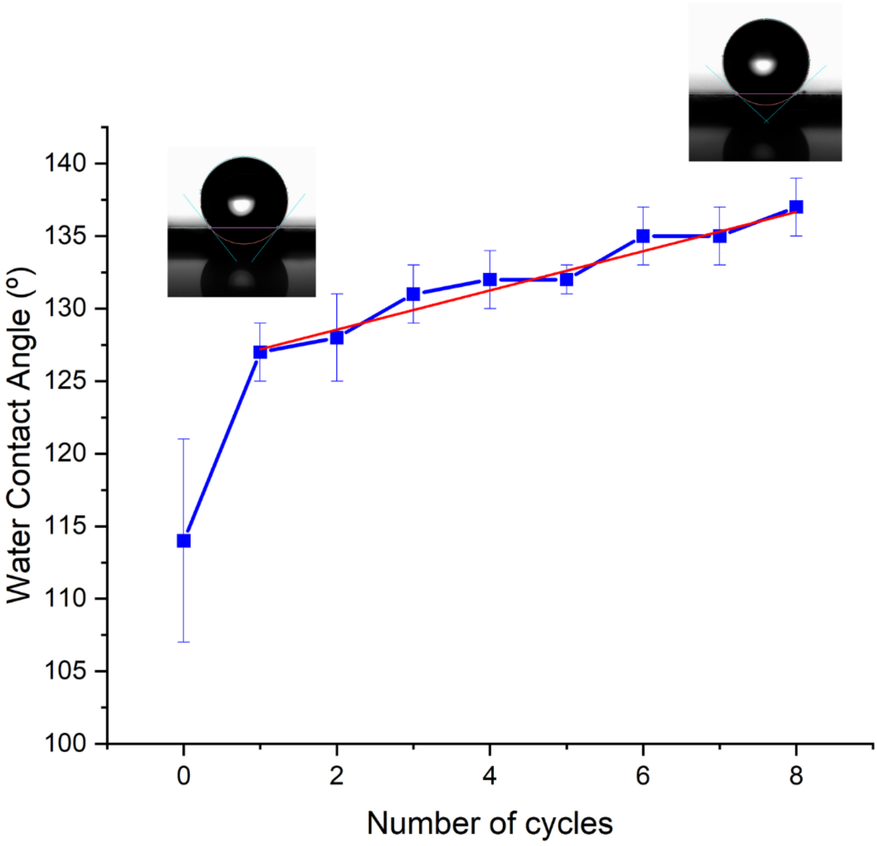

Figure 5.14. WCA as a function of PET deposition cycles.

5.8 Conclusions

In conclusion, ALD and MLD are effective for modifying the wettability of electrocatalysts. They allow the modification of the catalyst surface with ultra-thin coatings (sub-nanometer scale) to substantially change the wettability of the catalyst. Specifically, for PET deposition, MLD served as a method for controlling wettability. A linear relationship was observed between the WCA and the number of deposition cycles, with the WCA of the electrocatalyst increased from 119 ± 2° to 137 ± 2° after 8 PET cycles, representing an approximate 15% increase after coating. Conversely, SiO_2 deposition tuned the wettability of the electrocatalyst to be more hydrophilic, but unlike PET deposition, the WCA did not show a clear linear correlation with the number of deposition cycles. The WCA of the catalysts varied considerably between the two sets of samples. We speculate that this is due to the woven structure of the carbon fiber which results in the catalyst not being able to form a complete film on the surface of the carbon paper. Furthermore, SiO_2 deposition is less effective of improving the film integrity of the catalyst surface compared to PET deposition, as can be seen from the SEM characterization. This leads to the high fluctuation in the SiO_2 ALD modification results and only a decreasing trend can be observed instead of the linear correlation between WCA and the number of deposition cycles.

5.9 Further experiments and recommendations

We speculate that the high fluctuation in WCA results is due to the woven structure of the carbon fiber, which resulted in an incomplete film on the surface of the carbon paper electrodes. Therefore, repeating the experiments using solid glassy carbon electrodes instead of carbon paper is recommended.

Additionally, advancing and receding contact angle measurements should be performed to account for the influence of surface roughness on the WCA results.

The electrochemical performance of the ALD/MLD modified samples and the original Ag/CB samples should be tested. The first step could be using H-cell and chronoamperometry tests to identify the selectivity of the catalysts for CO_2 reduction. This will help to investigate the effect of the catalyst's wettability on selectivity and answer the question of whether catalyst selectivity is linearly related to the WCA of the catalyst surface.

The next step could be testing the stability of the ALD/MLD coating using H-cell in long-duration chronoamperometry tests and accelerated stability tests. This is essential for evaluating the stability of ALD/MLD coatings under electrochemical reactions and the viability of using ALD/MLD coatings in catalyst wettability modification applications.

If it is still not possible to achieve hydrophilic wettability of the electrode through SiO_2 ALD coatings, an alternative material known for tuning wettability to hydrophilic, such as TiO_2, is worth a try.

References

1. Li, K.; Zou, S.; Zhang, J.; Huang, Y.; He, L.; Feng, X., Superhydrophobicity-Enabled Efficient Electrocatalytic CO_2 Reduction at a High Temperature. *ACS Catalysis* **2023,** *13* (14), 9346-9351.

2. Li, M.; Idros, M. N.; Wu, Y.; Burdyny, T.; Garg, S.; Zhao, X. S.; Wang, G.; Rufford, T. E., The role of electrode wettability in electrochemical reduction of carbon dioxide. *Journal of Materials Chemistry A* **2021,** *9* (35), 19369-19409.

3. Wakerley, D.; Lamaison, S.; Ozanam, F.; Menguy, N.; Mercier, D.; Marcus, P.; Fontecave, M.; Mougel, V., Bio-inspired hydrophobicity promotes CO_2 reduction on a Cu surface. *Nat Mater* **2019,** *18* (11), 1222-1227.

4. Chang, Q.; Lee, J. H.; Liu, Y.; Xie, Z.; Hwang, S.; Marinkovic, N. S.; Park, A. A.; Kattel, S.; Chen, J. G., Electrochemical CO_2 Reduction Reaction over Cu Nanoparticles with Tunable Activity and Selectivity Mediated by Functional Groups in Polymeric Binder. *JACS Au* **2022,** *2* (1), 214-222.

5. Meng, C.; Wang, B.; Gao, Z.; Liu, Z.; Zhang, Q.; Zhai, J., Insight into the Role of Surface Wettability in Electrocatalytic Hydrogen Evolution Reactions Using Light-Sensitive Nanotubular TiO_2 Supported Pt Electrodes. *Sci Rep* **2017,** *7*, 41825.

6. Guo, D.; Wan, Z.; Fang, G.; Zhu, M.; Xi, B., A Tandem Interfaced (Ni_3S_2-MoS_2@TiO_2 Composite Fabricated by Atomic Layer Deposition as Efficient HER Electrocatalyst. *Small* **2022,** *18* (24), e2201896.

7. Sun, X.; Yang, X.; Xiang, H.; Mi, H.; Zhang, P.; Ren, X.; Li, Y.; Li, X., Nitrogen-doped CoO_x/carbon nanotubes derived by plasma-enhanced atomic layer deposition: Efficient bifunctional electrocatalyst for oxygen reduction and evolution reactions. *Electrochimica Acta* **2019,** *296*, 964-971.

8. Ding, Y.; Xu, S.; Zhang, Y.; Wang, A. C.; Wang, M. H.; Xiu, Y.; Wong, C. P.; Wang, Z. L., Modifying the anti-wetting property of butterfly wings and water strider legs by atomic layer deposition coating: surface materials versus geometry. *Nanotechnology* **2008,** *19* (35), 355708.

9. Martín-Palma, R. J.; Pantano, C. G., Ultra-thin hafnium oxide coatings grown by atomic layer deposition: hydrophobicity/hydrophilicity over time. *Materials Research Express* **2019,** *6* (8).

10. Zara, D. L.; Zhang, F.; Sun, F.; Bailey, M. R.; Quayle, M. J.; Petersson, G.; Folestad, S.; van Ommen, J. R., Drug powders with tunable wettability by atomic and molecular layer deposition: From highly hydrophilic to superhydrophobic. *Applied Materials Today* **2021,** *22*.

11. Liang, Y.; Han, Y.; Li, J.-s.; Wang, J.; Liu, D.; Fan, Q., Wettability control in electrocatalyst: A mini review. *Journal of Energy Chemistry* **2022,** *70*, 643-655.

12. Arl, D.; Roge, V.; Adjeroud, N.; Pistillo, B. R.; Sarr, M.; Bahlawane, N.; Lenoble, D., SiO_2 thin film growth through a pure atomic layer deposition technique at room temperature. *RSC Adv* **2020,** *10* (31), 18073-18081.

13. Li, M.; Saedy, S.; Fu, S.; Stellema, T.; Kortlever, R.; van Ommen, J. R., Enhancing the durability of Pt nanoparticles for water electrolysis using ultrathin SiO_2 layers. *Catalysis Science & Technology* **2024,** *14* (5), 1328-1335.

14. Kozbial, A.; Trouba, C.; Liu, H.; Li, L., Characterization of the Intrinsic Water Wettability of Graphite Using Contact Angle Measurements: Effect of Defects on Static and Dynamic Contact Angles. Langmuir 2017, 33 (4), 959-967.

15. Mugele, F.; Baret, J.-C., Electrowetting: from basics to applications. Journal of Physics: Condensed Matter 2005, 17 (28), R705-R774.

6

Conclusions and Outlook

6.1 Conclusions

Catalysts serve as pivotal components in the CO_2 electroreduction and water splitting processes, offering pathways to produce valuable fuels (for example, green hydrogen) and bulk chemicals (for example, formic acid and ethylene) while simultaneously mitigating greenhouse gas emissions. A wide array of catalyst materials, including Pt, Pd, Ag with different nanostructures and phases have been explored in this thesis with the aim of enhancing the efficiency, selectivity, and stability of these electrochemical reactions. Atomic layer deposition has been used to synthesize or modify these catalysts, in order to tailor the properties of these electrocatalysts and optimize their performance for specific applications. Moreover, the integration of advanced characterization techniques (for example, high-resolution STEM and area-scan XPS.) and various electrochemistry testing methods (for example, CV, LSV, EIS, ADT, CA, CP) has been instrumental in unraveling the reaction mechanisms and structure-property relationships inherent to catalyst materials, thereby facilitating the rational design of efficient and stable electrocatalysts for CO_2 electroreduction and water splitting. Different electrochemical cells, ranging from H-cell to MEA flow cell, have been used to bring the research topics closer to the practical application requirements. In general, the work presented in this thesis aimed at designing electrocatalysts using ALD to precisely control the catalyst structure and protect the catalysts from degradation and poisoning.

In Chapter 2, we have used atomic layer deposition to fabricate Pt-Pd bimetallic electrocatalysts with precisely controlled core-shell and alloy structures for the reduction of CO_2 to formic acid. Through this approach, we controlled the structure of the catalysts down to the sub-nanometer scale, allowing for an investigation into the influence of core-shell and alloy structures on Pt-Pd bimetallic catalysts. Our findings reveal that the Pt-Pd alloy catalyst exhibits a better selectivity towards formic acid compared to the core-shell structure, with a faradaic efficiency more than double that of the core-shell structure catalyst. Additionally, we observed that both core-shell bimetallic catalysts (Pd@Pt and Pt@Pd) exhibit instability under electroreduction conditions. These catalysts undergo structural rearrangements to form more thermodynamically stable configurations, such as segregated clusters or alloy particles, during the electrochemical reduction process, consequently altering the catalytic selectivity.

In Chapter 3, we use ALD to apply an ultra-thin SiO_2 coating on the surface of carbon black supported platinum nanoparticles (Pt/CB), aiming to prevent catalyst deactivation during hydrogen evolution. Our findings reveal that following an ADT, the current density at -0.2 V vs. RHE for the unprotected Pt/CB catalyst undergoes a 34% reduction. In contrast, when the Pt/CB catalyst is coated with 2 ALD cycles of SiO_2, the current density decrease after the ADT procedure is reduced by a factor 5, while coating with 5 ALD cycles of SiO_2 results in hardly any reduction in current density after the ADT. Analysis of Pt particle size post-electrochemical testing demonstrates a roughly 16% increase in average particle size for the uncoated Pt/CB catalyst after the ADT, compared to a nearly constant average particle size for the Pt/CB catalyst coated with 5 cycles of SiO_2 ALD. Additionally, the coating significantly mitigates Pt nanoparticle detachment, as evidenced by a substantial decrease in Pt concentration in the electrolyte following the ADT. However, the application of 20 cycles of SiO_2 ALD coating results in an excessively thick coating that hinders catalytic activity. In summary, our study highlights the Pt catalyst stability enhancement for the hydrogen evolution reaction achieved through the application of a few cycles of SiO_2 ALD coating.

In chapter 4, we explored the influence of SO_2 impurities on CO_2 electroreduction in two electrochemical cells: an H-cell and a membrane electrode assembly (MEA) system. Notably, we observed disparate behavior of the Ag on carbon black (Ag/CB) catalyst under SO_2 impurities between the H-cell and MEA reactors. In the H-cell system, SO_2 exerted a more pronounced effect on Ag/CB catalysts compared to the MEA system. We attribute this difference to the higher solubility of SO_2 in the electrolyte relative to CO_2, leading to an accumulation effect and resulting in variations in SO_2 concentration near the electrode between the H-cell and MEA systems. By employing atomic layer deposition (ALD) to deposit a thin SiO_2 coating on the outermost surface of the Ag/CB catalyst, we observed a reduction in the impact of SO_2 on the catalyst's selectivity. This phenomenon can be attributed to the permeability differences between CO_2 and SO_2 through the SiO_2 coatings, leading to local variations in SO_2 concentration between samples with and without SiO_2 coatings.

In Chapter 5, we explored the wettability adjustment of the Ag/CB catalyst on carbon paper electrodes. Our preliminary results demonstrated that the hydrophobicity of the catalyst-loaded carbon paper electrodes can be proportionally modified through PET MLD treatment.

Overall, in comparison to traditional wet chemistry methods, atomic layer deposition (ALD) is demonstrated as a valuable tool for electrocatalyst synthesis, offering additional benefits for catalyst design and protection strategies. It facilitates precise control over the deposition of thin films at the atomic level, allowing researchers to tailor the composition, thickness, and structure of catalyst materials with high accuracy. This level of control enables the creation of highly uniform and precisely engineered catalyst architectures, which can enhance the efficiency and selectivity of electrochemical reactions.

6.2 Outlook

The nanostructure of bimetallic catalysts plays a crucial role in determining their performance. Modifying the structure of bimetallic catalysts can significantly impact their selectivity and activity, although ensuring their structure during the reactions remains a key concern. Understanding how the nanostructure of a catalyst evolves during the reaction, when and under which specific conditions the catalyst's structure starts to reconstruct and what is the dominant factor triggering the reconstruction during the reaction are essential and crucial. All these questions deserve systematic research and concrete answers through comprehensive explanations and detailed experimental design. Exploring bimetallic or polymetallic catalysts is substantial to CO_2 reduction research, with further investigations needed to explore multi-metal combinations through computational and experimental approaches. The primary focus of bimetallic or polymetallic catalyst design should be on converting CO_2 into multicarbon (C_{2+}) alcohols. C_{2+} alcohols not only possess significant economic value and high energy density but also benefit greatly from the design of bimetallic or polymetallic catalysts. The primary challenge in electrochemically reducing CO_2 to C_{2+} alcohols lies in achieving an optimal binding energy between the reaction intermediates and the catalysts. This binding energy cannot be too strong, as it would hinder the detachment of reaction products from the catalyst. Conversely, it cannot be too weak, as insufficient electron transfer would limit the production of C_{2+} alcohols. Bimetallic catalysts offer effective strategies to tailor this binding energy to enhance selectivity and efficiency in CO_2 reduction processes.

The Pt catalyst protection research project occurred by coincidence. The project initially aimed to study Ag catalysts protection for CO_2 reduction, but due to delays in obtaining the Ag catalysts, we shifted the focus to investigating Pt catalyst protection. This unexpected turn led to the discovery that SiO_2 coatings can effectively protect Pt catalysts from agglomeration and leaching after accelerated durability testing (ADT). Nonetheless, some difficulties in this study are still not solved. Challenges persist in precisely determining the thickness of the ultrathin SiO_2 layers on the catalyst surface and accurately measuring Si content in the electrolyte before and after the ADT procedure. One method to address this issue is to use a high-resolution TEM with great magnification that can clearly characterize a 1 nm film to measure the actual film thickness on the substrate. Alternatively, applying fluidized bed ALD to powders for hundreds of cycles to increase the coated film thickness and employing TEM characterization to calculate the film growth per cycle, then using this growth per cycle number to calculate the synthesized film thickness and estimate the actual film thickness, could be another option.

Subsequently, the Ag catalyst protection project was successfully conducted using SiO_2 coatings to protect the Ag/CB catalyst from SO_2 impurities in the CO_2 stream. The mechanism proposed involves the permeability differences of SO_2 and CO_2 through the SiO_2 coating, which is supported by existing literature. However, further research is desired, including independent project investigating the permeability differences of various species, including SO_2, CO_2, H_2, CO, Ag^+, SO_3^{2-}, SO_4^{2-}, S^{2-} through SiO_2 coatings to fully understand this phenomenon. Questions arise regarding the potential influence of molecular polarity versus the dominance of kinetic diameter on permeability. Additionally, it is worth exploring the suitability of an ionic compound such as ZrO_2 for impurity protection, along with determining the permeability of these species through ZrO_2 films in neutral or acidic environments. Furthermore, the possibility of using a ZrO_2 film to protect the Ni anode in a PEM system against corrosion as an replacement of expensive IrO_2 used in PEM remains uncertain and definitely worth investigation. In MEA reactors, the relatively short testing time results in unclear conclusions. Solving the salt formation issue during MEA tests and prolonging the testing time is highly recommended for the follow-up research. Despite these challenges, ALD holds great promise for catalyst research in CO_2 reduction and water splitting fields, offering numerous possibilities for exploration and advancement.

Acknowledgements

Completing this PhD thesis has been an incredible journey for me. It has been a period in my life marked by immense personal and professional growth, a journey filled with moments of both challenge and triumph, pain and joy, obstacles and achievements. Looking back, I could never have imagined that I will stay in the Netherlands for such a long time to do research without returning home. I owe my deepest gratitude to the many individuals who have supported me along the way. Without your guidance, encouragement, and assistance, I could not complete this work. Thank you for being an integral part of this unforgettable chapter of my life.

First and foremost, I would like to sincerely thank my promotors, Prof. Dr. Ir. J. Ruud van Ommen and Dr. Ruud Kortlever, for their invaluable guidance, encouragement, and unwavering support throughout my PhD journey. Your expertise and insights have been instrumental in shaping both this work and my personal development. I am truly grateful for every group meeting we had, even though I always felt a bit nervous beforehand—haha! I also deeply appreciate the supportive and collaborative research environment you cultivated, as well as the friendly and inspiring team atmosphere. Without the opportunity generously provided by you, I would not have been able to join this group and embark on such a remarkable journey. Thank you for granting me the chance to pursue a PhD degree in the Netherlands—it has been an unforgettable and transformative experience. Finally, attending conferences with you was always a rewarding and enriching opportunity, and I thoroughly enjoyed those moments of learning and growth.

I am also profoundly grateful to the members of my doctoral committee- Prof.dr. A.J. Houtepen, Prof.dr. E.A. Pidko, Dr. T.E. Burdyny, Dr. A. Forner-Cuenca, and Prof.dr. J. Dendooven for taking the time to read my dissertation, providing constructive feedback, posing thought-provoking questions, and participating in my defense ceremony. I am especially thankful for your willingness to attend my defense at the very beginning of the new year—it truly means a great deal to me. Thank you all for your invaluable contributions!

Special thanks go to my colleagues and collaborators in PPE and Kortlever's group, who have shared their knowledge, expertise, and inspiration. Dr.ir. Gabrie Meesters, thank you so much for your advice and support in helping me navigate the job search process. Your guidance has been invaluable and has provided me with great direction in securing an offer in the days to come. Mojgan Talebi, Cas Veenhoven, Stefan ten Hagen, Duco Bosma and Michel van den Brink, thank you all for the management, maintenance and guidance in the lab. And also for your advice on purchasing chemicals, setting up lab equipment, booking lab equipment and lab safety considerations. Without the help from you, we can not finish all of the experiments in the lab. Leslie van Leeuwen and Elly Hikhuijsen, thank you both so much for your invaluable support as management assistants in the group. Leslie, I absolutely love the delicious fruits you bring from your amazing garden—they taste far better than the fruits from Jumbo! It's clear that you put a lot of care and effort into tending your garden, and it's greatly appreciated. Thank you for all the extra thoughtfulness and help you bring to the group. Elly, I'm so glad to see you enjoying a happy retirement from the PPE group and embracing life with so many exciting plans—painting your house, traveling to new countries, swimming, and even volunteering. Your vibrant approach to retirement is truly inspiring, and I hope that when the time comes for me to retire, my life will be just as fulfilling as yours. Thank you both for your kindness and for making the group a better place.

Shilong, Damiano, Fuweng, Feilong, Saeed, Isabell, and Dominik, you're the first colleagues I met when I came to the Netherlands. You've been a huge help in getting me into the group quickly. I still remember my first meeting with Shilong was at the e-refinery's annual meeting. At that time I didn't realize that we would have so much interactions and become such good friends afterwards. Your research insights and attitude towards research has impressed me a lot. You are a real time planning master and I've learnt a lot from you. Damiano, Fuweng, Feilong, you were the first colleagues I met at PPE, you provided immense help, particularly in teaching me how to operate the ALD system and guiding me through my initial experiments. Damiano, I cannot thank you enough for your patience and expertise—without your support, this study would never have gotten off the ground. Saeed, Isabell, and Dominik, I have genuinely enjoyed our discussions and various meetings. Saeed, your small chitchats always brightened my day and added a personal touch to our work environment. Rens, Albert, Kaiqiao, Mingliang, Peter, Bhavesh, Katherine, my ALD colleagues, we shared so many memorable moments working with the ALD equipment. From ALD meetings to maintenance tasks and scheduling equipment usage, our teamwork created an amazing experience that I'll always cherish. Daniel, Boaz, Nandalal, Asvin, Aleksandra, Hengameh, Iris, Katherine, Ahmed, Min, my electrochemistry colleagues, thank you for the stimulating group meetings and your collaborative spirit. Whether we were debugging and calibrating the gas chromatography, sharing chemicals, or designing and maintaining cells, your contributions made my electrochemical experiments so much smoother and more efficient! Christian, Nasim, Zaid, Margherita, Ruben, Ankur, Ida, Mahdiyeh, Sophie, Lena, Gao, Qing, Chengtian, Riccardo, Marc, Tanuj, Dominik, Giacomo, Lukas, Maximilian, I really enjoyed having lunch with you and chatting in the office. Interacting with all of you added so much joy to my days and has significantly improved my work life balance! The vibrant discussions and teamwork with all of you have made this experience both productive and enjoyable.

On a personal note, I am immensely thankful to my family and friends for their unconditional love, patience, and encouragement throughout this journey. I will always cherish the memories of our times together—dining out at restaurants, traveling, watching the sunrise, and playing countless board games. I can't imagine how I would have navigated the unprecedented and challenging COVID time— an event I could never have imagined—without you all by my side. The group of incredible people I met in the Netherlands holds a special place in my heart, and I will never forget you. No matter whether or not we meet in the future, no matter how much time passes, these memories will always remain vivid and cherished. Your insights and experiences have inspired me to see life from new perspectives and embrace its endless possibilities. Your belief in me has been my source of strength, and I will hold it forever, until death makes me forget.

Finally, I extend my heartfelt gratitude to everyone who has contributed to my PhD journey, directly or indirectly. This thesis is a reflection of collective support and inspiration from all of you.

Thank you all for being part of this journey!

Ming Li

Delft, December 2024

Curriculum vitae

Ming Li (李明) was born in August 1994 in Hunan, China. He earned his Bachelor's degree in Materials Science and Engineering from Beijing University of Chemical Technology, China, in 2016. In there, he received the first-class People's Scholarship three times and was recognized as an outstanding graduate. He then pursued a Master's degree in Master of Science in Materials Engineering at Beihang University, China, graduating in 2019. During his Master's studies, he was awarded the second-class scholarship for graduate students twice and completed a thesis titled 'Preparation and Property Regulation of High Dielectric and Low Conductivity Graphene Composite Film.' In September 2019, he joined the Product and Process Engineering group in the Department of Chemical Engineering at Delft University of Technology to pursue a Ph.D. focused on 'Designing Electrocatalysts via Atomic Layer Deposition for Carbon Dioxide Reduction and Hydrogen Evolution Reactions.'

List of Publications

Journal Articles - Within the scope of the dissertation:

1. **Ming Li**, Shilong Fu, Saeed Saedy, Aparna Rajendrakumar, Frans Tichelaar, Ruud Kortlever, J. Ruud van Ommen. Nanostructuring Pt‐Pd Bimetallic Electrocatalysts for CO_2 Reduction Using Atmospheric Pressure Atomic Layer Deposition. *ChemCatChem*, 2022, 14, e202200949.

2. **Ming Li**, Saeed Saedy, Shilong Fu, Teise Stellema, Ruud Kortlever, J. Ruud van Ommen. Enhancing the durability of Pt nanoparticles for water electrocatalysis using ultrathin SiO_2 layers. *Catalysis Science & Technology, 2024,* 10.1039/d3cy00996c.

3. **Ming Li**, Ruud Kortlever, J. Ruud van Ommen. The effects of SO_2 impurities on CO_2 electroreduction on bare silver and SiO_2 coated silver in different cell geometries. In preparation.

Journal Articles – Outside the scope of the dissertation:

1. Shilong Fu, **Ming Li**, Simone Asperti, Wiebren de Jong, Ruud Kortlever. Unravelling the Effect of Activators used in The Synthesis of Biomass‐Derived Carbon Electrocatalysts on the Electrocatalytic Performance for CO_2 Reduction. ChemSusChem, 2023, 16, e202202188.

2. Shilong Fu, **Ming Li**, Wiebren de Jong, Ruud Kortlever. Tuning the Properties of N-Doped Biochar for Selective CO_2 Electroreduction to CO. ACS Catalysis, 2023, 13, 10309-10323.

3. Shilong Fu, Asvin Sajeev Kumar, **Ming Li**, Wiebren de Jong, Ruud Kortlever. Electrochemical CO_2 Reduction in the Presence of SO_2 Impurities on a Nitrogen-doped Carbon Electrocatalyst. Submitted.

4. Shilong Fu, Boaz Izelaar, **Ming Li**, Qi An, Min Li, Wiebren de Jong, Ruud Kortlever. Ni-N-C catalysts for CO_2 electrochemical reduction to CO: The effects of carbon support. Submitted.

5. Shuo Zhang, **Ming Li**, He Tian, J. Ruud van Ommen, Luuk C. Rietveld, Sebastiaan G.J. Heijman. Low loading of palladium on ceramic ultrafiltration achieved by atomic layer deposition to enhance the removal of micropollutants by the activate peroxymonosulfate. In preparation.

6. Shuo Zhang, **Ming Li**, Yuning Ji, J. Ruud van Ommen, Luuk C. Rietveld, Sebastiaan G.J. Heijman. The effect of membrane fouling on the peroxymonosulfate-activated degradation of micropollutants. In preparation.

Oral and Poster Presentations:

2023 EUROCVD / Baltic ALD conference, Leuven, Belgium, Oral presentation

2022 AVS 22nd International Conference on Atomic Layer Deposition, Ghent, Belgium, Poster presentation

2022 23th Netherlands Catalysis and Chemistry Conference , Noordwijkerhout, Netherlands, Oral presentation

2021 72nd Annual International Society of Electrochemistry Meeting, Online, Oral presentation

2021 AVS 21st International Conference on Atomic Layer Deposition, Online, Oral presentation